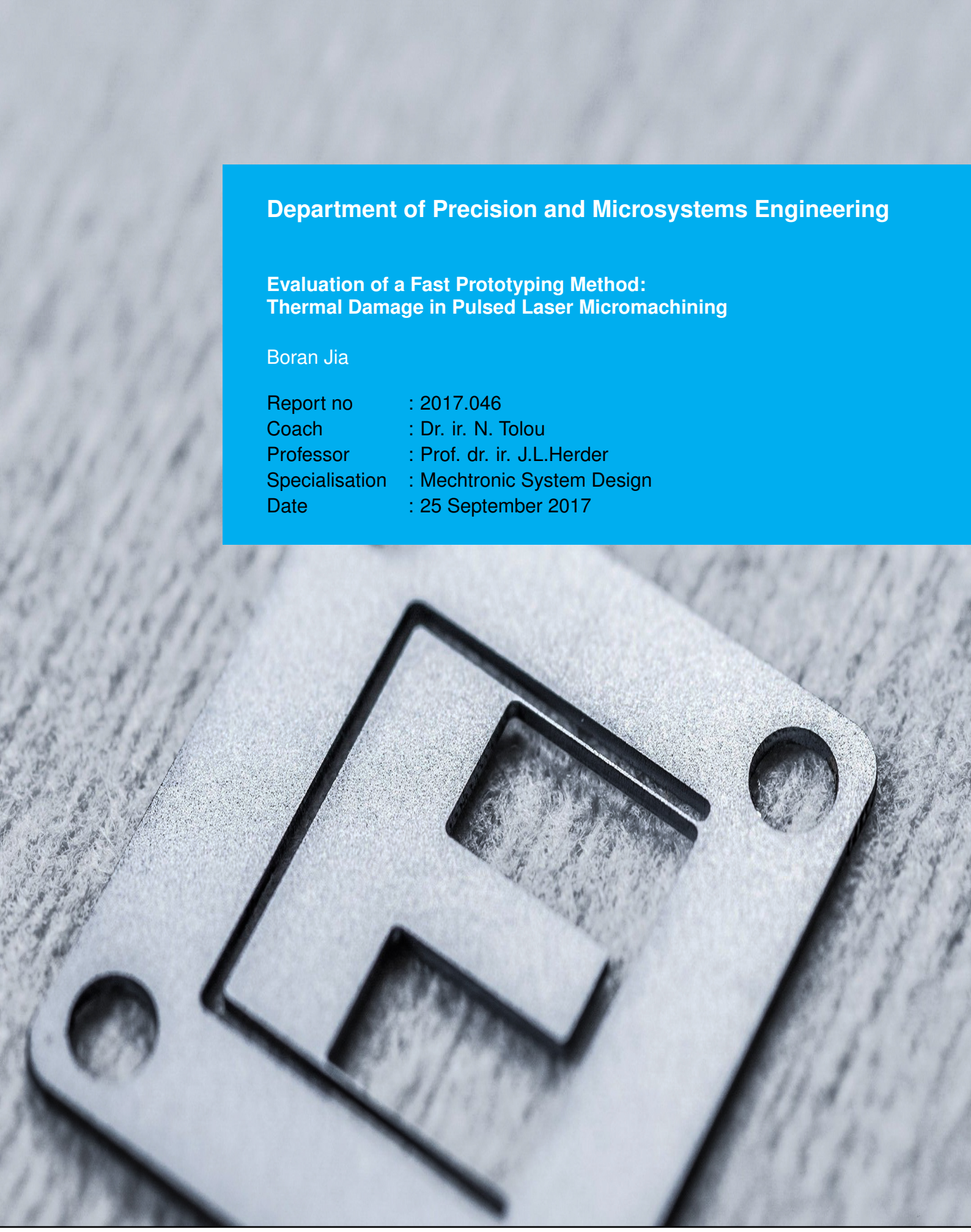

Department of Precision and Microsystems Engineering

Evaluation of a Fast Prototyping Method: Thermal Damage in Pulsed Laser Micromachining

Boran Jia

Report no	: 2017.046
Coach	: Dr. ir. N. Tolou
Professor	: Prof. dr. ir. J.L.Herder
Specialisation	: Mechtronic System Design
Date	: 25 September 2017

Evaluation of a Fast Prototyping Method: Thermal Damage in Pulsed Laser Micromachining

Department of Precision and Microsystems Engineering
Technical University of Delft

Boran Jia

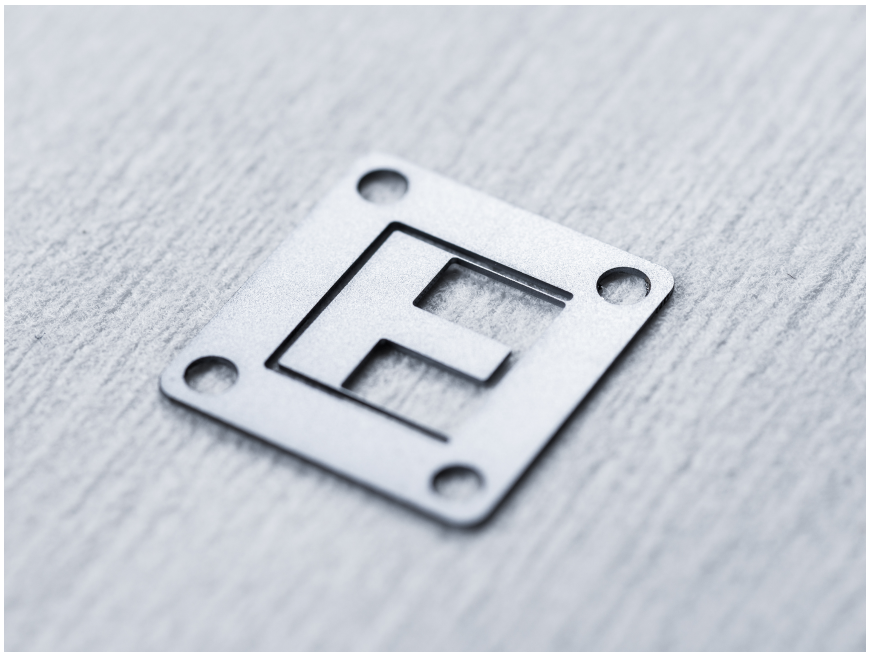

Committee Board: Prof. dr. ir. J.L.Herder
Dr. ir. N. Tolou
Dr. ir. MK. Ghatkesar

Defence date: 25-09-2017

Contents

Abstract

The theories of energy harvester and complaint mechanism on micro scale have been developed vastly, however prototyping and realization of conceptual designs of such devices is difficult. Currently, micro scale prototyping devices can only be manufactured by means of lithography. However, lithography is expensive, both in terms of time and cost. Alternatively, laser micro machining is considered to be capable of precise manufacturing in micro scale, be able to bring down process time from months to a few days. Yet, thermal damage and mechanical performance of laser fabricated device have not been quantified and evaluated properly in literature, which are the challenge and goal of this thesis. The operation of laser system has been thoroughly studied , which enables replication of previous research in this area with a state-of-art quality.

Firstly, thermal damage was quantified by means of the piezoelectric property loss under high temperature. A set of taguchi process optimizations was conducted for optimal operational settings. Secondly, a micro double-flexure stage was manufactured by laser micromachining. Structural properties of the micro devices such as side wall surface roughness and beam geometry were measured, and stiffness in translational direction of the micro flexure structures were tested.

It is found that the piezoelectric property can be preserved by 99% by systematically optimizing the parameters. And it was found that stiffness of the laser micro machined silicon compliant mechanism is 16%-36% lower than lithography made ones due to thermal damage. Therefore a fast prototyping method for micro scale devices has been thoroughly studied and can be used for further researches and applications.

1

Introduction and Background

1.1 Introduction

Since the electronic devices have been playing a dominant role in our lives, the Micro Electro Mechanical System (MEMS) gradually comes to public attentions. They are being used in variety of areas such as accelerometers, gyroscopes, pressure sensors, resonators, relays, switches, and micro pumps and values[1]. MEMS devices shows the great advantage of highly integrated functions into compact micro size. We might not be aware of it, but MEMS applications have penetrated into our daily lives and made our lives easier. However, there is still a vast potentials to be developed by scientists and researchers around the world for smaller, faster and more powerful devices.

MEMS devices are conventionally manufactured by means of lithography. Lithography is an extremely expensive and complex process that comprises multiple cycles of deposition, exposure and etching, specially for thick materials[6]. Also the heavy chemicals and delicate materials of lithography process requires highly trained operators. However, high throughput, meaning the highly automated and rapid parallel process of handling hundreds of thousands MEMS devices at the same time on a wafer, has made the price of a single device become affordable under vast industrial production.

Yet, lithography is normally not easily accessible, and it is relatively expensive to fabricate small amounts of devices. Therefore manufacturing of prototypes of new product has been an obstacle for researchers [2], and an alternative solution for this issue is craved.

In order to find a substitution method of rapid prototyping small amounts of micro devices, we investigated the requirements of fabrication. The size of the devices are normally in sub-millimetres or even micrometres scale, and high accuracy and resolution micromachining in both surface machining and internal 3-dimension structure are required [3]. Light Amplification by Stimulated Emission of Radiation, laser, has become one of the widely used innovative manufacturing methods in industry for decades[4]. This technique can be potentially considered as the alternative method of conventional lithography since it provides high intensity power as well as high precisions.

Conventional lithography is extremely time-consuming and expensive[7]. In contrast, Laser micro machining is relatively simple, without contact, no need for mask and time-efficient[8]. However, as a substitution of conventional manufacturing methods, laser micromachining is facing two main challenges when applied onto micro and nano scale.

1. **Thermal damage**, which is caused by the nature of laser technique, will immediately damage MEMS devices and also cause a series of problems such as cracking, waving, recast and debris around the cut. Generally the damaged area is also referred to as Heat Affected Zone (HAZ) [36]. The huge thermally introduced residual stress will jeopardize the structural properties with undesired deformation. Furthermore, other material properties such as piezoelectricity are also sensitive to thermal damage, which will diminish under certain temperatures.

2. **Side wall surface roughness**, which is very large in laser micro machining and this heavily influences the static and dynamic properties of device. Especially for micro structures, the small features on the surface plays bigger part in overall geometry compared to macro structures, this will dramatically decreases the performance of devices.

To circumvent negative effects such as thermal damage and high surface roughness, ultra fast laser micro machining has been introduced. It has accuracy that is high enough for MEMS devices with minimum thermal damage[3]. And this method is faster for prototyping compared to lithography, and it can dramatically decrease thermal effect on specimen while obtaining acceptable surface quality.

1.2 Background

By pulsing the laser, high energy density can be achieved with ordinary output power, also thermal effect is decreased. By further shortening the laser pulses, which changes the mechanism of material removal, while the thermal damage such as micro cracking, recast layer and debris can be eliminated. An illustration of comparison between long and short pulses of laser micromachining can be seen below.

1.2.1 What is ultra fast laser micro machining

Short and ultra short pulses The short or even ultra short light pulses are hard to be expressed in a way such that people could experience, just like the unit 'light-year' is used to show the very long distance, here we could also use light-length to show how short is the short pulses from laser. The distance of one nano second is roughly a foot long. And the distance of light travels for 100 fs pulse is only 30 um[18]. Between those tiny pulsed units, the comparison of a femto second to one second is equal to one second for 30 million years.

When distinguishing between short and ultra short, the interaction inside of material helps us to have a better understanding. The photons can be absorbed by the free electrons into a thin layer in a matter of magnitude of one femtosecond. And the relaxation time of the electrons is around one picosecond[20]. The

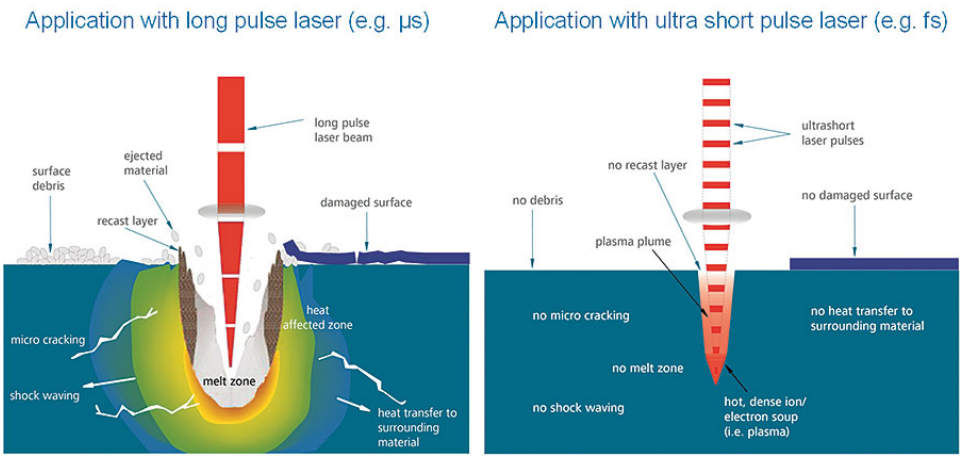

Fig. 1.1: Comparison between long and short pulsed laser micromachining[19]

energy will be stored in the electrons and then released as heat during the relaxation time.

Steel as an example, for 10fs, it diffuses a depth of 1nm, while over 1 ps, the heat diffuses more than 10 nm. The material takes 1 ps to convert photon energy into heat, and this heat diffusion layer happens in a 10nm thin layer. The optical penetration depth varies by different materials and wavelengths. The tale below shows a rough illustration of short pulses times for some common materials.

Material	Pulse length
Metals	1 ps
Ceramics	10 ps
Plastics	1 ns

Tab. 1.1: The range of ultra short pulses for common materials[18]

1.2.2 Mechanism of laser machining

In laser micromachining, femtosecond to nanosecond laser pulses are generated, the shorter pulse width brings extremely high peak power and power intensity while maintaining ordinary output power. The means of material removal changes from melting to sublimation when the time scales down to a tiny fraction of second. The discussion with respects to energy and time are introduced.

Two regimes of ablation mechanism In 1997, it is noticed that two ablation regimes existed that depend on the laser fluence [22]. Fluence is vastly used in literature to describe the energy applied on the surface of object, the fluence can be calculated as:

$$F = \frac{2E_{pulse}}{\pi\omega_0^2} \tag{1.1}$$

As the w is the frequency of the laser.

The first ablation regime is with relatively low influence, the ablation per pulse L was calculated as :

$$L = \alpha^{-1} ln(\frac{\phi}{\phi_{th}^{\alpha}}) \tag{1.2}$$

Where the α is the absorption coefficient and ϕ is the laser fluence and $\phi_{th}^{\alpha}$is the threshold fluence. While the laser fluence is increasing, the second regime appears with different coefficientλ:

$$L = \lambda^{-1} ln(\frac{\phi}{\phi_{th}^{\lambda}}) \tag{1.3}$$

In the lower fluence regime, no molten material and debris was found while it is inevitable in the higher fluence regime, meanwhile effective ablation can be guaranteed in both regimes. The physical reasoning behind this phenomena was due to two different mechanisms of material removal, respectively spallation and phase explosion.

Spallation is the fractures of material appeared when the tensile stress exceeds the material tensile stress limit, which leads to ejection of complete layers of material. This is introduced by the expansion and internal pressure of a solid material[23]. While the phase explosion is more complex, since not only more complicated phase transitions and thermodynamic behaviour happened, but also more ballistic electrons smash further into material as well as the higher temperature and pressure are induced[24, 25].

Two regimes of pulse duration For ultra short pulsed laser, the time duration is an important factor for laser micro machining[26]. Shorting pulses to certain extend can change the process fundamentally since the thermal effect can be removed theoretically. The heat diffusion depth l can be calculated as:

$$l = 2\sqrt{K\tau_p} \tag{1.4}$$

Where K is the diffusivity of thermal load of material and τ_p is the pulse duration. Therefore, at the first time regime, short pulse duration leads to smaller thermal diffusion depth. While the time duration gets short enough that there will be no thermal effect appeared.

Typically in laser system, this pulse duration varies from picosecond to femtosecond. For instance, this duration for silica glass is 1 ps and for silicon is 6 ps. A specific model for the ablation depth in silicon with certain laser pulse duration is explained in the following section.

1.2.3 Ablation rate on silicon

Since the silicon is one of the most common materials in the field of MEMS, the ablation behaviour of silicon has been studied specifically. The ablation of a silicon target of thickness T to a laser pulse is described as Stefan model[21], at position x and time t. The laser pulse propagates in the direction x. Mathematically, the laser ablation problem is a moving boundary problem which is transformed by a simple change of variables, into a fixed boundary problem, with the heated boundary located at $x = 0$. The model is :

$$\frac{\partial H}{\partial t} + u_{vap}\frac{\partial H}{\partial x} = \frac{\partial}{\partial x}\left(K(T)\frac{\partial T}{\partial x}\right) + \frac{\partial I}{\partial x} \tag{1.5}$$

H is enthalpy,

$$H = \rho(T)\, c_p(T)\, T \tag{1.6}$$

where ρ is the density of silicon, c_p is the heat capacity. The target surface is vaporized at velocity u_{vap}under heating by optical absorption of a laser pulse of intensity I; K is the thermal conductivity of the target.

Vaporization velocity u_{vap} is calculated using the Hertz–Knudsen relation[22]:

$$u_{vap} = \frac{\beta}{\rho} p_0(T_s)\left(\frac{M}{2\pi k_B T_s}\right)^{\frac{1}{2}} \tag{1.7}$$

where β is the evaporation coefficient of the sample, $T_s$is the temperature of the target surface,

$$T_s = T(0,t) \tag{1.8}$$

$p_0$is the vapour pressure at equilibrium, M is the molecular mass of silicon, and $k_B$is the Boltzmann constant.

The ablation depth Δz after s seconds, which s is normally equals to the period of laser:

$$\Delta z(s) = \int_0^s u_{vap}(t)\, dt \tag{1.9}$$

Based on the mathematical model aforementioned, a theoretical assumption of the energy and pulse condition needed can be obtained. However, due to the laser equipment and condition limitation, this theoretical approach is normally stochastic and random[22], since pulse duration, wavelengths and output energy of laser systems are not feasible.

1.2.4 Laser specification

The laser source is from a Spectra-Physics Q-switched Talon laser 355-15 with a maximum power of 15W at 50 kHz repetition frequency, and with 13W output at 100kHz. The maximum of frequency is 500 kHz and pulse width 35 ns. The M^2 factor is 1.1 which describes the accuracy of the Gaussian TEM00 mode laser, the closer the factor to 1, the closer the actual laser output to the theoretical Gaussian beam. The performance of laser in terms of output power and corresponding pulse width under different frequencies can be found below.

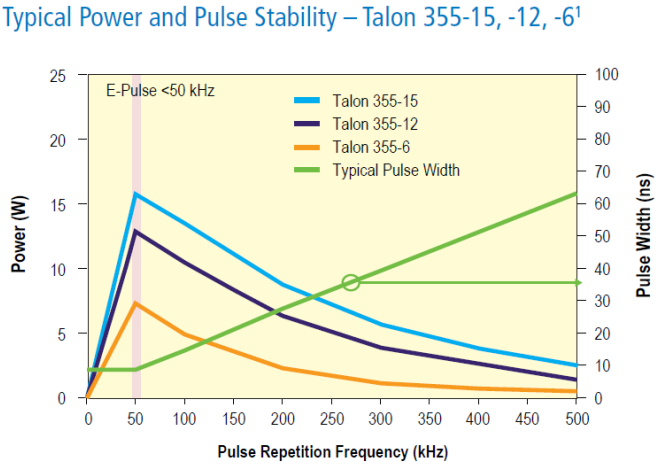

Fig. 1.2: specification of laser

The energy delivered per pulse can be calculated as :

$$E_{pulse} = \frac{W_{output}}{f_{laser}} \tag{1.10}$$

The W is the output power for the laser while irradiating obtained by the internal power monitor, which can be found by clicking 'refresh' button on the laser section Process Power software, and f is the laser frequency which is called as 'firing rate' in the system. For instance with Talon 355-15 laser, the maximum working mode with a 15w output at 50kHz, the energy delivered on every pulse is 300uJ.

The delivery of laser beam includes attenuator, energy monitor and steering mirrors. The vision system consists of a microscope inspection zoom associated to a CCD camera, focusing of laser beam is synchronized with the focusing of this camera.

The X-Y stage has a range of 80mm square with 1 um effective resolution. The laser beam scanning motion is done by a laser deflection systems based on the Lorentz force motors with internal active optical feedback in order of dramatically reducing sensitivity to external noise. Galvo head which manipulates

the laser path has the range of 46x46mm with local length of 100mm, the writing speed is 1300cm per second with position resolution of 8 urad.

1.3 State of the art

In this section the current state of art of laser micromachining and the means of the improving laser-machined devices are introduced.

1.3.1 Where is laser micro machining standing ?

The current stage of laser micro machining are mainly focused on the ablation behaviour with different laser types and variety of materials. Figure1.3 shows different behaviours of several piezoelectric materials cut by a picosecond laser. And figure1.4 shows the difference in ablation depth under different laser setting and fluence for silicon.

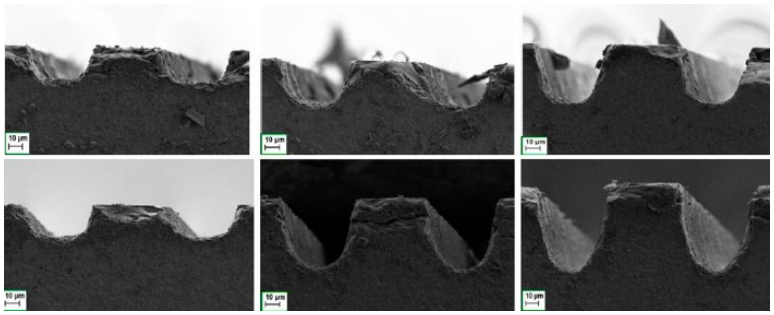

Fig. 1.3: Laser machined grooves on piezoelectric materials [29]

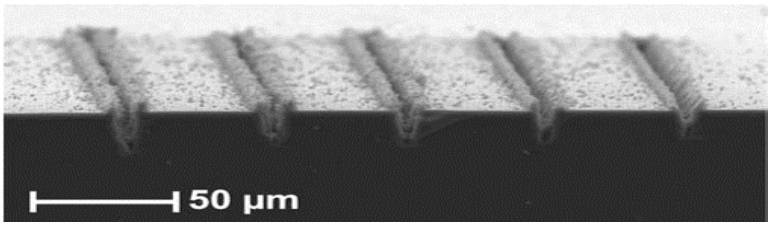

Fig. 1.4: Laser machined grooves on silicon[30]

The studies of laser cutting have also focused on drilling micro holes for interests from medical and micro fluid devices[33]. An example given below in figure1.5, micro holes are drilled in diamond and silicon.

Micro laser machining has also other potential application like improving the lubrication by graving micro patterns on sliding surface, an illustration can be seen below in 1.6. The MEMS devices manufactured by laser micro machining has not been found in literature yet.

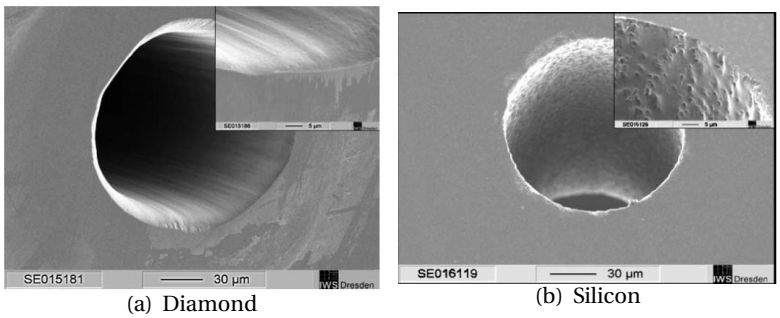

(a) Diamond (b) Silicon

Fig. 1.5: Different laser drilled holes on diamond (left) and silicon (right)[32]

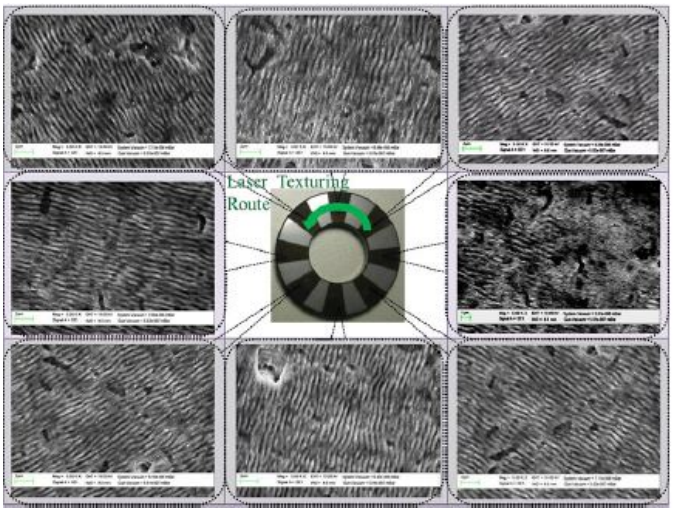

Fig. 1.6: Surface graving to improve lubrication[34]

1.3.2 How to improve the quality of laser-fabricated devices?

As aforementioned in introduction section, the laser micro machining is still facing two main obstacles, rough side wall surface and thermal damage (HAZ). There are small number of researches conducted for improving the overall quality of the laser micro machining, which is introduced in two parts: Minimize thermal damage and maximize surface quality.

Minimize thermal damage

In order to minimize the Heat Affect Zone, the amount of thermal damaged needs to be quantified. Currently the main method of quantifying the HAZ is by visual inspection, an example can be seen below at Fig1.7. Although it is not a relatively accurate method, so far the main criteria is the colour change on the surface along the cutting edge.

Other potential ways are measuring the mechanical property such as tensile

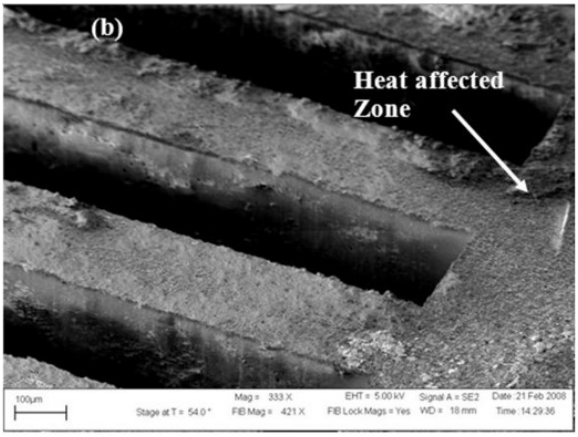

Fig. 1.7: The visually inspection of the HAZ[35]

strength, Young's modulus and yield tension. For piezoelectric material, since the piezoelectric material can be lost by applying the high temperature, measuring the piezoelectric coefficient is considered to be a trustworthy method to quantify the heat affected area. Both methods will be discussed in details in chapter 2 and 3 respectively.

Regarding to the minimize the thermal damage, or eliminating the thermal damage further more, water-assisted cutting is considered as an efficient solution. The water introduced into the cutting system could be still water, water flow or high-pressure water jet.

By putting a thin water laying beyond the working surface, the thermal effect can be dramatically decreased since the heat will instantly be dissipated into water . Although original ultra short pulse laser has the advantage of negligible thermal effect, minor thermal damage is still existed. There is certain band observed along the edges of laser path (Kerf band) that influences the quality of laser manufacturing. Another obstacle is caused by the high temperature debris recast and gathered around the cur area[37]. Several successful examples and comparisons are made by [36][38], pictures shown in Fig1.8.

As can be seen in Fig1.8, the water-assisted laser cutting show extensively advantages as debris and recast free, and no thermal damage[39].

Maximize side wall surface quality

As no external assistance or changes of laser cutting, by utilizing the parameters of the laser, the surface roughness can already be improved to a certain level. As an example, the silicon double-clamped beams with a side wall surface roughness as low as 370 nm[40], an illustration is in Fig1.9.

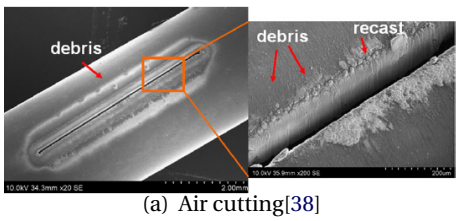

(a) Air cutting[38]

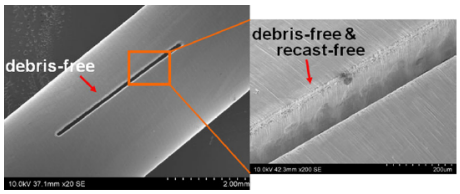

(b) Underwater cutting[38]

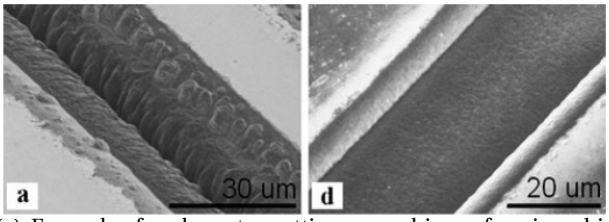

(c) Example of underwater cutting on saphire wafer, air ambient(left) and water ambient(right)[39]

Fig. 1.8: Comparison between dry and underwater cuttings

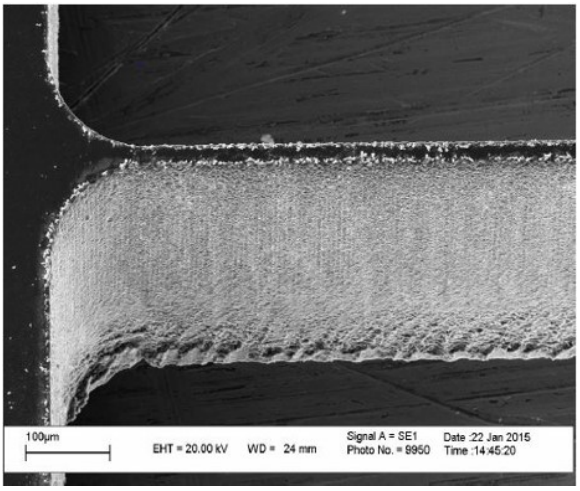

Fig. 1.9: Silicon double-clamped beam made by[40]

Reheat or reflow is a widely used post treatment method in conventional industry. This process can smooth out the defects and recrystallise the material to obtain an acceptable surface, as well as enhance the mechanical properties like strength. To improve the surface roughness of a resonator micro-machined by laser in a traditional lathe alike setting, a high temperature electric arc was introduced in [33]

Chemical etching or wet etching which was suggested to improve the surface condition, but it only subjects to certain types of materials but not all cases. Furthermore, etching method slows the manufacture efficiency[31]. one example

is introduced in [35], a micro channel chip is manufactured in the Poly Methyl Methacrylate (PMMA) and Cyclic Olefin Copolymer (COC) material by laser micro machining, and a vapour exposure method is used to improve the surface roughness, the outcome can be seen in 1.10.

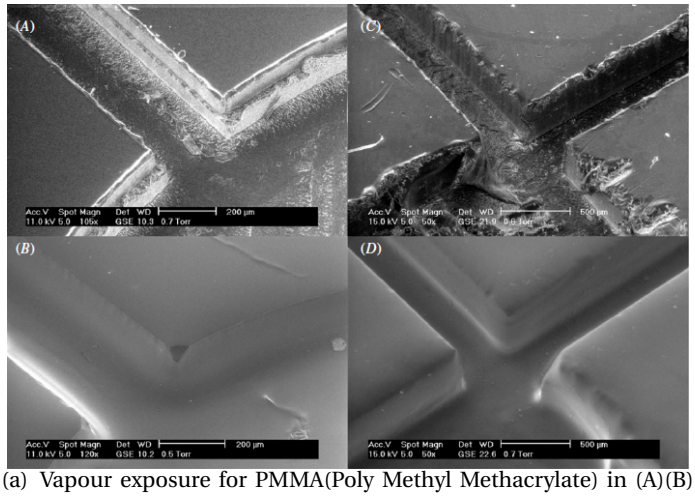

(a) Vapour exposure for PMMA(Poly Methyl Methacrylate) in (A)(B) and COC (Cyclic Olefin Copolymer) in (C)(D) under different time durations[35]

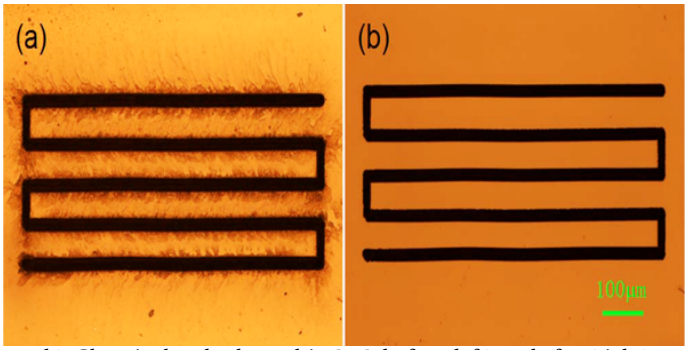

(b) Chemical etched sapphire[46], before(left) and after(right)

Fig. 1.10: Examples of chemical etching to improve surface quality on materials after laser machined

Underwater cutting is also referred as liquid immersion laser micromachining [39]. As mentioned in the previous section, this method is also beneficial for silicon structures cutting in terms of both less thermal damage and better surface roughness. Silicon based underwater cutting researches are shown in [41] and [42], but only single hole or groove were focused. Furthermore, no surface roughness details so far were quantitatively recorded but only observation of 'smoother' result[36].

Discussion

Direct cutting by ultra fast laser micromachining has been developed by over decades, and a number of researches have been carried out. In [40] an advanced optimizing model was used to obtain the best cutting result. A minimum surface roughness of 370nm was achieved on cutting through silicon samples, and the HAZ was negligibly small due to the ultra fast laser pause.

Reflow and etching method as post processing are the most commonly used and adapted methods for improving the surface roughness after cutting. However, as considering manufacturing MEMS devices, there are multiple layers of materials cut at the same time. This brings serious problems even for the most commonly used silica and silicon substrates used in this field, since silicon is much more thermal conductive than silica[47]. Different conductivities between layers make the reflow process difficult to achieve.

Although the underwater cutting technique is still being developed, this is the a promising method for improving the surface roughness and heat affected zone. Moreover the specific roughness data has not been found in literature yet.

Conclusion

Surface quality of the silicon structure obtained by laser manufacturing is relatively low compared to lithography. Currently the rough and coarse surface is unacceptable for laser machined MEMS devices applied in industry[31] since it would heavily influence the mechanical and structural properties of devices. However, the direct relation between surface roughness and mechanical performance has not been verified in literature.

In addition, ultra fast laser still introduces small thermal effect, the thermal interaction between the laser and the specimen is hard to simulate and be measured since it all happens at a small area instantly[9]. Specifically for piezoelectric materials, the most common building block for energy harvester and actuators, the thermal damage leads to a loss of piezoelectric property. Normally the HAZ can be minimized by carefully tuned laser parameters[9]. However the quantification of the HAZ is done by visual measurement of indication which is not precise and reliable, a systematic approach to quantify the thermal damage is missing.

To sum up, although ultra fast laser micro machining technique as a new fabrication method has its unique advantages, it also brings drawbacks, such as poor surface quality and HAZ. Several attempts on groove cutting and micro drilling on semiconductor and piezoelectric materials have been carried out[2, 7, 8, 10, 11, 12, 13, 14, 15]. But producing practical MEMS devices with minimizing those drawbacks has not been found, which draws great research potential for future study. Moreover, the thermal damage and low surface quality have not been connected to the actually structural and mechanical performance. There-

fore, the quantification of HAZ and evaluation of thermal damage in terms of mechanical performance draw great interest for this project.

1.4 Challenges and knowledge gap

1.4.1 Challenges

So far we have discussed the laser micro machining in basic mechanism, current studies conducted and the methods to enhance the performance. The research questions of this project are :

1. **Drawbacks**, what is limiting laser micro fabrication compared to other methods as lithograph, what are the drawbacks?

2. **Quality**, how to achieve a acceptable result of the laser micro machining, without external assistance but only by optimization of laser parameter setting ?

3. **Quantifying**, how sever the drawbacks of laser micro machining are, in terms of the thermal damage and low surfacer roughness?

4. **MEMS fabrication**, how to integrate the laser micro machining techniques into MEMS device fabrication?

Based on the previous introduction and the project research questions, the main challenges can be concluded as below:

1. **Operation**, since the ultra-fast laser system has not only the conventional process parameters but also more complexly the laser beam parameters such as frequency, out put power and pulse duration. Moreover, the link between input parameters to certain outcome criteria is an unknown and highly non-linear related. Furthermore. there is no previous experience or reliable guide for the specific laser system accessible. Therefore, to start the operation and understand the mechanism is the first difficulty for this research.

2. **Optimization with only laser**, here 'only' means there is no external methods to facilitate the cutting to obtain better results, but solely optimizing the parameters setting and combination. Hence a experimental parameter optimization method called 'Taguchi method' has been widely adapted to obtain optimal quality for complex laser systems based on different materials. Although this method has chosen a relatively small amount of samples, still a whole set of test needs to be conducted, which includes sophisticated experiment design and enormous experiment time.

3. **Quantifying and evaluation**, after the manufacturing, test and measurement is needed to quantify the thermal damage and certain drawbacks of the laser cut device in terms of mechanical and electrical performance. Yet there is no current test equipment available existed currently which requires either external corporation or building by the author.

4. **Integration**, laser cutting technique has been developed for several decades, however, a fully integrated MEMS system fabricated by laser micro machining has not been found in literature. An example of attempt can be seen below in Fig1.11, as a lateral resonator has been cut with femtosecond laser. But this structure has not been integrated with electrical connection and furthermore actuated or sensed, neither examined passively.

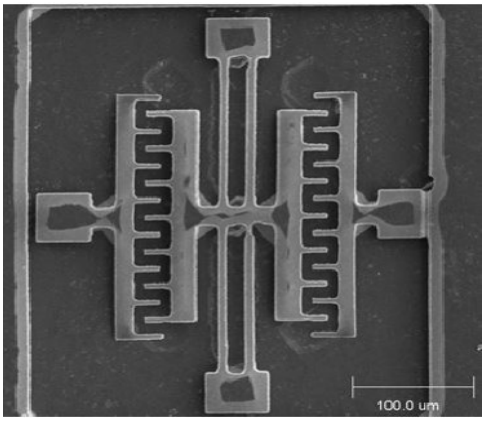

Fig. 1.11: A lateral resonator without functioning[48]

1.4.2 Knowledge gap

Although laser micro machining has been developed to a relatively deep extend, the author still find that there is few aspect and knowledge existed which have not been found in literature.

From value to performance Side wall surface roughness, machining time, HAZ width, tapper angle are the main judgement of current studies in this field. However, how those criteria affect the outcome of the laser cut devices has not been studied, especially for thermal damage and side wall surface roughness.

From cutting to devices There is a huge gap between current laser fabrications such as cutting, graving, and drilling, to a fully functioning device or integrated MEMS system. The minimum feature sizes, enough high accuracy and tolerance, reliable electrical connection and processing multi-layer structures are all obstacles that need to be conquered.

1.4.3 Thesis structure

The fundamental principles of laser micromachining and material removal mechanisms are introduced in Chapter 1. Then a study of quantification of Heat Affected Zone is presented in Chapter 2. In order to quantify the thermal damage laser micromachining brought on micro structures, a material feature which piezoelectric property gets lost under temperature above Curie point on piezoelectric material has been utilized. Then another study of evaluation of mechanical performance on micro compliant mechanism fabricated by laser is introduced in Chapter 3. Mechanical performance in term of stiffness has been investigated for a double-flexure silicon micro stages. Furthermore, some supportive outcome and other relative work conducted are presented in Chapter 4. Additionally, a manual of recipes of common materials are collected and presented for helping further researchers.

Bibliography

[1] Huang, Yunhan, et al. "MEMS reliability review." IEEE Transactions on Device and Materials Reliability 12.2 (2012): 482-493.

[2] X. Jiang, J.R. Yuan, A. Cheng, K. Snook, P.J. Cao, P.W. Rehrig, W.S. Hackenberger, G. Lavalelle, X. Geng, T.R. Shrout, Proc. IEEE Symp. on Ultra (2006) 922.

[3] Crawford, T. H. R., A. Borowiec, and H. K. Haugen. "Femtosecond laser micromachining of grooves in silicon with 800 nm pulses." Applied Physics A 80.8 (2005): 1717-1724.

[4] Cheng, Jian, et al. "A review of ultrafast laser materials micromachining." Optics Laser Technology 46 (2013): 88-102.

[5] Bäuerle, Dieter W. Laser processing and chemistry. Springer Science Business Media, 2013.

[6] Peng, Jue, et al. "Micro-patterning of 0.70 Pb (Mg 1/3 Nb 2/3) O 3–0.30 PbTiO 3 single crystals by ultrasonic wet chemical etching." Materials letters 62.17 (2008): 3127-3130.

[7] Lam, K. H., et al. "Kerf profile and piezoresponse study of the laser micromachined PMN-PT single crystal using 355nm Nd: YAG." Materials Research Bulletin 48.9 (2013): 3420-3423.

[8] Han, Yukun, et al. "Femtosecond laser-induced silicon surface morphology in water confinement." Microsystem technologies 15.7 (2009): 1045-1049.

[9] Zheng X J, Zhou Y C, Nin M Z. Thermopiezoelectric response of a piezoelectric thin film PZT-6B deposited on MgO (100) substrate due to a continuous laser[J]. International journal of solids and structures, 2002, 39(15): 3935-3957.

[10] Tangwarodomnukun, Viboon, Jun Wang, and Philip Mathew. "A comparison of dry and underwater laser micromachining of silicon substrates." Key Engineering Materials. Vol. 443. Trans Tech Publications, 2010.

[11] Karatodorov, S., and M. Grozeva. "The Effect of Process Parameters in Femtosecond Laser Micromachining." Bulg. J. Phys 43 (2016): 110-120.

[12] El Fissi, Lamia, Victor Xhurdebise, and Laurent A. Francis. "Effects of Laser Operating Parameters on Piezoelectric Substrates Micromachining with Picosecond Laser." Micromachines 6.1 (2014): 19-31.

[13] Corbari, Costantino, et al. "Femtosecond versus picosecond laser machining of nano-gratings and micro-channels in silica glass." Optics express 21.4 (2013): 3946-3958.

[14] Li, Xiaomeng, et al. "Lead-Free Piezoelectric Diaphragm Biosensors Based on Micro-Machining Technology and Chemical Solution Deposition." Sensors 16.1 (2016): 69.

[15] Knappe, Ralf, et al. "Scaling ablation rates for picosecond lasers using burst micromachining." SPIE LASE. International Society for Optics and Photonics, 2010.

[16] Chen, Chien-Yu, et al. "Microstructure and lubricating property of ultrafast laser pulse textured silicon carbide seals." Applied Physics A 107.2 (2012): 345-350.

[17] Kam, D. H., L. Shah, and J. Mazumder. "Femtosecond laser machining of multi-depth microchannel networks onto silicon." Journal of Micromechanics and Microengineering 21.4 (2011): 045027.

[18] Meijer J, Du K, Gillner A, et al. Laser machining by short and ultrashort pulses, state of the art and new opportunities in the age of the photons[J]. CIRP Annals-Manufacturing Technology, 2002, 51(2): 531-550.

[19] GEOFF SHANNON, "comparison the effects of using a micro second with a femtosecond laser", LASER TECHNOLOGY MANAGER,MIYACHI AMERICA

[20] Corbari, Costantino, et al. "Femtosecond versus picosecond laser machining of nano-gratings and micro-channels in silica glass." Optics express 21.4 (2013): 3946-3958.

[21] Cheng J, Liu C, Shang S, et al. A review of ultrafast laser materials micromachining[J]. Optics Laser Technology, 2013, 46: 88-102.

[22] Nolte S, Momma C, Jacobs H, et al. Ablation of metals by ultrashort laser pulses[J]. JOSA B, 1997, 14(10): 2716-2722.

[23] Perez D, Lewis L J. Molecular-dynamics study of ablation of solids under femtosecond laser pulses[J]. Physical review B, 2003, 67(18): 184102.

[24] Cheng C, Xu X. Mechanisms of decomposition of metal during femtosecond laser ablation[J]. Physical Review B, 2005, 72(16): 165415.

[25] Kelly R, Miotello A. Contribution of vaporization and boiling to thermal-spike sputtering by ions or laser pulses. Physical Review E 1999;60:2616–25.

[26] Krüger J, Kautek W, Lenzner M, et al. Structuring of dielectric and metallic materials with ultrashort laser pulses between 20 fs and 3 ps[C]//PROCEEDINGS-SPIE THE INTERNATIONAL SOCIETY FOR OPTICAL ENGINEERING. SPIE INTERNATIONAL SOCIETY FOR OPTICAL, 1997: 40-47.

[27] Tao, Sha, et al. "Thermal modeling and experimental study of infrared nanosecond laser ablation of silicon." Journal of Applied Physics 106.12 (2009): 123507.

[28] Cournoyer, Alain, et al. "Maximizing laser ablation efficiency of silicon through optimization of the temporal pulse shape." SPIE LASE. International Society for Optics and Photonics, 2014.

[29] EL Fissi L, Xhurdebise V, Francis L A. Effects of laser operating parameters on piezoelectric substrates micromachining with picosecond laser[J]. Micromachines, 2014, 6(1): 19-31.

[30] Wee L M, Ng E Y K, Prathama A H, et al. Micro-machining of silicon wafer in air and under water[J]. Optics Laser Technology, 2011, 43(1): 62-71.

[31] Bärsch N, Körber K, Ostendorf A, et al. Ablation and cutting of planar silicon devices using femtosecond laser pulses[J]. Applied Physics A: Materials Science Processing, 2003, 77(2): 237-242.

[32] Otani T, Herbst L, Heglin M, et al. Microdrilling and micromachining with diode-pumped solid-state lasers[J]. Applied Physics A: Materials Science Processing, 2004, 79(4): 1335-1339.

[33] Kam D H, Shah L, Mazumder J. Femtosecond laser machining of multi-depth microchannel networks onto silicon[J]. Journal of Micromechanics and Microengineering, 2011, 21(4): 045027.

[34] Chen C Y, Chung C J, Wu B H, et al. Microstructure and lubricating property of ultra-fast laser pulse textured silicon carbide seals[J]. Applied Physics A: Materials Science Processing, 2012, 107(2): 345-350.

[35] Kim H U, Bedekar V, Islam R A, et al. Laser-machined piezoelectric cantilevers for mechanical energy harvesting[J]. IEEE transactions on ultrasonics, ferroelectrics, and frequency control, 2008, 55(9).

[36] Han, Yukun, et al. "Femtosecond laser-induced silicon surface morphology in water confinement." Microsystem technologies 15.7 (2009): 1045-1049.

[37] Tangwarodomnukun, Viboon, Jun Wang, and Philip Mathew. "A comparison of dry and underwater laser micromachining of silicon substrates." Key Engineering Materials. Vol. 443. Trans Tech Publications, 2010.

[38] Muhammad, Noorhafiza, and Lin Li. "Underwater femtosecond laser micromachining of thin nitinol tubes for medical coronary stent manufacture." Applied Physics A 107.4 (2012): 849-861.

[39] Mak, Giuseppe Y., Edmund Y. Lam, and H. W. Choi. "Liquid-immersion laser micromachining of GaN grown on sapphire." Applied Physics A 102.2 (2011): 441-447.

[40] Pusch, Tim P., et al. "Laser Micromachining of Thin Beams for Silicon MEMS: Optimization of Cutting Parameters Using the Taguchi Method." ASME 2015 International Design Engineering Technical Conferences and Computers and Information in Engineering Conference. American Society of Mechanical Engineers, 2015.

[41] Tada, Kazunari, et al. "Fabrication of high-Q microresonators using femtosecond laser micromachining." IEEE Photonics Technology Letters 25.5 (2013): 430-433.

[42] Ogilvie, I. R. G., et al. "Reduction of surface roughness for optical quality microfluidic devices in PMMA and COC." Journal of Micromechanics and Microengineering 20.6 (2010): 065016.

[43] Mak, Giuseppe Y., Edmund Y. Lam, and H. W. Choi. "Liquid-immersion laser micromachining of GaN grown on sapphire." Applied Physics A 102.2 (2011): 441-447.

[44] Wee, L. M., et al. "Micro-machining of silicon wafer in air and under water." Optics and Laser Technology 43.1 (2011): 62-71.

[45] Das, Alok Kumar, and Partha Saha. "Micromachining of silicon with excimer laser in air and water medium." International Journal of Manufacturing Technology and Management 21.1-2 (2010): 42-53.

[46] Wang X H, Lai P T, Choi H W. Laser micromachining of optical microstructures with inclined sidewall profile[J]. Journal of Vacuum Science Technology B: Microelectronics and Nanometer Structures Processing, Measurement, and Phenomena, 2009, 27(3): 1048-1052.

[47] Armani D K, Kippenberg T J, Spillane S M, et al. Ultra-high-Q toroid microcavity on a chip[J]. Nature, 2003, 421(6926): 925-928.

[48] Dong Y, Zorman C, Molian P. Femtosecond pulsed laser micromachining of single crystalline 3C–SiC structures based on a laser-induced defect-activation process[J]. Journal of Micromechanics and Microengineering, 2003, 13(5): 680.

2

Quantifying Thermal Damage in Piezoelectric Material

Quantifying the Heat Affected Zone in Laser Micro-Machined Piezoelectric Structures

B.Jia* and T.W.A. Blad*, D. Farhadi Machekposhti, P.R. Kuppens and N. Tolou
*Both authors contributed equally

***Abstract*—As a manufacturing method for fast prototyping of MEMS (Mechanical Electro Micro System), laser micro machining with fast pulsed laser source has drawn great attention. Yet the limited thermal damage has not been quantified precisely. A set of piezoelectric material has been processed under different sets of parameters from Taguchi process optimization. And the piezoelectric coefficient was measured for both laser cut and natural broken pieces as the indication of the piezoelectric property loss due to thermal damage, thus the Heat Affected Zone is quantified precisely. The lowest surface roughness of 755 nm was obtained and no obvious piezoelectric property loss was found after one Taguchi iteration. Furthermore, a beam micro-actuator was fabricated based on the optimal laser parameters found in this research.**

***Index Terms*—Vibration energy harvesting, Piezoelectric materials, Heat affected zone, Laser micromachining.**

I. Introduction

PIEZOELECTRIC materials exhibit a coupling between the mechanical and electrical domains which makes them well suited for sensing and actuation. One advantage of piezoelectric transducers is their retained efficiency when miniaturized [1]. On this scale, applications include micro-surgery, micro-positioning stages, wireless sensor networks and micro-energy harvesters. Moreover, piezoelectric materials make excellent candidates for distributed sensing and actuation applications in compliant mechanisms. Research in these fields is often of an experimental nature, which inevitably requires the design and fabrication of numerous prototypes.

Due to their high coupling factors, piezoelectric ceramics are the most commonly used. The brittle properties of the ceramics, however, limit the use of conventional cutting and grinding machining at the small scale. Traditionally, the manufacturing of miniaturized sensors and actuators from piezoelectric material is done with processes such as lithography and chemical vapor deposition. These processes usually have a very long cycle time, making each iteration during prototyping very time consuming. An alternative to these methods may be laser micro-machining, which has the potential to shift the prototyping time scale for miniaturized devices from months to minutes. Therefore, laser micro-machining may allow for rapid prototyping of miniaturized piezoelectric devices.

The material removal of laser micro-machining is achieved by ablation process which is thought to be a combination of main steps: energy absorption, energy transfer and material removal [2]. The chemical connections in the material are directly broken by the absorption of high energy photons which results in the detachment of micro particles [3]. During this process, heat that is generated as a result of ablation is diffused into surrounding material through conduction. This results in a heat affected zone (HAZ) where material properties have been altered.

When laser micro-machining of piezoelectric material is considered, temperatures above the Curie temperature (typically $200 - 400\,^{\circ}\mathrm{C}$ [4]) may be reached in the HAZ. As a result, the piezoelectric properties may be lost locally. When the length scales of the piezoelectric structures are in the order of the HAZ dimensions, the performance of the device may be severely reduced. Especially during the prototyping of miniaturized piezoelectric sensors and actuators this is a problem as it may lead to non-functional devices.

Prior art on the quantification of the dimensions and effects of the HAZ in laser micro-machining of piezoelectric structures is mostly limited to visual inspection of color changes of the material surface [5]–[7]. Reduced performance as a result of laser micro-machining with a $355\,\mathrm{nm}$ YAG laser were reported by Zeng et al. (2004) [8]. It was found that the piezoelectric properties were reduced as a result of the loss of Pb and the existence of a pyrochlore phase. The solution proposed in this paper was the annealing at $1150\,^{\circ}\mathrm{C}$ under PbO-controlled environment for $1\,\mathrm{h}$. Lam et al. (2013) [9] investigated the machining of PMN-PT single crystal with a $355\,\mathrm{nm}$ YAG laser. The main conclusion was that the piezoelectric properties were reduced in an area of about $50\,\mu\mathrm{m}$ from the cutting line. Furthermore, it was shown that a narrower cut can be obtained by using less power per pulse, and a higher amount of repetitions. In Nadig et al. (2013) [10], [11] it was observed that the piezoelectric properties of bulk PZT-5H were lost entirely after laser micromachining with a $355\,\mathrm{nm}$ UV laser. The smallest features in this design were $125\,\mu\mathrm{m}$ with a thickness of $500\,\mu\mathrm{m}$. Another attempt resulted in successful fabrication of these features from PZT-4A, which was presumed to be a result of the higher curie temperature of the material. On the contrary, Kim et al. (2008) reports no significant loss of macroscopic performance after machining features of $500\,\mu\mathrm{m}$ with a $1064\,\mathrm{nm}$ YAG laser. This result was found to be consistent with a previous study [12] where the piezoelectric properties of PZT were found to be unaffected as a result of femtosecond laser-machining (FLM). In that study, however, it was argued that substantial HAZ effects were expected for lasers with pulse durations in the order of nanoseconds.

The objective of this research is to investigate the effects of

the laser parameters on the HAZ in laser micro-machined piezoelectric structures. This will lead to insights that could aid in the development of a novel design guidelines for the laser micro-machining of piezoelectric structures.

Part II will present the designs of the piezoelectric actuator and sensor test pieces and the methods used for the manufacturing. This will include the selection of the laser parameters, selection of the array, cleaning the piezoelectric material and testing the capacitance and d_{33} piezoelectric coefficients. The results of the experimental tests will be presented in chapter III and discussed in chapter IV. Furthermore, the discussion will include an example of how these results can be integrated in a micro-compliant mechanisms with distributed actuation. Lastly, the most important conclusions will be summarized in part V.

II. Method

Laser micromachining processes remove material through the ablation of the target material as a result of the laser energy. Associated with the laser-material interaction is the conduction of heat through the target material. This may result in a *heat affected zone* in which the material properties are altered. When the fabrication of miniaturized piezoelectric sensors or actuators is considered, temperatures above the Curie temperature of the material may be reached. As a result, the piezoelectric properties, and thereby the performance of the device, may be severely reduced. In this research, piezoelectric test structures will be manufactured using a laser micro-machining process to quantify the resulting HAZ. This is illustrated in Fig. 1.

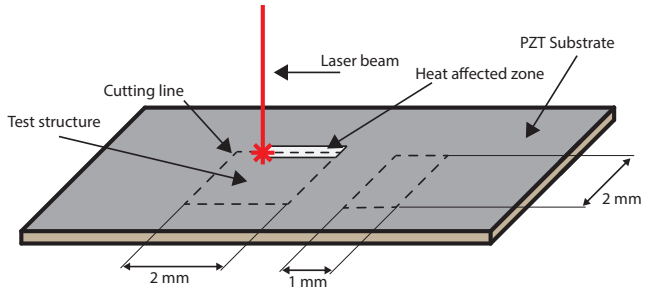

Fig. 1: Laser micro-machining of piezoelectric structures results in a HAZ. This research aims to quantify this HAZ through measurement of piezoelectric properties.

First, laser parameters will be selected using the method of orthogonal arrays. With these parameters, test structures will be manufactured from a plate of piezoelectric material by laser micro-machining. Each test structure will be manufactured individually and numbered. Next, the test structures are cleaned using an ultra-sonic cleaner while immersed in isopropyl alcohol. Finally, the capacitance, piezoelectric strain coefficient and the surface roughness of the side walls are measured. The measured piezoelectric strain coefficients are compared to theoretical values from datasheets to quantify the HAZ. Using these measurements, the effects of the laser parameters on the manufacturing of piezoelectric structures is quantified.

TABLE I: Overview of material and geometrical parameters used in the experiment. The resulting properties of the test structure were calculated using Eq. 1-3.

	Parameter	Symbol	Value
Material	Type		PIC252
	Curie temperature	T_c	$350\,^{\circ}\mathrm{C}$
	Elastic modulus	E	$62\,\mathrm{GPa}$
	Relative permittivity	ϵ_r	1750
	Density	ρ	$7.8\,\mathrm{g\,cm^{-3}}$
Geometry	Length	L	$10\,\mathrm{mm}$
	Width	w	$1\,\mathrm{mm}$
	Thickness	h	$100\,\mu\mathrm{m}$
	Capacitance (square)	C_p	$620\,\mathrm{pF}$
	Capacitance (beam)	C_p	$310\,\mathrm{pF}$

A. Material and geometry

The piezoelectric structures are squares with the dimensions of $2\,\mathrm{mm} \times 2\,\mathrm{mm}$ and beams of $2\,\mathrm{mm} \times 1\,\mathrm{mm}$. The test structures are expected to be sensitive to material degradation in the HAZ due to the small dimensions. The piezoelectric material that will be used are plates of PIC 252 from PI ceramics with a thickness of $t = 100\,\mu\mathrm{m}$. The Curie temperature of this material is $350\,^{\circ}\mathrm{C}$ and the relative permittivity is $\epsilon_r = 1750$ [4]. The expected capacitances, C_p, of the test structures were calculated by the following equation.

$$C_p = \frac{\epsilon_r \epsilon_0 A}{t} \tag{1}$$

Where ϵ_r is the relative dielectric constant, ϵ_0 the permittivity of free space, A the electrode surface area and t the thickness of the piezoelectric material. The results are a capacitance of $620\,\mathrm{pF}$ for the squares and a capacitance of $310\,\mathrm{pF}$ for the beams. The material parameters and geometries are summarized in Table I.

B. Manufacturing procedure

The material is fixed on a ceramic substrate which is fixed by the vacuum extractor from beneath. A gap between substrate and sample is created by adding substrate material of $1\,\mathrm{mm}$ thickness at all edges, in order to prevent the accumulation of thermal energy at the bottom of the sample.

A Spectra-Physics Talon 355-15 diode pumped solid-state (DPSS) UV laser system with a wavelength of 355nm and maximum power of 15 watts at 50 kHz is adapted in this project. The maximum frequency is 500 kHz with pulse width 35ns. A BOFA extractor and filter is integrated in order to exhaust fumes. The laser beam delivery including energy attenuator, mirrors and steering mechanism. The optical steering is achieved by a Galvo head from Rhothor with a scan range of 46x46mm and focal length of 100mm. An overview of the setup is illustrated in Fig. 2.

The X-Y stage has a range of 80mm square with $1\,\mu\mathrm{m}$ effective resolution. The laser beam scanning motion is done by a laser deflection systems based on the Lorentz force motors with internal active optical feedback in order of dramatically reducing sensitivity to external noise. Galvo head had the range of 46x46mm with local length of 100mm, the writing speed is 1300cm per second maximum.

All the test pieces were cleaned by using an ultra-sonic cleaner while immersed in isopropyl Alcohol [13].

C. Laser parameter selection

The three laser parameters that were controlled in this experiment were the diode current, A, laser pulse frequency, f, and the overlap, O. These parameters were selected because the diode current is directly related to laser power, and the pulse width varies depending on the frequency in the configuration of the laser system. The overlap is related to the scanning speed, v, by the following relation.

$$v = f \cdot r \cdot (1 - O) \tag{2}$$

Where r is the spot size of the laser. The method that will be used for the selection of the process parameters is the orthogonal array method, which finds its origin in the Taguchi method [14]–[16]. In this method, *orthogonal arrays* are used to study the relation between process parameters and an objective function. For each process parameter, a finite number of values is selected called the *level settings*. We adapt three variables with three levels for each variable. The combinations of the level settings of different parameters are arranged into orthogonal arrays, which ensure that every pair of parameter levels occurs an equal amount of times. Due to this pair-wise balancing of level settings, the effects of multiple process parameters can be studied simultaneously without distorting the effects of individual process parameters. As a result, the orthogonal array method allows the maximum amount of information to be derived by using the fewest experiments [17].

Initially, the applied energy of each shot was fixed as constant which is the maximum value of the laser, which will decrease the variant output from laser pulses, at the same time the trend between thermal damage and output power is more obvious to be observed. The lower boundary of the range of the controlled parameters was set such a reproducible cut-through would be achieved for every combination. These values were

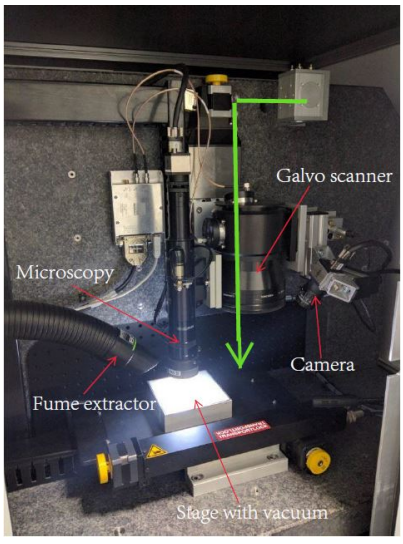

Fig. 2: Laser beam delivery setup

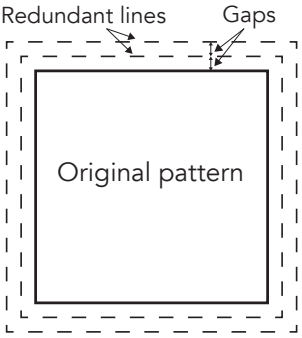

Fig. 3: Schematic representation of redundant lines and separating gaps used in laser micro-machining. These features are added to help the laser move into the workpiece.

empirically determined to be $A = 6\,\mathrm{A}$, $A = 20\,\mathrm{kHz}$ and $A = 70\,\%$. The upper boundary of the range was set at the maximum settings of the machine, which were $A = 7\,\mathrm{A}$, $A = 30\,\mathrm{kHz}$ and $A = 90\,\%$. This range is divided into three levels for every factor.

A second experiment was conducted variant energy pulses which is no long fixed as constant, meaning the pulse energy varies depending on frequency and using a narrower range of the controlled parameters. This will decrease the overall energy applied in order to find the optimal parameter sets in a lower energy regime. Again, the lower boundary was set to $A = 6\,\mathrm{A}$, $A = 15\,\mathrm{kHz}$ and $A = 60\,\%$, such that every experiment would result in cut-through. The upper boundary of the range was set at $A = 7\,\mathrm{A}$, $A = 25\,\mathrm{kHz}$ and $A = 80\,\%$, which was chosen because .

During both experiments, the other parameters were fixed as suggested by prior art [18]. They include the wavelength, pulse width, number of redundant lines and gap size between those lines. Redundant lines are often used in laser micro-machining in order to help the laser beam move into the work piece . In Fig. 3 the redundant lines and gaps are depicted schematically. Here, 3 redundant lines were used with a gap size of $20\,\mu\mathrm{m}$ which was suggested in [19], which corresponds to the laser spot diameter of the laser beam. A complete overview of the level settings for the controlled parameters and the values of the fixed parameters is shown in Table II.

D. Measurement procedure

After cleaning, the capacitance and dielectric loss coefficient of the piezoelectric structures was measured using an Agilent 4263B LCR meter at 1 kHz. The piezoelectric charge constant, d_{33} was measured using a PiezoTest PM300 Berlincourt type d33 meter. The piezoelectric charge coefficient measurements were conducted twice for each test structure. Between the two measurements the sample was flipped such that both a positive and a negative value was obtained for the piezoelectric charge constant.

TABLE II: Overview of parameters used in this research

Symbol	Factor name	Level 1	Level 2	Level 3
A	diode current [A]	6.0	6.5	7.0
B	frequency[KHz]	20	25	30
C	overlap [%]	70	80	90

Symbol	Factor name	Level 1	Level 2	Level 3
A	diode current [A]	6.0	6.5	7.0
B	frequency[KHz]	15	20	25
C	overlap [%]	60	70	80

The surface roughness of the side walls of the samples were measured using a white light interferometer (Bruker Nano Surfaces Division), and was processed by integrated software of (Vision 64). For the measurement, the R_a value is measured over the whole side wall area. This value measures the deviations from the mean of the roughness profile and is corrected for tilt angle. The surface roughness measurements are conducted three times in order to limit random errors.

The surface is considered as non-periodic profile instead of conventional laser manufacturing profile as the result shows surfaces under specific settings are non-periodic where is laser path is no longer obviously existed.

Finally, the samples were inspected using a Scanning Electron Microscope (SEM) from Jeol JSM-6010LA.

E. Data analysis

The controlled parameters were analyzed for each level setting by taking the average of the measured properties of all the test structures manufactured with that particular level setting. This resulted in 9 averages for the surface roughness and the piezoelectric charge constant. The effects of the individual controlled parameters is given by the variance between the three averages for that particular control parameter. For more information on this method we refer the reader to [17] .

TABLE III: Application of the orthogonal array result

Mean value of one parameter level
$A_1 = Set\,(1+2+3)\,/3$
$A_2 = Set\,(4+5+6)\,/3$
$A_3 = Set\,(7+8+9)\,/3$
$f_1 = Set\,(1+4+7)\,/3$
$f_2 = Set\,(2+5+8)\,/3$
$f_3 = Set\,(3+6+9)\,/3$
$O_1 = Set\,(1+6+8)\,/3$
$O_2 = Set\,(2+4+9)\,/3$
$O_3 = Set\,(3+5+7)\,/3$

F. Fabrication of piezoelectric beam micro-actuator

Using the manufacturing procedure described in the previous section and the parameters that were found to result in a minimal heat affected zone, a micro-scale piezoelectric actuator/sensor was fabricated. The device consists of a piezoelectric beam with a length of $5\,\mathrm{mm}$ and a width of $100\,\mu\mathrm{m}$. The electrode layer on the top side of the beam was removed along a $30\,\mu\mathrm{m}$ wide line over the total length of the beam. A section of the design is illustrated in Fig. 4.

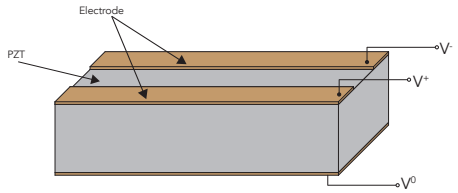

Fig. 4: Schematic indication of the design of an in-plane piezoelectric beam micro-actuator.

By applying a voltage across the terminals, the beam can be used as an in-plane micro-actuator. Alternatively, the device can be used as a sensor by measuring the voltage across the terminals to sense the deflection of the beam. The structure could also be used as a resonance energy harvester which would operate in the natural frequency of the beam, ω, that can be estimated by the following equation [20].

$$\omega = 2\pi f = \sqrt{\frac{k}{\frac{33}{140}m}}, \tag{3}$$

In this formula, m is the mass of the test structure and k is the stiffness which can be approximated by linear beam theory.

$$k = \frac{3EI}{L^3} = \frac{Ewt^3}{4L^3}, \tag{4}$$

Where E is the elastic modulus of the material, I is the moment of inertia, and L, w, t are the length, width and thickness, respectively. For the proposed beams, a mass of $m = 0.39\,\mathrm{mg}$ and a stiffness of $k = 12.4\,\mathrm{N\,m^{-1}}$ were estimated. As a result, the resonance frequency of the beam was estimated to be $5.64\,\mathrm{kHz}$.

III. Results

The results are listed in Table IV.

As can be seen in the table the smoothest surface had a value of $R_a = .755\mu\mathrm{m}$ and was obtained by parameters of set 4. And based on the parameters of set 4, a micro-beams were successfully manufactured and illustrated in Fig. 5a. The resulting beam had a tapered shape, where the width of the top side was measured at $79\,\mu\mathrm{m}$ and the bottom side at $109\,\mu\mathrm{m}$. As shown in Fig5a the two sides of the beam are covered with different types of electrode materials. And the yellow side (left) of the beam, the electrode surface is separated by a line of laser engraving which was tested by a resistance measurement.

TABLE IV: Results of the measurements and orthogonal array method. Surface roughness measurements of a) experiment 1 and b) experiment 2, electrical properties of the test pieces from c) experiment 1 d) experiment 2, mean value of per parameter of surface roughness

(a) surface roughness of experiment 1

Set number	A	B	C	Power (W)	2x1mm	2x2mm	Average (µm)
1	1	1	1	4.434	4.24	3.918	4.176
2	1	2	2	3.405	5.23	4.459	3.932
3	1	3	3	4.718	6.44	5.242	4.980
4	2	1	2	3.589	4.02	3.424	3.506
5	2	2	3	6.690	6.29	3.620	5.155
6	2	3	1	6.230	3.24	2.966	4.598
7	3	1	3	4.436	5.57	4.142	4.289
8	3	2	1	7.549	6.61	6.310	6.929
9	3	3	2	6.052	8.06	8.327	7.189

(b) rusface roughness of experiment 2

Set number	A	B	C	2x1mm	Power	2x2mm	Average (µm)
1	1	1	1	0.910	1.12	0.840	0.875
2	1	2	2	1.633	1.24	1.143	1.388
3	1	3	3	0.864	2.25	0.877	0.870
4	2	1	2	0.759	1.35	0.751	0.755
5	2	2	3	0.885	1.73	0.939	0.912
6	2	3	1	0.659	2.42	0.860	0.759
7	3	1	3	0.796	1.60	1.172	0.984
8	3	2	1	0.828	1.96	1.293	1.060
9	3	3	2	1.254	2.88	1.127	1.190

(c) Electrical properties of experiment 1

Identification	Dimensions	Capacitance	δ coefficient	d_{33} value
1	2 x 2 mm	510 pF	0.0213	172 pC N^{-1}
2	2 x 2 mm	520 pF	0.0213	176 pC N^{-1}
3	2 x 2 mm	544 pF	0.0353	150 pC N^{-1}
4	2 x 2 mm	512 pF	0.0217	166 pC N^{-1}
5	2 x 2 mm	501 pF	0.0283	153 pC N^{-1}
6	2 x 2 mm	497 pF	0.0300	131 pC N^{-1}
7	2 x 2 mm	523 pF	0.0315	162 pC N^{-1}
8	2 x 2 mm	502 pF	0.0215	143 pC N^{-1}
9	2 x 2 mm	487 pF	0.0319	132 pC N^{-1}
1	1 x 2 mm	265 pF	0.0242	161 pC N^{-1}
2	1 x 2 mm	254 pF	0.0272	111 pC N^{-1}
3	1 x 2 mm	232 pF	0.0386	102 pC N^{-1}
4	1 x 2 mm	240 pF	0.0223	114 pC N^{-1}
5	1 x 2 mm	220 pF	0.0346	40 pC N^{-1}
6	1 x 2 mm	217 pF	0.0264	52 pC N^{-1}
7	1 x 2 mm	242 pF	0.0249	111 pC N^{-1}
8	1 x 2 mm	237 pF	0.0250	85 pC N^{-1}
9	1 x 2 mm	217 pF	0.0344	19 pC N^{-1}

(d) Electrical properties of experiment 2

I.d.	Dimensions	Capacitance	Positive d_{33} value	Negative d_{33} value
1	2 x 2 mm	497 pF	180 pC N^{-1}	−163 pC N^{-1}
2	2 x 2 mm	500 pF	170 pC N^{-1}	−170 pC N^{-1}
3	2 x 2 mm	498 pF	168 pC N^{-1}	−170 pC N^{-1}
4	2 x 2 mm	491 pF	185 pC N^{-1}	−162 pC N^{-1}
5	2 x 2 mm	504 pF	170 pC N^{-1}	−161 pC N^{-1}
6	2 x 2 mm	497 pF	156 pC N^{-1}	−175 pC N^{-1}
7	2 x 2 mm	514 pF	152 pC N^{-1}	−151 pC N^{-1}
8	2 x 2 mm	502 pF	175 pC N^{-1}	−174 pC N^{-1}
9	2 x 2 mm	514 pF	164 pC N^{-1}	−167 pC N^{-1}
1	1 x 2 mm	250 pF	136 pC N^{-1}	−123 pC N^{-1}
2	1 x 2 mm	257 pF	119 pC N^{-1}	−166 pC N^{-1}
3	1 x 2 mm	249 pF	140 pC N^{-1}	−142 pC N^{-1}
4	1 x 2 mm	255 pF	117 pC N^{-1}	−124 pC N^{-1}
5	1 x 2 mm	243 pF	158 pC N^{-1}	−135 pC N^{-1}
6	1 x 2 mm	252 pF	146 pC N^{-1}	−122 pC N^{-1}
7	1 x 2 mm	250 pF	128 pC N^{-1}	−105 pC N^{-1}
8	1 x 2 mm	254 pF	111 pC N^{-1}	−121 pC N^{-1}
9	1 x 2 mm	248 pF	159 pC N^{-1}	−133 pC N^{-1}
Ref.1	-	548 pF	155 pC N^{-1}	−160 pC N^{-1}
Ref.2	-	595 pF	149 pC N^{-1}	−165 pC N^{-1}
Ref.3	-	891 pF	162 pC N^{-1}	−178 pC N^{-1}

(e) Mean value of surface roughness of experiment 1

Per parameter level	Roughness (µm)	Ra(Max)-Ra(Min)
A_1	4.362	
A_2	4.419	1.773
A_3	6.135	
f_1	3.990	
f_2	5.338	1.599
f_3	5.589	
O_1	5.234	
O_2	4.875	0.423
O_3	4.811	

(f) Mean balue of surface roughness of experiment 2

Per parameter level	Roughness µm	Ra(Max)-Ra(Min)
A_1	1.044	
A_2	0.809	0.269
A_3	1.078	
f_1	0.871	
f_2	1.120	0.249
f_3	0.940	
O_1	0.898	
O_2	1.068	0.170
O_3	0.922	

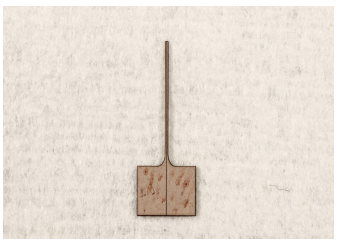

(a) Beam with seperated electrode

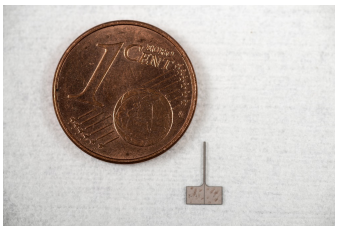

(b) A one euro coin beside as a reference

Fig. 5: Resulting micro-beam with electrode removed in the centre along the length; manufactured with the laser parameters from set 4

IV. Discussion

A. Surface roughness

The findings of best surface roughness is found under parameters of set 4, and the worst is at set 2. The SEM images in Fig 6 provide a visual comparison between these surface qualities. In a) there is material irregularly accumulated at the bottom of the work piece while the rest part of the cross section area show smooth and clean cut. However in b) the cut shape is straight and uniform along all the cross section area. A potential explanation of this phenomenon is the interaction between substrate material and pzt ceramic. The ablation threshold of substrate material is higher than the fluence of set 4 while lower than the fluence of set 2, which huge amount of heat is accumulated at the bottom for set 4 and created melted material while in set 2 laser directly cut through the whole pzt material

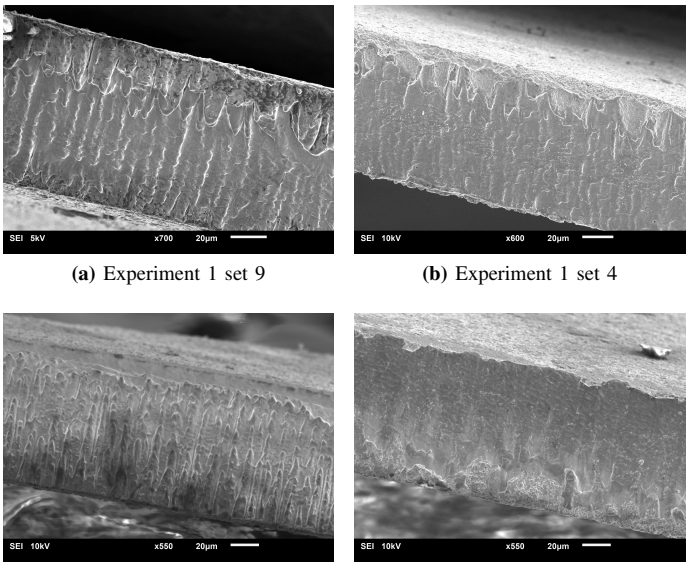

(a) Experiment 1 set 9 **(b)** Experiment 1 set 4

(c) Experiment 2 set 9 **(d)** Experiment 2 set 4

Fig. 6: SEM photage of side wall view for best and worst surface.

and into substrate material. Further experiment with variety of substrate materials can be conducted to further testify this reasoning.
It can be seen from the SEM images6 that the right image is obviously more clear and clean compared to the left figure, the laser foot path is less presented in the cross section area. From table IV e and f, it can be concluded from the results of experiment 1 that amongst the three controlled variables, the diode current (A) has the most severe effect on both the surface roughness and the piezoelectric coefficient loss. While the overlap has the least influence on the surface roughness.Furthermore, both sets of Taguchi optimization loops indicated the same trend in optimal setting, despite of the different levels of pulse energy.

B. HAZ

Generally, the HAZ is strictly related to the the amount of energy applied, specifically the energy introduced into per unit area material also known as fluence. From TabIV c, we can firstly conclude that the clear existence of thermal damage, because of the differences in d_33 value of samples with different sizes under the same settings. Secondly, we can observe the clear trend of more piezoelectric property loss with more output power applied. However, the surface roughness is non-linearly affected by multiple factors of the process. The experiment prove can be found in measurements results. The set of minimum HAZ is not necessarily the same as the set with the smoothest surface. which means the optimal settings varies base on different criteria.

As the reference, there are also three sets of un-cut samples measured during the experiential. However, the results showed measured value is far lower than the theocratic value. This could be leaded by either limited accuracy of the piezo-measurement set-up, or the poor fabrication quality of the material. Yet this offset does not affect the outcome overall trend obtained in this research.

It is needed to notice that for experiment sets with low energy applied, the d_{33} values are accidentally higher than the reference un-cut value, this could be leaded by the random error of measurement equipment. It could also be the instant temperature at the laser spot is near sintered temperature of PZT material while the laser beam acts as electromagnetic wave which change the piezoelectric coefficient of the samples [21], [22].

C. Methods

In a full set of typical Taguchi optimization, an outer ray is expected to be chosen, which is normally noise factors. However, for this particular project, noise factors are believed not controllable, nor cheap to control in other words.Thus there is no outer ray selected. Because noise factors are factors such as weather environment and humidity, which could be investigated by adding an outer array in further research.
Gas or water assistance are also considered not applicable in this research, but could be interesting in the further studies to eliminate the thermal damage.

V. Conclusion

In this research the influences by parameters of diode current, pulse frequency, overlap, along with the surface roughness and heat affected zone were investigated during the laser micro-machining of PZT material. The heat affected zone was quantified by comparing the measured values for the $d_3 3$ coefficient to the theoretically predicted results. As shown in this study, the piezoelectric property of laser machined test structures can be reserved tremendously to $99\,\%$ by using the optimized machining settings. And the by applying higher energy, the more piezoelectric property lost.
Side wall surface roughness can be significantly improved to reach $759\,\mathrm{nm}$. While the setting for minimum HAZ is not subject to the setting for best surface roughness. Furthermore, it was demonstrated that a piezoelectric beam micro-actuator can be fabricated using the optimized machining settings.

References

[1] Takeshi Morita. Miniature piezoelectric motors. *Sensors and Actuators A: Physical*, 103(3):291–300, 2003.
[2] S Karatodorov and M Grozeva. The effect of process parameters in femtosecond laser micromachining. *Bulg. J. Phys*, 43:110–120, 2016.
[3] Claas Willem Visser. *Fundamentals and applications of fast micro-drop impact*. Universiteit Twente, 2014.
[4] Physik Instrumente. *Piezoelectric Ceramic Products*, 2016.
[5] Dirk Herzog, Peter Jaeschke, Oliver Meier, and Heinz Haferkamp. Investigations on the thermal effect caused by laser cutting with respect to static strength of cfrp. *International journal of machine tools and manufacture*, 48(12):1464–1473, 2008.
[6] Viboon Tangwarodomnukun, Jun Wang, and Philip Mathew. A comparison of dry and underwater laser micromachining of silicon substrates. In *Key Engineering Materials*, volume 443, pages 693–698. Trans Tech Publ, 2010.
[7] V Tangwarodomnukun, J Wang, CZ Huang, and HT Zhu. An investigation of hybrid laser–waterjet ablation of silicon substrates. *International Journal of Machine Tools and Manufacture*, 56:39–49, 2012.

[8] DW Zeng, K Li, KC Yung, HLW Chan, CL Choy, and CS Xie. Uv laser micromachining of piezoelectric ceramic using a pulsed nd: Yag laser. *Applied Physics A: Materials Science & Processing*, 78(3):415–421, 2004.

[9] KH Lam, Y Chen, K Au, J Chen, JY Dai, and HS Luo. Kerf profile and piezoresponse study of the laser micro-machined pmn-pt single crystal using 355nm nd: Yag. *Materials Research Bulletin*, 48(9):3420–3423, 2013.

[10] Sachin Nadig, Serhan Ardanuc, and Amit Lal. Planar laser-micro machined bulk pzt bimorph for in-plane actuation. In *Applications of Ferroelectric and Workshop on the Piezoresponse Force Microscopy (ISAF/PFM), 2013 IEEE International Symposium on the*, pages 152–155. IEEE, 2013.

[11] Sachin Nadig, Serhan Ardanuç, and Amit Lal. Monolithic 2-axis in-plane pzt lateral bimorph energy harvester with differential output. In *Micro Electro Mechanical Systems (MEMS), 2015 28th IEEE International Conference on*, pages 1129–1132. IEEE, 2015.

[12] Nitin Uppal, PANOS S SHIAKOLAS, and Shashank Priya. Micromachining of pzt using ultrafast femtosecond laser. *Ferroelectric Letters*, 32(3-4):67–77, 2005.

[13] Lal A Nadig S, Ardanuc S. Planar laser-micro machined bulk pzt bimorph for in-plane actuation[c]//applications of ferroelectric and workshop on the piezoresponse force microscopy (isaf/pfm). *IEEE International symposium on the.*, 2013.

[14] Kirby E D. Zhang J Z, Chen J C. Surface roughness optimization in an end-milling operation using the taguchi design method[j]. *Journal of Materials Processing Technology*, 2007.

[15] Taguchi G. System of experimental design: engineering methods to optimize quality and minimize costs[m]. *UNIPUB/Kraus International Publications*, 1987.

[16] J. Li and G. Ananthasuresh. A quality study on the excimer laser micromachining of electro-thermal-compliant micro devices. *J. Micromech. Microeng*, 2001.

[17] Jun Li and GK Ananthasuresh. A quality study on the excimer laser micromachining of electro-thermal-compliant micro devices. *Journal of Micromechanics and microengineering*, 11(1):38, 2001.

[18] M DAuria and N Tolou. Uv-laser cutting for silicon mems prototyping: Improving etching rate and quality. In *Proceedings of the 14th euspen International Conference, Dubrovnik, Croatia*, 2014.

[19] N. Tolou M.D'Auria. Uv-laser cutting for silicon mems prototyping: Improving etching rate and quality. In *proceedings of the 14th euspen internation conference*, 2014.

[20] Alper Erturk and Daniel J Inman. *Piezoelectric energy harvesting*. John Wiley & Sons, 2011.

[21] Donny Wang, Yevgeniy Fotinich, and Greg P Carman. Influence of temperature on the electromechanical and fatigue behavior of piezoelectric ceramics. *Journal of applied physics*, 83(10):5342–5350, 1998.

[22] Matthew W Hooker. Properties of pzt-based piezoelectric ceramics between-150 and 250 c. 1998.

3

Laser Micro-machined Silicon Compliant Mechanism Devices

Structural and Mechanical Evaluation of Laser Micromachining Fabricated Compliant Mechanism Structures

B. Jia, P. R. Kuppens, and N. Tolou

Precision and Microsystems Engineering, Technology University of Delft, the Netherlands

***Abstract*—Along with the vast development of micro compliant mechanism (CM), prototyping of such devices in a micro scale has drawn huge interest in this field. Laser micro machining is considered as a potentially alternative method for prototyping which has advantages as fast manufacturing and accessible cost. However, main challenges such as low side wall surface roughness and Heat Affected Zone (HAZ) are still restraining development of this technique. In this paper, we investigated performance of laser micro machined CM devices in structural and mechanical properties. A Finite Element Analysis (FEA) model is used as an inter media to compare laser micromachining with lithography, since the direct relationship is not possible to build up due to different intrinsic natures. This FEA is verified by (Deep Reactive Ion Etching) DRIE made devices. Then a set of compliant mechanism devices have been designed, simulated, fabricated and tested. surface roughness, taper angle and stiffness of laser micro-machined silicon structures have been obtained.**

***Index Terms*—Laser Micromachining, Compliant Mechanism, Heat affected zone, prototyping.**

I. Introduction

Traditional rigid body mechanisms are becoming less attractive in fields of precision engineering or energy harvesting because high performance are expensive. For Micro Electro-Mechanics System (MEMS), miniaturization is a big obstacle and hygiene is a great issue in medical or space environment [1]. While Compliant Mechanisms (CM, also known as flexure mechanisms) can be a perfect alternative since its intrinsic advantages, there is no lubrication or wear needed, elimination of backlash and friction, and less assembly parts.

Manufacturing CM devices in micro scale is conventionally by means of lithography. Lithography is not only a time-consuming and expensive process, especially for thick materials [2], but also requires experts with sufficient experience [3].
The high throughput and parallel handling has made the price of single device of mass production become relatively affordable. However, for prototyping of new concepts, lithography is normally not easily accessible and very expensive for small amounts of devices. Therefore prototyping of new product has been an obstacle for researchers [5].

To achieve fast prototyping, ultra fast laser micromachining has been introduced as an alternative for prototyping, it has high accuracy for micro devices along with negligible thermal damage [6]. In this method, femtosecond to nanosecond laser pulses are generated. The shorter pulse width brings extremely high peak power and power intensity while maintaining ordinary output power. The mechanism of material removal changes when the time scales down to a tiny fraction of second. Compared to lithography, this method is explicitly faster, relatively simple, without contact, no need for mask and effective [7].
This technique has been developed for several decades [8], however current researches are mainly focused on groove cutting [9], [10] and micro drilling [11], [12] on semiconductor and piezoelectric materials [13], [14]. A fully functional CM device fabricated by laser micro machining has not been found in literature. Because several factors are still limiting this technique, such as low surface roughness at side wall, thermal damage introduced micro cracking, minimum feature size and taper angle [22].A prior study that a lateral resonator has been cut a with femtosecond laser [15], but the mechanical performance has neither been examined, nor with a high cross sectional aspect ratio which is interested for CM. Furthermore, the direct relation between surface roughness along with thermal damage and mechanical performance of micro CM has not been verified.

The present paper evaluates cutting quality structurally by side wall surface roughness, and mechanically by deformation behaviour of CM structures. In part II, Research method and Finite Element Model (FEM) are introduced in part A and B, equipment of the experiment, parameter selection and measurement are introduced following. Then result and discussion are presented in part II and IV.

II. Method

A. CM devices

Lase micro machined structures inevitably have the trapezoid shaped cross section area due to the curvature of focal path, which is refereed as taper angle. Additional, the minimum feature size and side wall roughness are difficult to achieve at the same level as lithography. Therefore, the direct comparison between laser micromachining and lithography is not possible. Therefore we introduce FEM as an intermediary to link two methods together. The offsets in stiffness between FEM model and two fabrication methods, laser micro machining and DRIE (Deep Reactive Iron Etch), are quantified and compared. The difference between FEM model and DRIE is in order to verify the accuracy of FEM. While for laser micromachining, FEM is used as an indication of weak performance introduced by

thermal damage and low surface roughness. A flowchart of constructing the comparison is shown in Fig1.

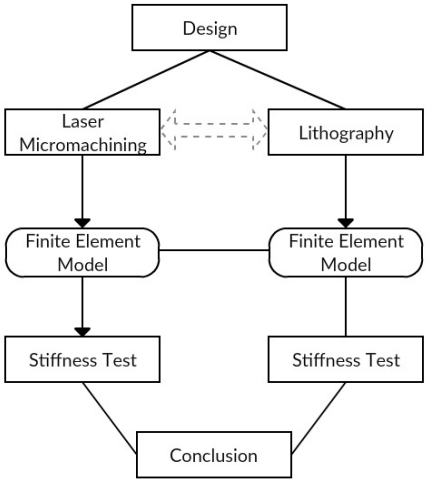

Fig. 1: Flow chart of the comparison approach

For simplicity, a fundamental building block in CM design, which is a compliant stage fixed by two parallel flexure has been designed as can be seen in Fig2. Two flexure fixed at two ends of the centre mass, only horizontal translational movement is achieved while rest of degrees of freedom (DOF) are constrained for a small range of deflection. The widths of flexure is normally where the minimum feature sizes are, $20\,\mu\mathrm{m}$ for DRIE and $30\,\mu\mathrm{m}$ for laser micromachining. It is needed to mentioned that the thin beam width of laser cut flexure is fixed to $70\,\mu\mathrm{m}$ due to the high aspect ratio (>10) and larger taper angle, and for better experiment repeatability.

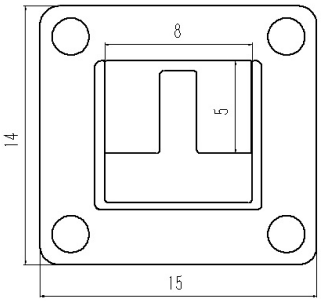

Fig. 2: Illustration of design of CM device

B. FEM model

A Finite Element Model in *ANASYS APDL* has been developed to model mechanical behaviour for DRIE devices, and several simplification has been applied. 4 Degrees of Freedom (DOF) have been fixed except for the horizontal translational and vertical deflection, the parasitic displacement in vertical direction is negligible because the displacement regime is small; the middle body part is treated as totally rigid connection (mass) and the two beams are meshed using element *beam 188* . This beam module is generally used for analysing slender to moderately thick beam structure, and it is based on Timoshenko Beam Theory which includes shear-deformation effects.

Furthermore, careful treatment of cross section area shape has been applied for each model since the laser micro machining has unique taper angle profile along cutting edge, which can be seen in Fig3 where the cross sectional information of flexure are included. And as discussed in [17], the Young's Modulus is adapted as 130GPa which take orientation of devices into account since the anisotropic property on (100) silicon wafer.

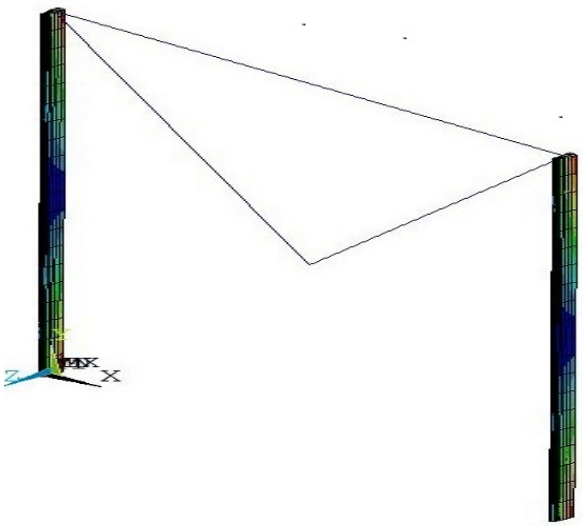

Fig. 3: Illustration of FEM model

Next, the experimental result has verified this simulation model for the same design and dimension of the flexure device. The verification device is fabricated by DRIE which is the most common technique for micro CM prototyping. The stiffness obtained by the same measurement and condition of DRIE made device can be seen below in Fig4. The measurement result fits the stiffness behaviour of simulated model, which verifies the simulation model.

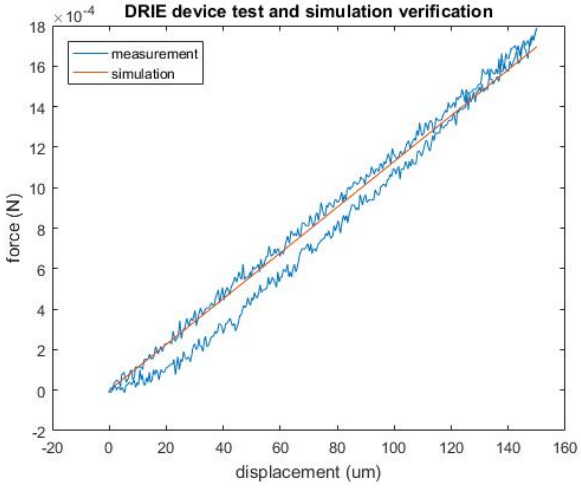

Fig. 4: Test verification of FEM model

Devices are made under different parameter sets, each beam width is determined under Scanning Electron Microscope (SEM). Three data point where at two ends and middle point of beam were measured, and four measurement at each point were carried out. Then the obtained width of beams are used as input for building specific FEM model for every parameter set.

C. Laser system

Devices are fabricated by a Spectra-Physics Talon 355-15 diode pumped solid-state (DPSS) UV laser system with a wavelength of 355nm and maximum power of 15 watts at 50 kHz. The maximum frequency is 500 kHz with pulse width 35ns. A BOFA extractor and filter is integrated in order to exhaust fumes. The laser beam delivery including energy attenuator, mirrors and steering mechanism. The optical steering is achieved by a Galvo head from Rhothor with a scan range of 46x46mm and focal length of 100mm. An overview of the setup is illustrated in Fig. 5.

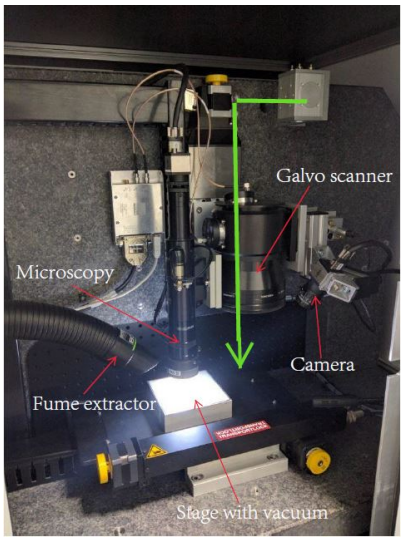

Fig. 5: Laser beam delivery setup

The X-Y stage has a range of 80mm square with $1\,\mu\mathrm{m}$ effective resolution. The laser beam scanning motion is done by a laser deflection systems based on the Lorentz force motors with internal active optical feedback in order of dramatically reducing sensitivity to external noise. Galvo head has the range of 46x46mm with local length of 100mm, the writing speed is $1300\,\mathrm{mm/s}$ maximum. The material is fixed on a Alumina ceramic substrate which is fixed by the vacuum extractor from beneath.

D. Laser parameter selection

In the field of fast-pulsed laser micromachining, ablation behaviour varies with different types of laser and material. Material removal principle changes when the pulses shorten down to pico second regime,because the electron relaxation time is generally around picosecond [18] which is normally recognized as 'ultra-fast' laser. Here we only consider fast-pulsed laser micromachining (nano second pulsed duration) for silicon wafer processing.

Generally parameters are divided into two categories, laser settings as pulse frequency, output power and overlap, and process settings as repetition times, re-focus level and redundant patterns. Pulse frequency is the frequency of laser pulses which is also called 'repetition rate' in literature. Output power is the energy carried by laser beam, while the energy per pulse is also considered. The overlap is dependent on pulse frequencies and moving speed, which is fixed to 90% since the prior art [19] suggests that the higher overlap helps obtaining relatively lower surface roughness.
For improving the cutting quality while the focal point moving inward to the material, re-focus after certain depth is necessary to avoid out of focus. Ideally the number of laser is refocused (levels) and step size of focal point shift down should be based on the ablation depth of laser. Redundant lines added to help the rear part of laser beam can move inward to materiel since the laser beam is not a perfect cylinder, moreover added redundant lines help dissipation of accumulated heat. An illustration of redundant line is shown in Fig6.

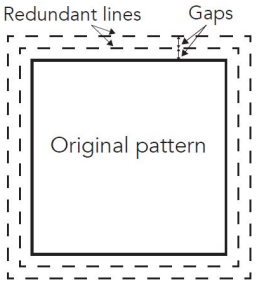

Fig. 6: Laser beam delivery setup

On one hand, the Taguchi method has been applied laser setting optimization of silicon cutting for minimum taper angle and surface roughness in [20] with a identical laser set-up. On the other hand, process parameters optimization was carried out for minimum surface roughens and shorter machining time in [19] under the same equipment. Therefore, with both laser and process parameters found in literature for optimal structural properties, a selection of parameters is chosen for further investigation of mechanical property which can be seen below in table I and II. All combinations of settings have been verified that can ensure a smooth cut-through performance and clear releasing of samples.

Based on the chosen parameters shown above, trenches with single laser path of three frequencies are carried out, in order to examine the ablation rate and behaviour or material removal performance. All samples are cleaned with 5 minutes of ultrasonic cleaning in Isopropanol Alcohol (IPA).
The relationship of frequencies and trench shapes are presented in Fig 7. Trenches show U-shape for lower pulse energy at 10 and 15KHz, while it is more likely V-shape for high energy at 20KHz. This phenomenon matches the prior study in similar

TABLE I: Overview of laser parameters

Set	Frequency (KHz)	Power (W)	Speed (mm/s)	Energy (uJ/pulse)
1	10	1.8	10	180
2	15	3.0	15	200
3	20	5.1	20	255

TABLE II: Overview of process parameters

Parameter	Lines	Gap	Levels	step	wafer thickness
Value	3	15 µm	11	30 µm	300 µm

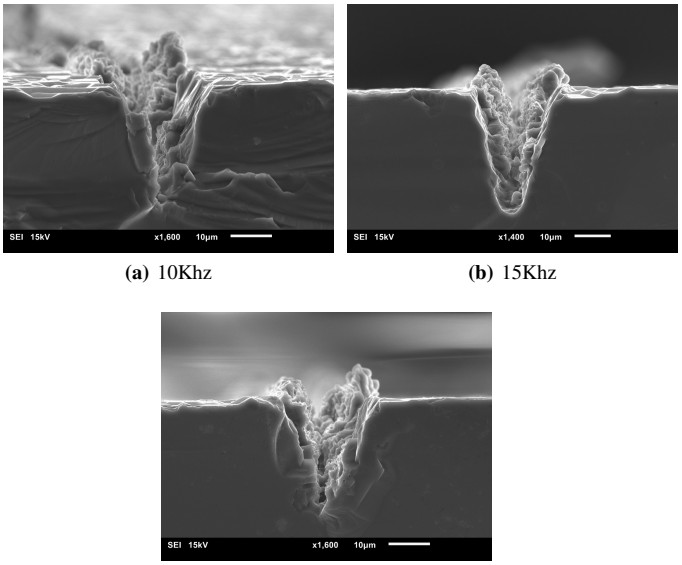

(a) 10Khz **(b)** 15Khz

(c) 20Khz

Fig. 7: Cross sectional views of trenches on silicon from under different sets of laser parameters

laser micromachining for piezoelectric substrates [21]. It was found that lower pulse energy with lower scanning speed results more evenly ablation, and high energy pulse with high scanning speed has V-shape ablation trench since the central region is ablated earlier than the adjacent region. This phenomenon is more dominantly affected by scanning speed, which is pre-determined according to the frequencies to ensure high overlap.

All of three parameter sets can effectively grave the silicon substrate with an ablation depth roughly of 30 µm, which at the same time proves the selection of process parameters are effective and efficient. However, the debris and recast material on the cutting surface indicate that further cleaning method is necessary.

E. Cleaning

cleaning methods are crucial for this project, since both structural properties as side wall surface and beam width and mechanical properties as stiffness and strength are affected by the debris accumulated around the cutting edge. A set of SEM of the debris is in Fig8. Some of the prior study generally used ultra-sonic cleaning and IPA resin for simple structures as grooves and holes, while others combine HF (Hydro Florid) etching in order to remove silicon-dioxide. Here for the identical cutting setting, different cleaning resulting in stiffness curves can be seen in Fig8c. VHF (Vapour Hydro Florid) method is not commonly used in laser micro machining therefore the cleaning setting is not well developed. More remaining debris on the beam, resulting in high stiffness. While KOH etching seems thoroughly cleaned silicon dioxide however silicon structure were attacked as well, therefore thinner beam width show dramatically lower stiffness.
Overall, a cleaning method that can effectively remove the debris while keep the silicon structure intact is needed, which is direct HF immersing for author's aware, However, the compromise of clean room access has to be made which slows the whole prototyping speed.

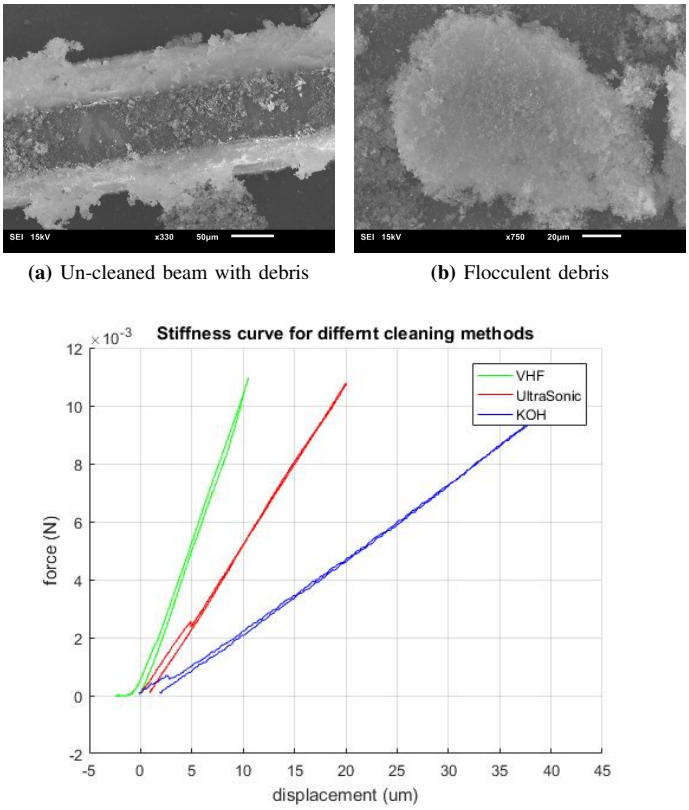

(a) Un-cleaned beam with debris **(b)** Flocculent debris

(c) Stiffness profile under different cleaning methods

Fig. 8: (a,b)SEM photages of debris without cleaning (c)stiffness curves of cleaning methods

The debris composition has been determined by Energy-dispersive X-ray spectroscopy (EDS), and the result shows the main contamination is silicon dioxide. In addition, since the complex and delicate structures in this project are not able to survive through the harsh ultra-sonic vibration, a suspended ultrasonic shake system is adopted which ensure the vibration waves only delivered by liquid.

F. Surface roughness determination

The surface roughness of the side walls of the samples were measured using a white light interferometer (Bruker Nano Surfaces Division), and was processed by integrated software

of (Vision 64). For the measurement, the roughness value is measured over the whole side wall area. This value measures the deviations from the root mean square of the roughness (R_a) and is corrected for tilt angle. The surface roughness measurements are conducted 3 times in order to limit random errors.
The surface is considered as non-periodic profile in contrast of conventional laser manufacturing, since the periodic profile (path shape of laser beam) on the surfaces under specific settings are no longer obviously existed. At the end, the samples were observed and the using a Scanning Electron Microscope (SEM) from Jeol JSM-6010LA as an optical inspection.

G. Stiffness measurement

The force-displacement test set-up consists of a force sensor and a translational stage properly. The force sensor is FT-S100000 from *Femto Tools* with the maximum range of 10 gram force (10mN) and resolution of 0.05mg, and it is mounted with an angle of 30 degree to horizontal plane. Certain pre-described displacement are applied by the translational stage, and the reaction force is obtained by force sensor. An illustration can be seen below in Fig9

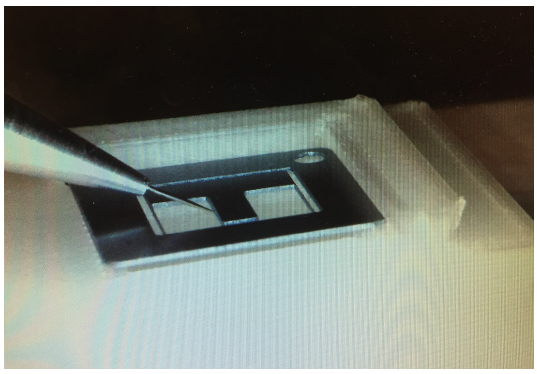

Fig. 9: The illustration of test set-up

III. Result

A. Structural measurement

In order to simulate the behaviour of laser micro-machined CM devices, the basic geometry of device should be determined as the input of FEM model. The rest of the body is built as totally rigid body, but only the thin beams where the deformation appeared, also where is carefully treated and modelled under different laser setting. Therefore, the beam geometries are measured and result can bee seen in TableIII. To be noticed that since the laser machined surface is relatively rough, resulting the irregularity existed, therefore the deviation of each beam is recorded as well.

TABLE III: Beam width measurement

Set	Top (µm)	Bottom (µm)	Mean (µm)	Deviation
1	36.001	116.061	76.031	4.1%
2	32.112	114.532	73.322	6.5%
3	28.085	112.950	70.518	6.2%

Surface roughness (Ra) is also measured and can be seen under table IV as an indication of how smooth the laser cut surfaces are. As a referenced value, the values of DRIE manufactured device also recorded. The 15 KHz frequency laser setting has the lowest Ra among the laser machined while is indeed relatively high compared to the DRIE device. Since all the process parameters are fixed, the taper angle varies in a limited range due to the taper angle is most sensitive to the number of redundant lines, however, it is a trade-off between better releasing of device with delicate beams and smaller taper angle.

TABLE IV: Structural properties

	1	2	3	DRIE
Ra	0.905 µm	0.802 µm	1.103 µm	0.173 µm
Taper	15.19°	15.66°	15.94°	0.46°

The surface profile obtained by white light interferometer can be seen below in Fig10. The side wall of the laser machined is relatively rough and the wave-like shape caused by the laser path column is observed at the left. And in DRIE devices, the marks along the side wall can be observed due to the etching process is done layer by layer inward to the silicon, especially at the top and bottom.

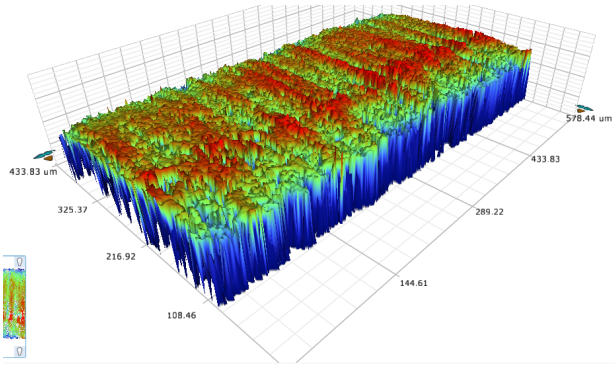

(a) Set 2

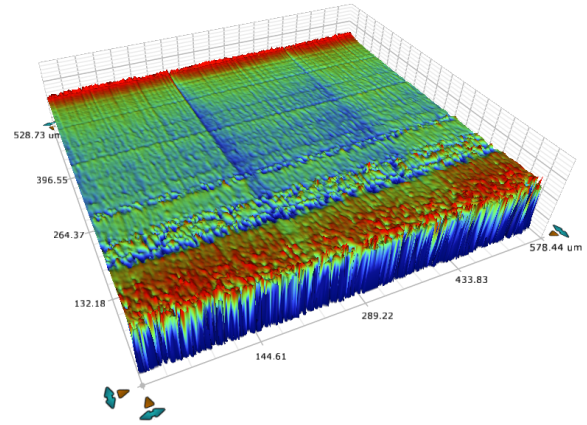

(b) DRIE device

Fig. 10: Surface profile of laser machining and DRIE by White Light Interferometer

B. Mechanical measurement

The stiffness measurement result is presented in the Fig11. The dashed lines represent the values of simulation and the solid is from measurement. The offset percentage for set 1,2 and 3 are 65%, 64% and 84% respectively. Here the offset between simulation and measurement is large, since the comparison between simulation and measurement is intended to be an indirect comparison of two different manufacturing methods, instead of the conventional idea of proof of design in reality scenario.

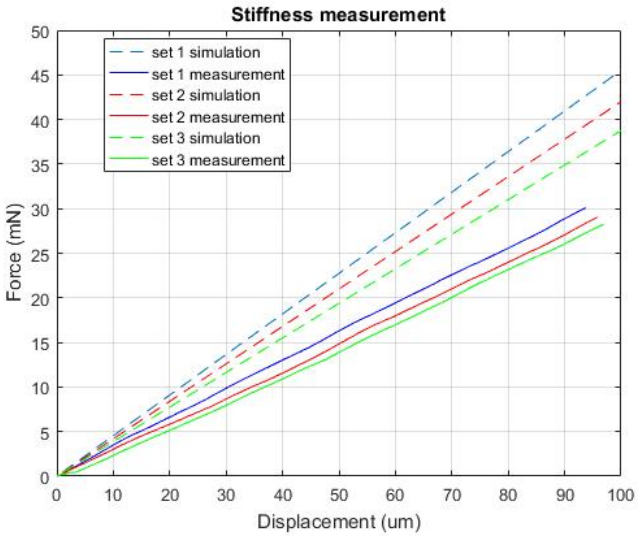

Fig. 11: Stiffness profile of laser micro-machined flexure

IV. Discussion

A. Beam width deviation and stiffness measurement

All devices with different parameter sets are designed with the same geometry. Yet because the higher frequency carrying more energy onto the unit area resulting more material removal, therefore the beam width of set 3 is thinner than the set 1.
The beam widths under 20KHz frequency laser set (set 3) has higher deviation in the beam width, however the beams are also relatively thinner which makes the variance in beam width takes bigger portion of the whole. Furthermore, the deviation of the beam width will propagate further in the stiffness, however, the offset in stiffness between measurement from laser micro machined devices and simulation is larger than this deviation. Therefore, this offset in stiffness profile is believed to be from the thermal damage solely of the laser.

B. Stiffness

Since the laser source we adapted in this project has pulse duration in nano second regime, the thermal damage still takes large part of ablation behaviour. The micro cracking inside of the silicon can cause the decrease in overall stiffness. Beside of that due to the high temperature of the laser, a thin layer of silicon transforms from original solid state to liquid state then re-solidified. Therefore, the crystal property is potentially changed from single crystal to poly crystal which brings down the active young's module.

However, the difference in youn's module between poly crystal and single crystal is roughly 10-20 percent due to different materials references, meaning this stiffness offset can be explained solely by re-solidification, only if the most of the material of flexure has been transformed from one orientation to the other. While in the other hand, the micro cracking affects more dramatically on the stiffness behaviour, since the beam width changes the second moment of area very sensitively. Therefore, the cause of this low stiffness are more likely to be a combination of two factors which are all from thermal affection, while with micro cracking as dominant factor.

V. Conclusion

The indirect comparison between two manufacture methods has been established and realized, in terms of both structural and mechanical properties. Laser pulse with higher frequency results in more materiel removal thus relatively smaller feature is obtained, while the best side wall surface found in the parameters of set 2. The stiffness of laser micro machined overall lower than the simulated value which is believed due to the thermal damage, specifically micro cracking dominantly and crystal re-solidification. For deeper investigation of this study, the factor of yield strength and exact cause of the low stiffness could be further researched. For applying laser micromachining as prototyping method, improvement of water-assisted cutting can be investigated along with smaller minimum feature size.

VI. Acknowledgement

The authors would like to thank *Flexous B. V.* and Davood. Farhadi Machekposhti for their helps in stiffness measurement.

References

[1] Hao G, Yu J, Li H. A brief review on nonlinear modeling methods and applications of compliant mechanisms[J]. Frontiers of Mechanical Engineering, 2016, 11(2): 119-128.
[2] X. Jiang, J.R. Yuan, A. Cheng, K. Snook, P.J. Cao, P.W. Rehrig, W.S. Hackenberger, G. Lavalelle, X. Geng, T.R. Shrout, Proc. IEEE Symp. on Ultra (2006) 922.
[3] Peng, Jue, et al. "Micro-patterning of 0.70 Pb (Mg 1/3 Nb 2/3) O 30.30 PbTiO 3 single crystals by ultrasonic wet chemical etching." Materials letters 62.17 (2008): 3127-3130.
[4] Machekposhti D F, Tolou N, Herder J L. A review on compliant joints and rigid-body constant velocity universal joints toward the design of compliant homokinetic couplings[J]. Journal of Mechanical Design, 2015, 137(3): 032301.
[5] Crawford, T. H. R., A. Borowiec, and H. K. Haugen. "Femtosecond laser micromachining of grooves in silicon with 800 nm pulses." Applied Physics A 80.8 (2005): 1717-1724.
[6] Cheng, Jian, et al. "A review of ultrafast laser materials micromachining." Optics Laser Technology 46 (2013): 88-102.
[7] Lam, K. H., et al. "Kerf profile and piezoresponse study of the laser micro-machined PMN-PT single crystal using 355nm Nd: YAG." Materials Research Bulletin 48.9 (2013): 3420-3423.
[8] Buerle, Dieter W. Laser processing and chemistry. Springer Science Business Media, 2013.
[9] Knappe, Ralf, et al. "Scaling ablation rates for picosecond lasers using burst micromachining." SPIE LASE. International Society for Optics and Photonics, 2010.
[10] Kam, D. H., L. Shah, and J. Mazumder. "Femtosecond laser machining of multi-depth microchannel networks onto silicon." Journal of Micromechanics and Microengineering 21.4 (2011): 045027.
[11] El Fissi, Lamia, Victor Xhurdebise, and Laurent A. Francis. "Effects of Laser Operating Parameters on Piezoelectric Substrates Micromachining with Picosecond Laser." Micromachines 6.1 (2014): 19-31.

[12] Li, Xiaomeng, et al. "Lead-Free Piezoelectric Diaphragm Biosensors Based on Micro-Machining Technology and Chemical Solution Deposition." Sensors 16.1 (2016): 69.
[13] Corbari, Costantino, et al. "Femtosecond versus picosecond laser machining of nano-gratings and micro-channels in silica glass." Optics express 21.4 (2013): 3946-3958.
[14] Chen, Chien-Yu, et al. "Microstructure and lubricating property of ultrafast laser pulse textured silicon carbide seals." Applied Physics A 107.2 (2012): 345-350.
[15] Dong Y, Zorman C, Molian P. Femtosecond pulsed laser micromachining of single crystalline 3CSiC structures based on a laser-induced defect-activation process[J]. Journal of Micromechanics and Microengineering, 2003, 13(5): 680.
[16] Karatodorov, S., and M. Grozeva. "The Effect of Process Parameters in Femtosecond Laser Micromachining." Bulg. J. Phys 43 (2016): 110-120.
[17] Hopcroft M A, Nix W D, Kenny T W. What is the Young's Modulus of Silicon?[J]. Journal of microelectromechanical systems, 2010, 19(2): 229-238.
[18] Corbari, Costantino, et al. "Femtosecond versus picosecond laser machining of nano-gratings and micro-channels in silica glass." Optics express 21.4 (2013): 3946-3958.
[19] M.D'Auria, N. Tolou "UV-Laser Cutting for Silicon MEMS Prototyping: Improving Etching Rate and Quality". proceedings of the 14th euspen internation conference, 2014.
[20] Pusch, Tim P., et al. "Laser Micromachining of Thin Beams for Silicon MEMS: Optimization of Cutting Parameters Using the Taguchi Method." ASME 2015 International Design Engineering Technical Conferences and Computers and Information in Engineering Conference. American Society of Mechanical Engineers, 2015.
[21] EL Fissi L, Xhurdebise V, Francis L A. Effects of laser operating parameters on piezoelectric substrates micromachining with picosecond laser[J]. Micromachines, 2014, 6(1): 19-31.
[22] Han, Yukun, et al. "Femtosecond laser-induced silicon surface morphology in water confinement." Microsystem technologies 15.7 (2009): 1045-1049.
[23] Zheng X J, Zhou Y C, Nin M Z. Thermopiezoelectric response of a piezoelectric thin film PZT-6B deposited on MgO (100) substrate due to a continuous laser[J]. International journal of solids and structures, 2002, 39(15): 3935-3957.
[24] Tangwarodomnukun, Viboon, Jun Wang, and Philip Mathew. "A comparison of dry and underwater laser micromachining of silicon substrates." Key Engineering Materials. Vol. 443. Trans Tech Publications, 2010.

4

Self reflection

4.1 Line of thoughts

4.1.1 Paper Design

This graduation project started with a goal of fast prototyping and fabrication of MEMS devices, for example as energy harvester. The line of thoughts of paper design can be seen in Fig4.1.The whole laser fabrication of MEMS devices concludes several main factors such as improving laser cutting quality, minimization of the feature size, integration with electrical connection and testing. Minimization of the feature size and integration are challenges for laser micro machining. It is difficult to obtain the same feature size as small as lithography is capable to make, since the intrinsic process property of lithography can provide layers of different materials with nanometer size structures. However, in order to conduct any further investigation of those challenges, optimizing the laser tooling is essential. Tapper angle affects uniformity of high aspect ratio structures and rough side wall surface quality affect mechanical and dynamical performances.

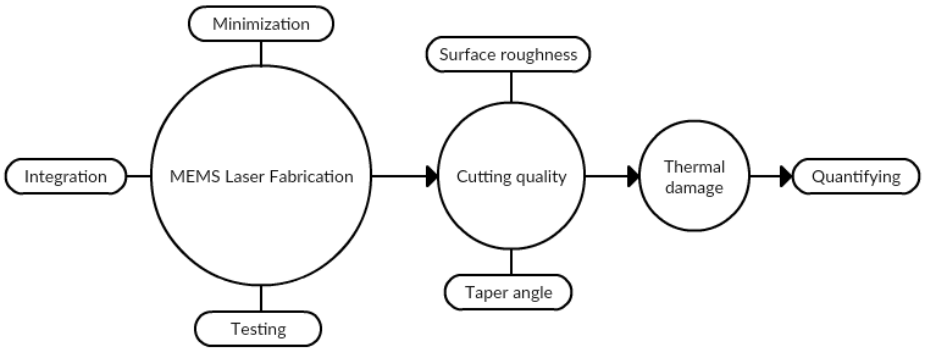

Fig. 4.1: The flowchart of lines of paper design, the approach towards quantifying thermal damage.

Currently, Heat Affect Zone (HAZ) is quantified by the visual inspection which provide very poor accuracy. The first mean of quantifying is utilizing the piezoelectric property loss under temperatures above Curie point. Since the main interest is based on the application of energy harvester, PZT-5H bulk ceramic with 100µm thickness. The second mean of quantifying is focused on the mechanical performance of silicon structure based on the other interest applica-

tion of complaint mechanism prototyping. Silicon micro stages are fabricated and compared with lithography-made devices verified Finite Element Method simulation.

4.1.2 Supporting materials

Experimental Analysis for silicon debris composition

Since the cleaning application of this project is rare to see in a normal clean room laboratory, the composition of the contamination needs to be confirmed before operating a HF etching. Therefore, a Energy Dispersive X-ray Spectroscopy (EDS) has been carried out for chemical characterization of un-cleaned samples. The result can be seen in Figure4.2.

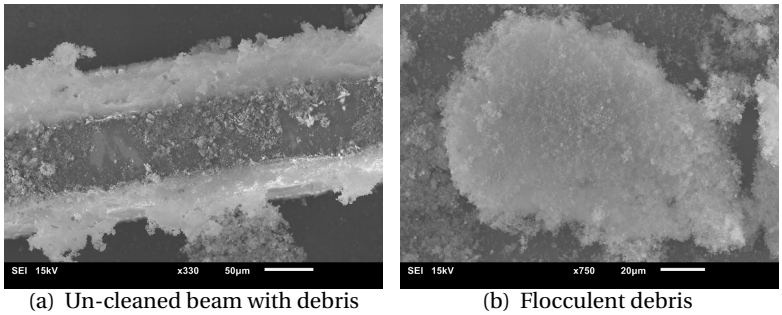

(a) Un-cleaned beam with debris (b) Flocculent debris

Fig. 4.2: SEM photos of the un-cleaned sample for EDS analysis

The result of the EDS analysis can be seen below in figure4.3, the black markers are the name of the element, and the 'Ka' following the element is the typically strongest X-ray spectral line for electron emission, also called 'K-alpha'. There are two highest lines are both for Silicon, at the left side and right side of the picture, and the second highest is the Oxygen. There are also Boron, carbon and Nitride are determined, Boron is related to a very thin doped layer and Nitride is related to the compound previously discussed.

Therefore, the main contamination is silicon dioxide and no obvious nitride compound determined by EDS. Surprisingly, there is no Boron found but wafer is supposed to have a Boron doped layer of 10um. Hydro Fluoride can only attack silicon dioxide which suits this project.

Cleaning method

The main structural criteria of this project are surface roughness, taper angle, feature size along with the mechanical criteria, stiffness. All of these criteria are heavily affected by the debris and recast on the sample. Therefore the suitable cleaning method needs to be chosen and conducted. Common methods for cleaning are ultra-sonic bath which vibrates in a ultra-sonic range(10-30KHz),

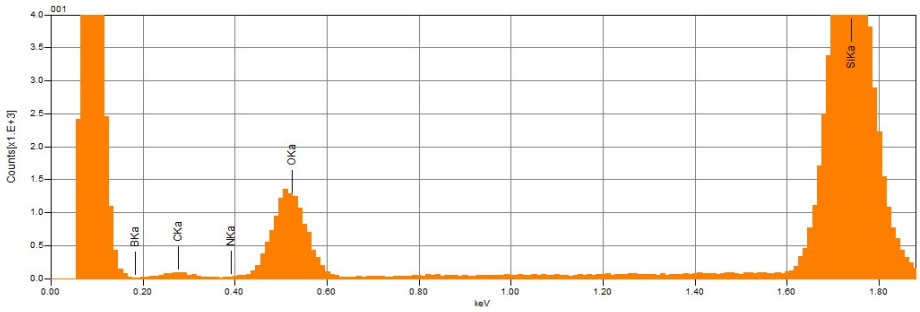

Fig. 4.3: EDS result

Chemical	formula	Mass%	Atom%
B			
C	14.91	24.38	0.09
N			
O	30.53	37.47	0.17
Si	54.56	38.15	0.24
Total	100	100	

Tab. 4.1: EDS result in chemical element

Isopropanal Alcohol (IPA) and acetone bath resining, Vapour Hydro Florid acid cleaning and normal wet Hydro Florid bath and KOH heated bath. Ultrasonic bath and IPA will not affect the cutting quality but simply remove the debris on the surface physically, and partially.

KOH heated bath can provide a proper clean of debris and recast but at the same time silicon structure will also be etched, as shown in Fig4.4(a-d). On other sides, the HF only attaches the silicon dioxide and any other organic contamination, but HF is a very aggressive chemical that requires trained operation in clean room environment, which will decrease the fabrication speed.

Vapour HF cleaning has been carried out since it brings less chemical hazard compared to the wet HF etching. The result can be seen in Fig4.4(e,f), and there is still minor debris left on the surface on the beam, since the VHF technique is not normally used for bulk beam and large structures therefore the recipe is not found.

Other devices

As the original approach to the MEMS devices fabrication, U-shape thermal actuators are cut with Boron doped silicon as electrical connection. The devices can be seen in Fig4.5a,b. However, the overall size in this field is much smaller and workload that is needed to make this actuation system is out of the time line of a graduation project.Therefore this direction was no longer carried on.

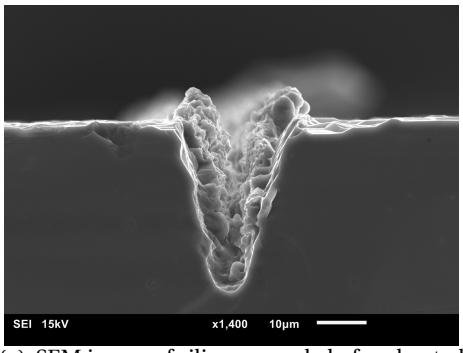

(a) SEM image of silicon sample before heated KOH etching

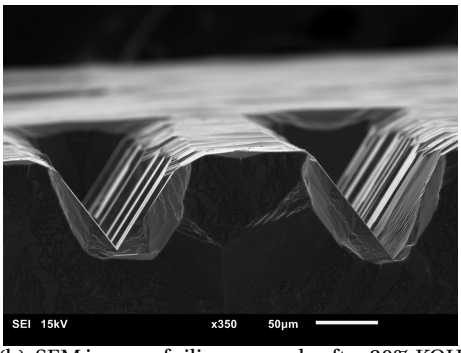

(b) SEM image of silicon sample after 30% KOH bath at 50 °C for 1 hour

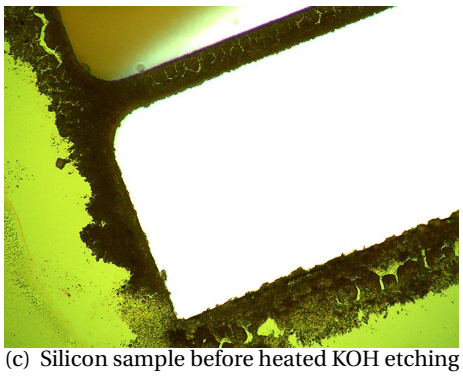

(c) Silicon sample before heated KOH etching

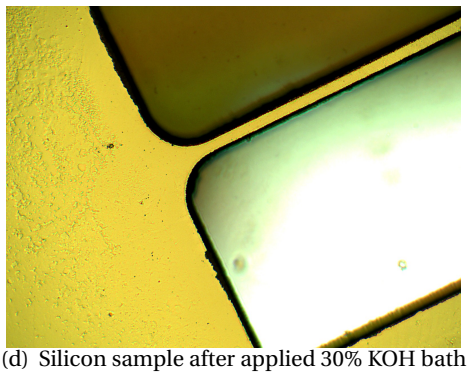

(d) Silicon sample after applied 30% KOH bath at 50 °C for 40 minutes

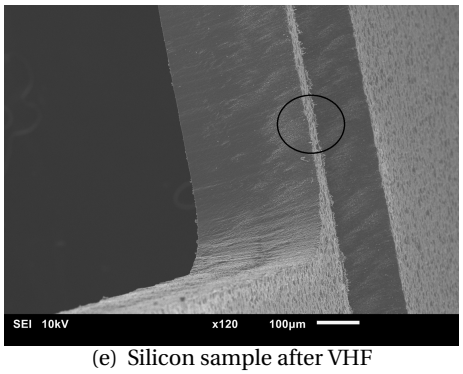

(e) Silicon sample after VHF

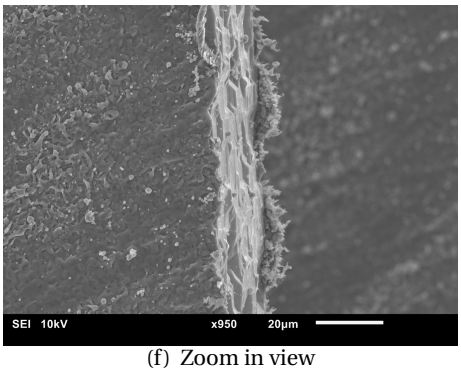

(f) Zoom in view

Fig. 4.4: Images of samples before and after different cleaning methods

A cantilever with very thin feature were fabricated as an indication of the capability of current equipment as seen in Fig4.5c. And since all the delicate features and structures in this project are not capable to survive through the conventional cleaning method of ultrasonic cleaning, a suspended setup for ultrasonic cleaning can be seen below, and it ensure all the harsh vibration can only conduct through liquid which acts as a damped buffer.

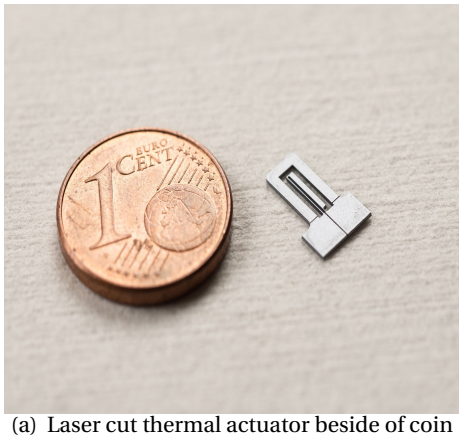
(a) Laser cut thermal actuator beside of coin

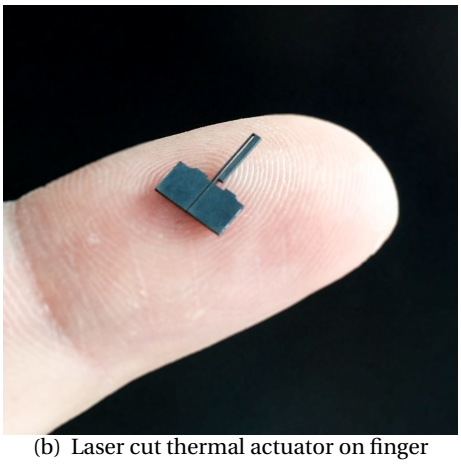
(b) Laser cut thermal actuator on finger

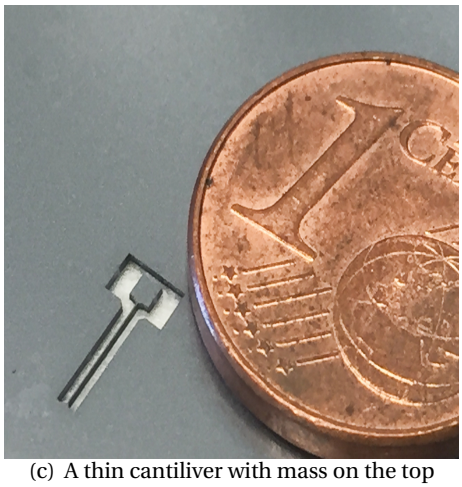
(c) A thin cantiliver with mass on the top

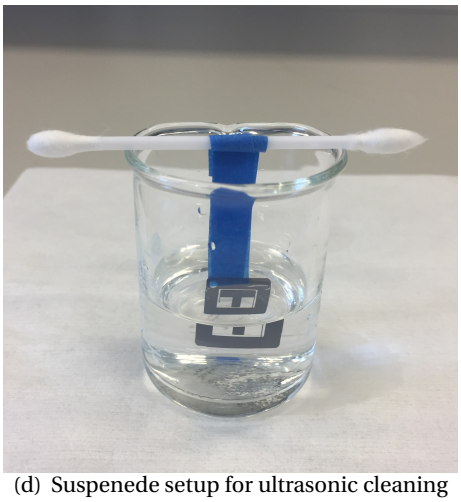
(d) Suspenede setup for ultrasonic cleaning

Fig. 4.5: Other devices fabricated during master project

The project of quantifying thermal damage on piezoelectric material shows that the piezoelectric property loss is limited, therefore a micro beam actuator was cut as shown in Fig4.6. And the electro on one side is separated by laser path (verified by the resistance test) and the beam width was measured (top73µm,bottom107µm). Finally the cases made by 3-D printing was adapted to set up the electrical connection.

Fast prototyping application

As the background of this project which is to develop a fast prototyping method for new design and concept of compliant mechanism, a prototype with micro scale has been manufactured by laser micromachining which can be seen in Fig4.7. This innovative design is for energy harvesting under low frequency for

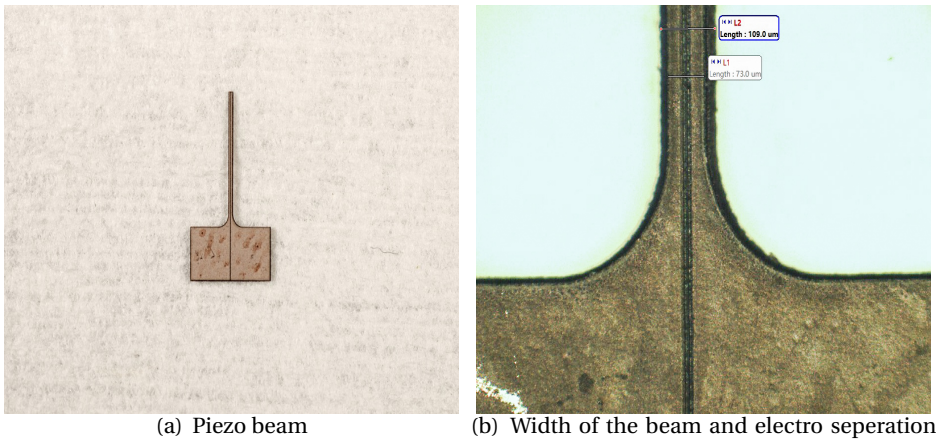

(a) Piezo beam (b) Width of the beam and electro seperation by laser

Fig. 4.6: Piezoelectric beam manufactured by laser micro machining

wearable devices. The sets of large flexure are designed as pre-loaded bistable structure, and smaller inner parts are designed as free standing double-flexure stages which vibrates at higher frequency.

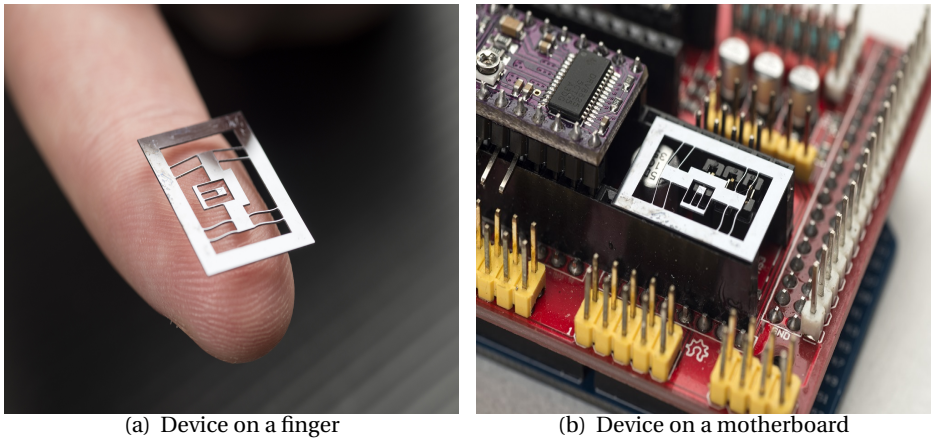

(a) Device on a finger (b) Device on a motherboard

Fig. 4.7: Concept prototype of a low frequency energy harvester

4.2 Work timeline

As can be seen in Tab 4.2.

Month	Phase	Plan	Reality
09.2016	Literature	Background	——
10.2016	Literature	Knowledge learning	——
11.2016	Literature	Prior research	——
12.2016	Literature	State of art	——
01.2017	Traineeship	Equipment training	Design of paper
02.2017	Traineeship	Experiment conducting	Manufacturing
03.2017	Traineeship	Documentation	Testing and Documentation
04.2017	Thesis	Fabrication	MEMS devices
05.2017	Thesis	Fabrication	Silicon cutting
06.2017	Thesis	Simulation	simulation and design
07.2017	Thesis	Testing	Measurement and analysis
08.2017	Thesis	Documentation	testing
09.2017	Thesis	——	Documentation

Tab. 4.2: Research timeline

4.3 Contributions and collaborations

Contribution to research group

The main contribution for this project is establishment of a fast prototyping method for concept proving and testing for compliant mechanism design, possibly in the further also beneficial for energy harvesting devices. Current work happening within the compliant mechanism group is based on the concept design and theory investigation, therefore a fast prototyping methods in a micro scale which is accessible within the campus and fast (from few months by DRIE down to few days) is highly desired.

In order to applying laser micro manufacturing, quantifying the drawbacks and evaluation of the mechanical performance is essential, which is achieved by this graduation project and had not been done before. With the knowledge and experience obtained by this project as a ground base, the further promising research topics as micro actuator (micro gripper), MEMS devices (thermal), energy harvester and water-assisted laser cutting are made possible.

Joint work

The first paper of the chapter 2 was originally intendedly arranged as the traineeships project for another master student Thijs Bald and author, however, the endless passion and great effort brought this project to a much deeper extend as planed. And the author is fully aware and grateful for the inspiration and suggestion from Thijs.

More importantly, it is not possible without the all the supports from staffs of PME. For instant from the other research group of Nano and Micro Engineering

(MNE), Murali Ghatkesar provided great support for this project and among the devices, the thermal actuator was provided to his group for printing conductive nano particles on the surface as electrical connection, and the process is still on going.

Also, the close cooperation from company *Flexous B.V* and Else Kooi Laboratory (EKL) has played important roles in testing and cleaning of the devices.

Personal development

From the project during the past year, I gained knowledge of Laser micromachining, process optimization, MEMS design and fabrication process, Finite Element Method simulation, testing and measurement environment and scientific writing.

Moreover, I deeply mastered the experimental skills for variety of equipment such as Scanning Electron Microscopy (SEM), Atomic Force Microscopy(AFM), White Light Interferometer, HF and VHF operation, chemical laboratory, and abundant experience of working in high class Clean Room.

Apart from technical aspects, I also learned other crucial and important professional skills such as communicating and working together as a team with different specialities, conquering obstacles of project with a limited time budget.

Acknowledgement

First of all, I am deeply truly grateful to my parents who always support me on every matter, I would have never reached so far without their supports and love.

I would like to thank Just Herder and Nima Tolou for their patient supervisions, all the inspiring guides and scientific advices have made my project extremely fruitful. Reinier Kuppens, my daily supervisor, has given me so much help all the way along the project from the very beginning, and patiently helped me in great depth with academic writing. Other members in MSD group also helped me with variety of matters, help of simulation and test from Davood Farhadi, great discussions and personal skills learned from Thijs Blad, instructions of MEMS process from Murali Ghatkesar , reliable laboratory support from Rob Luttjeboer, Patrick van Holstand and Spiridon van Veldhoven.

And all the staff from PME department have provided great supports and knowledge, which made this two year experience not only a giant milestone of my life, but also a very happy memory to carry into my future.

Part I

APPENDIX

1

Appendix A: Supportive material for silicon flexure

1.1 Main contaminations of devices for VHF

The wafer which is intended to be etched are <100> silicon wafer, and optionally doped wafer with boron (depends on wafers), and device on the wafer are mainly suspended structures as flexure or thin beams which are cut by laser micromachining. The production environment is air ambient without clean room condition. Laser cutting introduces huge amount of heat as high as 2500k, therefore the main reactions applied are oxidation and nitrification of pure silicon under heat, while other reactions with rare gas and sub-reactions are considered.

Theoretical assumption

oxidation

Under temperature between 600 and 1200°C the silicon reacts with water and oxygen as follow :

$$Si + O_2 \rightarrow SiO_2 \tag{1.1}$$

$$Si + 2H_2O \rightarrow SiO_2 + 2H_2 \tag{1.2}$$

nitrification

Under temperature between 1300-1400°C the silicon also reacts with nitrogen as follow :

$$3Si + 2N_2 \rightarrow Si_3N_4 \tag{1.3}$$

Expect for the Si_3N_4 in solid form, there are also Si_2N SiN and Si_2N_3 in gaseous state which is not considered in this case.

conclusion

The main contaminations are SiO_2 and Si_3N_4. Other organic contaminations like finger print are negligible. Both of them can be attacked by HF.

1.2 Error analysis

Background

The testing of the compliant silicon stages are based on the force-displacement measurement, the displacement is contributed from a moving stages. And the force is from the elasticity of silicon beams. Each one of two beams can be simplified as a cantilever with an end load, which maximum deflection can be calculated as 1.4:

$$\delta_{MaxDef} = \frac{FL^3}{3EI} \tag{1.4}$$

While the δ is the deflection at the end point of the beam and L is the length of the beam and E is the Young's modules of the silicon. And the second moment of area I of the beam with a trapezoidal cross section area where the narrow or top side width is a and the other is b.

$$I = \frac{h(a+b)(a^2+b^2)}{48} \tag{1.5}$$

The general stiffness of the beam k can be calculated in equation 1.6, by dividing term I to the left side of the equation, we can eliminate the effect of different cross section shapes created by variety of tapper angles of laser micromachining. Then the 'active Young's modules' E^* can be calculated by equation1.7. Originally, E is fixed by material itself, however, in our application of laser micro machining, there are certain factors, mainly Heat Affect Zone and roughness profile, introduced which can affect the finally outcome of the silicon beam.

Here the assumed factors which can influence this 'Active E' are low side wall surface roughness and thermal damage which may change the inner property of silicon lattices. However, Based on the current experiment measurement, these two factors are coupled together shown as the drawbacks or poor behaviour compared to the theoretical values. Nevertheless, this quantification which can point out the offset of ideal performance and laser machined performance in terms of elasticity and yield strength, is still valuable and helpful for further designed in the field of compliant mechanism.

$$k = \frac{F}{\delta} = \frac{3EI}{L^3} \tag{1.6}$$

$$E^* = \frac{L^3 k}{3I} \tag{1.7}$$

As we can see in equation 1.5, the I is linear to the maximum deflection while a and b the cross section area dimension is critical to the δ_{MaxDef}.Therefore getting the accurate profile of the cross section area is important to obtain a solid argument for both simulation and testing. The following discussion would be mainly about the error, or the deviation, of measuring the cross section dimension.

Error determination

In order to determinate the error that exists in the measurement of beam width, several measurements have been carried out. For consideration of the time duration and repeatability, only a simple structure of double clamped beam with a designed beam width of 70 um has been manufactured, the same study was shown in [1] with similar design but thicker beam. A Scanning Electron Microscopy (SEM) picture can be see below in Fig1.1.

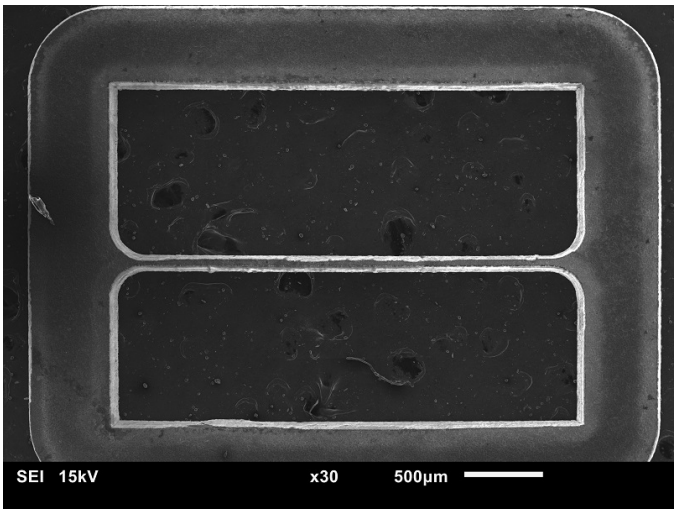

Fig. 1.1: SEM photos of simplified measurement structure

The samples are fixed into a plat sample holder for the SEM and observation direction is vertical to this plane. Due to the tapper angle, from the vertical direction there are two beam widths are visualized, which are the top and bottom sides of the beams. Due to vibration and debris attached on cutting edge, the beam width may vary along with the whole length, therefore three different positions are selected as sampling point, which points near two ends and one at the middle. And these three positions are identical for each set of measurement and samples. In order to minimize the random error, each sample is manufactured three times under same condition, and each measurement has been carried out four times. A illustration of sampling points is shown in Fig1.2a.

And one example of the measurement can be seen in Fig 1.2b, where 4 measurement for both top and bottom width are carried at one position of one sample. In order to find the error, also called as fractional deviation, the standard deviation are carried out.

$$d_i = x_i - \bar{x} \tag{1.8}$$

$$\sigma_x = \sqrt{\frac{1}{N-1}\sum(x_i - \bar{x})^2} \tag{1.9}$$

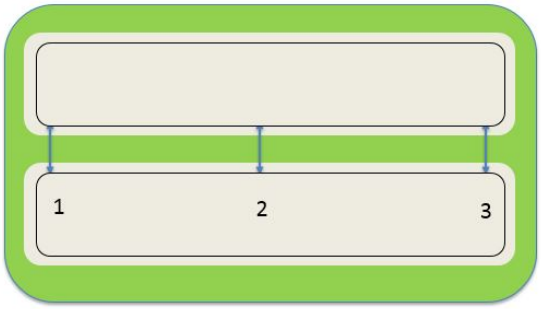

(a) Illustration of the measuring positions, 1 and 3 are near ends and 2 is at the middle

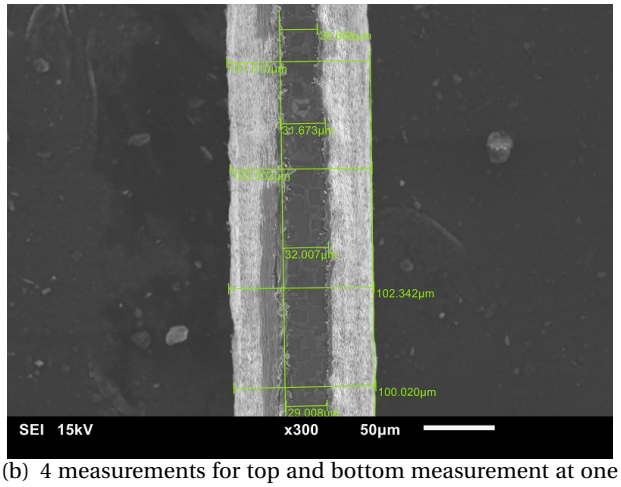

(b) 4 measurements for top and bottom measurement at one position

Fig. 1.2: Illustration(a) and example(b)of the double-clamped beam measurement

The error of each measurement for both top and bottom beam width is calculated based on the SEM length measurement result, the error ϵ is fractional deviation as in equation 1.10.

$$\epsilon = \frac{\sigma_x}{\bar{x}_i} \tag{1.10}$$

The result of the error statics for all the beams under different cutting parameter from set 1 to 5 can be seen in Fig1.3a, the average error for SEM beam width measurement is about 9% overall. The Root Mean Square (RMS) value of beam width is in Fig1.3b. Furthermore, this error will propagate along the equation of stiffness and through out all the test process.

1.3 Testing under different cleaning methods

The first test set-up is with cooperation with *Flexous*, which consists of a force sensor and a translational stage. The force sensor is FT-S10000 from *Femto Tools* with the maximum range of 1 gram force (10mN) and resolution of 0.05mg, and it is mounted with an angle of 30 degree to horizontal plane. Certain pre-described displacement are applied by the translational stage, and the force sensor output the force signal. The result of the first time measurement can be seen in Fig1.4

As shown in Tab1.4b, due to the existence of tapper angle at side wall, the horizontal deflection force is separated into two directions, and the vertical load creates lifting while increasing of the applied load. Therefore, on the side wall surface, there is a 'slip' effect appearing after 20µm . In addition. this effect may be also due to the low deflection stiffness at the force sensor tip. By attaching a small block which has perfect vertical side wall while does not affect horizontal force-deflection behaviour of the devices since theoretically the flexure stages have very high stiffness in vertical direction.

	Top width	Bot width	Measured Stiffness	I ($mm^4 x10^-5$)
VHF	65 (um)	147 (um)	1041.3 N/m	3.4230
Ultrasonic	38(um)	116 (um)	506.6 N/m	1.4341
KOH 1	39 (um)	118 (um)	211.5 N/m	1.5155
KOH 2	30 (um)	126 (um)	130.2 N/m	1.6357

Tab. 1.1: Beam dimension and measured stiffness

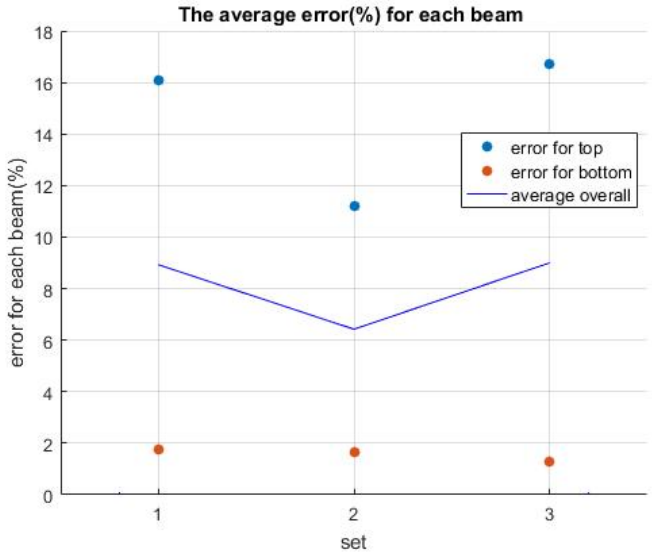

(a) Error statics for every measurement

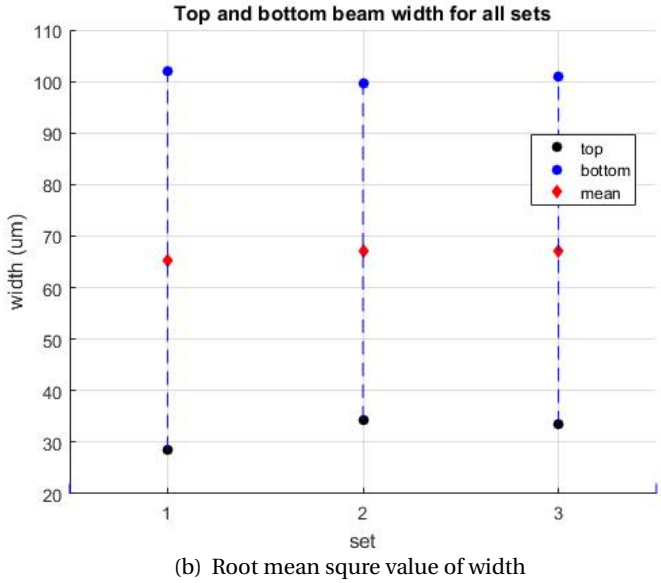

(b) Root mean squre value of width

Fig. 1.3: Result of error analysis

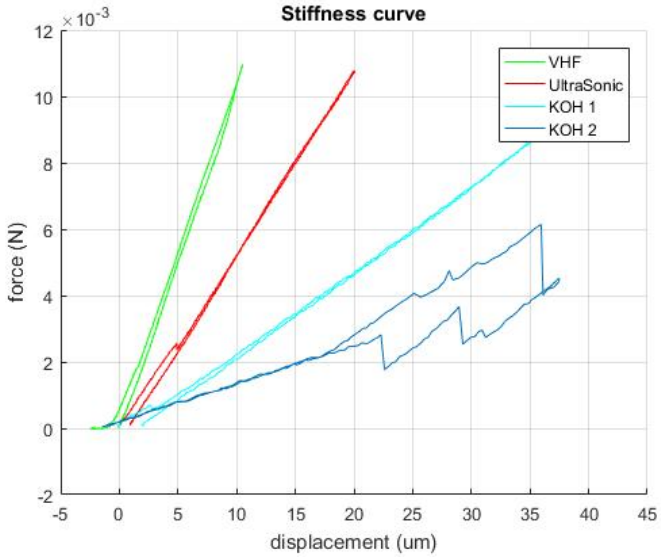

(a) All curves of samples under different cleaning methods

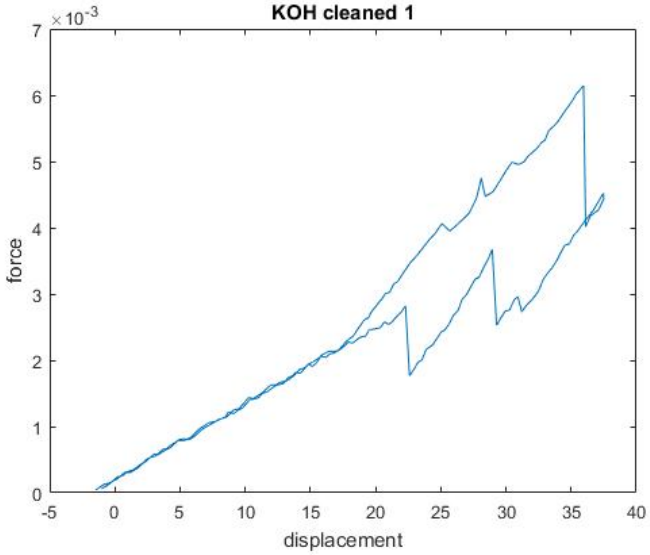

(b) Stiffness curve due to 'slipping'

Fig. 1.4: Stiffness measurement (first time)

2

Appendix B: Traineeships report

This traineeships is conducted as a part of the master graduation project. In previous literature study, basic knowledge of laser system and state of art have been studied. Specifically, improving the cutting quality, in terms of higher surface roughness and smaller thermal damage, is the main concern and focused area. The main aims are to obtain practical experiences and skills of working with ultra fast pulsed laser system, as well as the corresponding examination equipment, which are essential and supportive for further research and project. The correlating between settings found in literatures and existed system in laboratory has been established, which enables to attempt replica of previous research in this area.

Multiple materials have been tested and cut, such as stainless steel, piezoelectric thin film and ceramic. Then the sample pieces are observed and processed by several equipment as Scanning Electron Microscopy, Atomic Force Microscopy, White Light Interferometer and basic chemical cleaning. A project of quantifying the Heat Affected Zone in micro laser machined piezoelectric material has been conducted and optimal settings for this project have been obtained by Taguchi process parameter optimal method.

Several findings that have not noticed in the literature study period have been obtained, especially the process parameters as speed, re-focus step in vertical direction, overlap and cutting path. Other than the laser parameters like fluence, frequency and pulsed width which have been vastly studied, process parameters also extraordinarily influence the cutting quality.

Apart from technical skills and depth understanding of laser system that I obtained during this traineeships, I also learned other crucial and important professional skills as communicating and working together as a team with different specialities, conquering obstacles of project with a limited time budget.

2.1 Cutting Training

Some training cutting has been achieved to get a basic understanding of the laser and process parameters specifically for the equipment existed in the laboratory.

The initial approach to find the optimal setting for cutting is utilizing the clone function in the process power software. In order to find the optimal setting between two variables at one time, a two-array pattern with each variable value can be changed in a certain step size can be generated. Then inspection on the test piece by the CCD camera in the system can help to check the cutting

outcome and also give a direct illustration of the behaviour of the laser cutter of different parameters.

The fluence of the laser, the energy applied on the surface is most importance factor of the cutting quality. And fluence is affected by not only the laser parameters like frequency and out put power, but also the processing parameters like scanning speed and repetition number. Therefore while conducting this two-array method of finding the optimal setting, only look at one category of parameters is recommended. For instant, the two-array that are selected initially could be frequency and power , the the parameters that influence the fluence. After several iterations, then the process parameters could be considered.

2.2 Stainless Steel

Stainless steel as the most accessible and cheap material is considered to be the starting material to help understanding the operation of laser system.

2.2.1 Recast

The recast phenomenon is significant while cutting the stainless steel with laser cutting since huge thermal load applied instantly on the surface, the material experienced from solid state to liquid state and then reformed back to solid sate. This reformation is called recast, which can dramatically negatively influence the surface roughness of the cutting edge since the shape of re-solidification is not well controlled and randomly. As shown in the Fig2.1, the recast is severe since there was no cleaning or etching procedure involved after cutting. An immersing of acid solution can be expected to dramatically improve the quality, however by doing which will also affect the original structure.

Fig2.2 shows the local view of the cross section of cutting surface. The path of the laser beam column can be noticed on this figure, yet the pat is not intact curve since the a relatively high overlap rate is applied. The relationship of overlap op, speed v, spot size ss and frequency f is shown in equation[1] below:

$$v = f \cdot ss \cdot (1 - op) \tag{2.1}$$

A sets of thin beams with a width of (100µm) have been manufactured as the potential application of energy harvester substrate. The Fig2.3 and Fig2.4 are the SEM image of beams under different angles. As can be seen that there are a layer of oxidation material existed which could prove the assumption of polycrystalline layer due to re-solidification for silicon application discussed in previous chapter.

Recast phenomenon is random compared to the original material, yet it also follows certain behaviour, as seen in the Fig2.5, there is a peak of accumulated debris sprayed along the cutting edge. During the experiment, it is found that the recast is sensitivity to a speed range which was not expected. The reason of

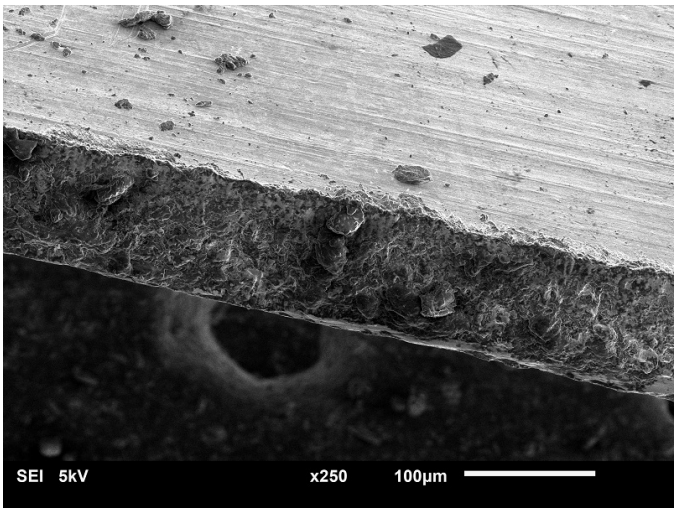

Fig. 2.1: Recast on the stainless steel

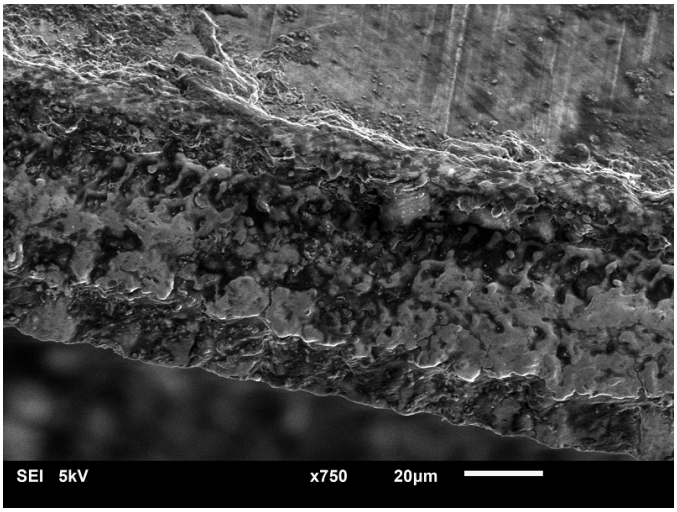

Fig. 2.2: Local view of cast on the stainless steel

this effect may be the small size of the cutting piece comparing with the high scanning speed. The spot of laser beam scanned is scanned a second time, the laser finished the whole pattern and came back to the same spot again. Furthermore with the fast scanning speed, the time period of two passes is not enough for heat dissipation on the material.

2.2.2 Corner Effect

Interestingly, there is another behaviour called 'corner effect' found during the laser cutting process. This effect is commonly existed in the conventional Computer Numerical Control (CNC) machine tool due to the line speed of cor-

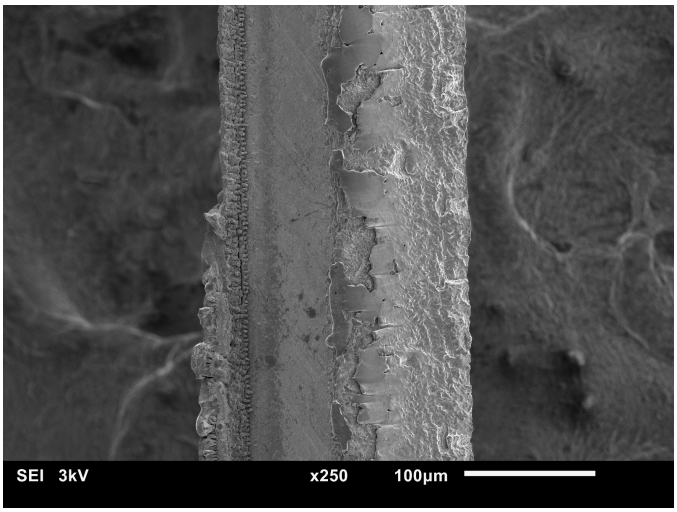

Fig. 2.3: Recast on the stainless steel beam (100µm) from a tilted angle

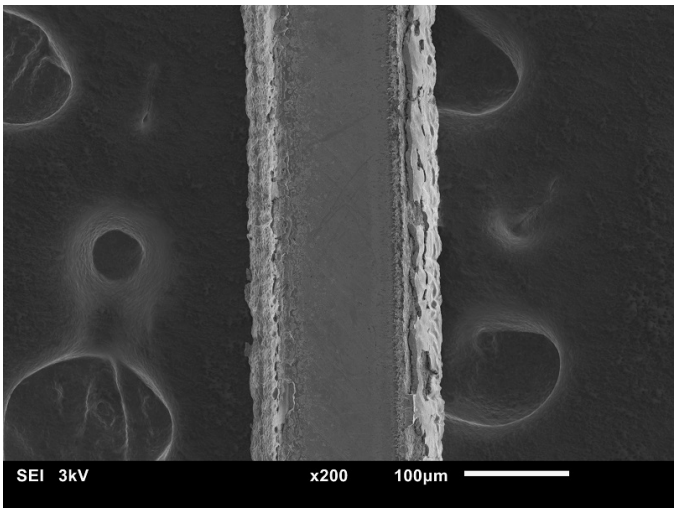

Fig. 2.4: Local view of cast on the stainless steel (100µm) from vertical direction at the top

ner is smaller than the straight line, which applied more energy at the corner position. However, this effect is not expected for ultra fast micro laser machining since the inertia of manipulating the laser beam is extremely small.

Eliminating this effect can be achieved by improving design of the cutting trajectory. Instead of directly cutting along the desired shape on the material, extra path that exceeds the line element before corner is added. After the changing on the spare material, the same extra path applied on the other line element after corner. By improving the deign, the corner effect is expected to be avoided, however it also may restrict the minimum feature size of a complex structure.

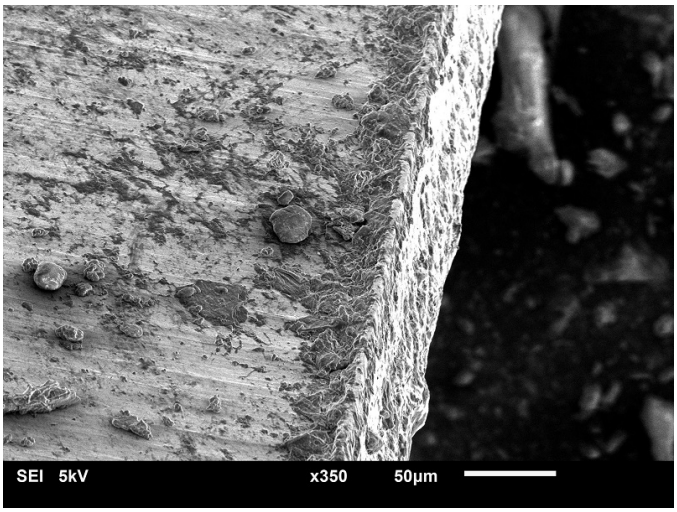

Fig. 2.5: Debris and recast accumulated along the edge

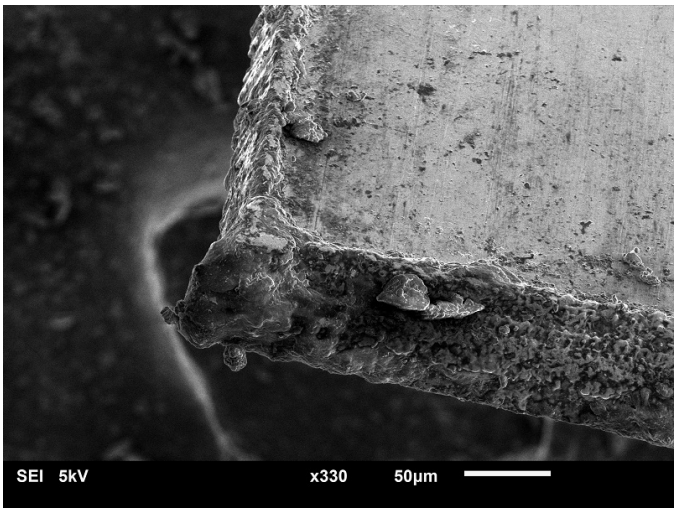

Fig. 2.6: The accumulated material at the corner

2.3 Piezo Film

Soft material, not like ceramic or crystal (including metal), has specific recast behaviour that influence the structure releasing. Due to the low thermal capacity and conductivity of the polymer, the liquefaction and solidification phase take longer time than ceramic and metal, which introduces more severe recast behaviour. This feature makes the cutting piece hard to be released after the laser cut through the whole material. Lower energy results not hight enough ablation rate for cutting through, while higher energy creates severe recast which makes the piece hard to release. A different cutting profile can be seen below

in Fig2.7, the darker part of the figure with huge hollows is the substrate of SEM examination.

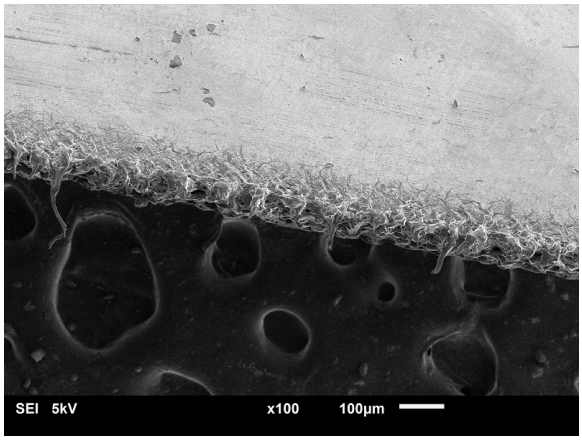

Fig. 2.7: Surface profile of pzt film

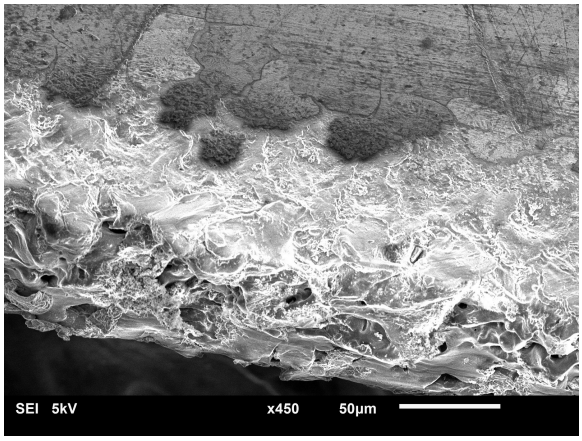

Fig. 2.8: Local view of surface profile of pzt film

As a result, an inspection of already released piece shows that the releasing was not clear and sharp. There are some extra strips on the surface which can be interpreted as the releasing force was actually stretching the attached part till yield and break. The strips was due to the displacement was larger than the elastic strength, and those strips remain the shape. This effect is certainly not desired for high accuracy cutting.

The improvements can be achieved by cutting thinner piece or shorter pulse width. Thinner piece subjects to smaller fluence to be enough to cut through. And shorter laser pulse width introduced less thermal effect while provides higher energy intensity to ablate material.

2.4 Pzt Ceramic

2.4.1 Project Motivation

There is a small amount of heat introduced by the plasma generated of ultra fast last micro machining. Therefore, there is thermal interaction between plasma and specimen called burnt. During this phenomenon the material properties are negatively affected due to overheating. The burnt area is also referred to as Heat Affected Zone (HAZ). The structural properties of the material such as strength could be negatively influenced by the high temperature reached within the HAZ. Currently, the quantification of HAZ is based on the visual inspection as stated in studies of ultra-fast laser machining [2, 3, 4]. Yet the natural advantage of piezoelectric material, capacitance, can indicate the level of damage due the HAZ, which potentially gives another mean of quantifying the HAZ accurately.

2.4.2 Taguchi Method

Taguchi design method was developed by Dr. Genichi Taguchi and proposed in 1987[5],This technique has became popular in worldwide industries after the 1980s. It is suitable for fast determination of important factors, but for construction of statistical models and optimization of machining regimes is barely studied[6]. The advantage of this method is that multiple factors can be considered at one time.

However, it is worthy to notice that Taguchi method does not guarantee to give the universal optimal result among the whole parameter space. Because it assumes an namely additivity of the main effect while ignoring further interactions. Which means, Taguchi method only looks into the primary order of various parameters on the objective function. Nevertheless, this method has helped to obtain tremendous improvements for most of the practical occasions[7].

The main goals of this project is to identify the optimal cutting conditions that yield the lowest surface roughness value Ra and the minimal width of heat affect zone, before to quantify the heat affect zone by the change of electrical property. The key step in the design of experiments is so called the orthogonal array will be explained next.

2.4.3 Array Selection

In order to achieve a relatively fast optimization process for this project, a part of the process parameter of drilling function are fixed. According to the result proposed in [8], process parameters such as the redundant patterns in order to help the laser beam to move into work piece and the Gap between those lines were investigated. The redundant line number was recommended as 2 or 3, and the gap size was chosen as 20 um which is the foot size of the laser beam. The z direction step which is the refocus procedure during the focus point moves

into the work piece, the step is chosen as the middle point of the thickness of the sample.

A list of variable value and levels can be seen in table2.1. Those values are chosen based on the principle of combination of each factor can ensure a reproducible cut-through performance. Thus, those values stands the maximum range of which any arbitrary combination could be enable cut through. Then the range is divided into three levels for every factor in order to obtain a constructional result and insight while maintaining a practical number of experiment

Tab. 2.1: Taguchi parameters

symbol	Factor name	level 1	level 2	level 3
A	diode current [A]	6.0	6.5	7.0
B	frequency[KHz]	20	25	30
C	overlap [%]	60	70	80

In a full set of typical Taguchi optimization, an outer ray is expected to be chosen, which is normally noise factors. However, for this particular project, noise factors are believed not controllable, nor cheap to control in other words.Thus there is no outer ray selected. Because noise factors are factors such as weather environment and humidity, which could be investigated by adding an outer array in further research.

In this experiment, interactions within factors are neglected since there are no any correlation effect as the author knows that could potentially affect the result. Furthermore, Taguchi's recommendation is considered to rather dig into more individual factors than interactions within factors. The degree of the freedom is calculated as 9, which is the number of the orthogonal array.

2.4.4 Cleaning Procedure

All the test piece was cleaned by an ultra-sonic cleaner machine while immersed in isopropyl Alcohol, this recipe was found in [9]. A large part of the existed research, there was no cleaning procedure involved. By applying this cleaning methods, the surface roughness value and HAZ width are decreased by roughly 4 to 5 and 50 micron.

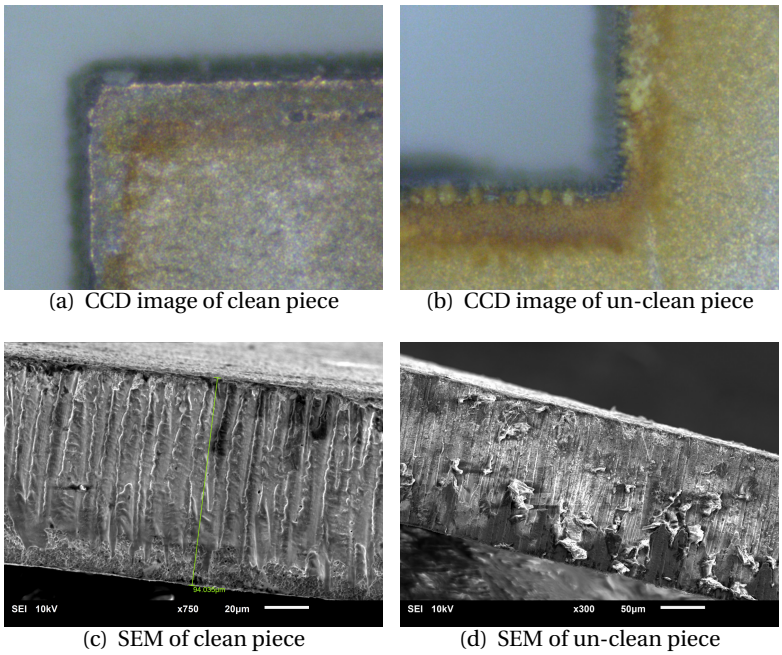

(a) CCD image of clean piece (b) CCD image of un-clean piece

(c) SEM of clean piece (d) SEM of un-clean piece

Fig. 2.9: Comparison of clean and un-clean piece

2.4.5 Experiment

The orthogonal array and result is listed in the table below in table2.2, every set of test is done by three time and then adapt the mean value of three in order to eliminate the random error.

Test Set	Level			Result	
Number	A	B	C	Ra (um)	HAZ (um)
1	1	1	1	5.907	62
2	1	2	2	7.269	41
3	1	3	3	5.356	51.5
4	2	1	2	4.023	35
5	2	2	3	7.427	41
6	2	3	1	5.022	50
7	3	1	3	8.769	85
8	3	2	1	5.940	76.6
9	3	3	2	7.601	86

Tab. 2.2: Table of array and result

2.4.6 Result

As can be seen in the table above, the best result, in terms of the lowest Ra value of 4.023 um, is obtained by the experiment set of number 4. A comparison between the best and the worst can be seen below in 2.10. The right figure is obviously more clear and clean compared to the left figure, the laser foot path is less presented in the cross section area. Although the SEM voltage applied on two samples are different, this is not a dominant error that severer enough to affect the overall result.

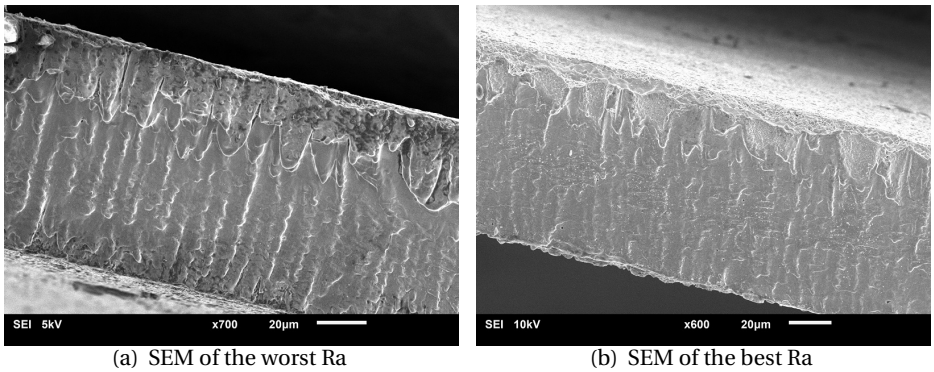

(a) SEM of the worst Ra (b) SEM of the best Ra

Fig. 2.10: Comparison between the best and worst Ra

The white light interferometer profile of the lowest Ra value is shown below in Fig2.11. The interferometer profile highly matches the SEM inspection. It is worth to mention that the location of white light interferometer may not be the identical location under SEM, however, the overall value should not be affected much between different locations since the whole test piece is cut by identical parameters under same environment.

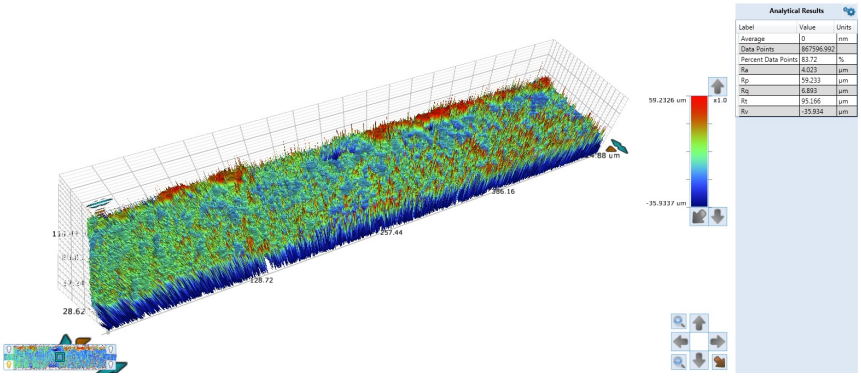

Fig. 2.11: White light interferometer image of minimum surface roughness

2.4.7 Discussion

HAZ Quantifying

Heat affect zone, as one of the two metrics that are chosen, has relatively rough accuracy in defining the exact width with huge variance and error factor. First of all, the debris and fumes may heavily influence the measurement of the width although certain cleaning procedure is involved. Secondly, the colour changing zone follows an irregular gradient which gives no obvious boundary between affected and non-affected zone. Thirdly, although certain shadow-ish pattern can be observed under SEM, SEM is not supposed to give chromatography information, and this shadow later is proved to be changed by different configurations of SEM examination.

Therefore. the value of HAZ for this project is not considered as a trust worthy factor to lead to a conclusion, which is the exact motivation of this project that quantifies the HAZ by different metric as piezoelectricity.

Bottom Adhesion

Since the white interferometer gives one more dimension information. As a result, we can see in Fig2.11, at the bottom part of the cutting surface, the shape no longer follows the straight laser path but accumulated to a peak. This effect is also found in previous research in similar configuration[1], an illustration can be seen in Fig2.12. One of the two potential reasons of this phenomenon is that laser beam is out of depth of field at the bottom part, the other reason is that the substrate underneath the cutting piece behaves as thermal tank.

In order to investigate this issue, firstly, the test piece is lift up and suspending in the air, therefore the influence of substrate is eliminated by this setting, secondly, a re-focus with the half of the sickness is applied during cutting which helps to prove the 'out of focus' assumption. This procedure introduces another issue which will be discussed in the further section. However, in conclusion, as can be seen in the Fig2.11, this issue still existed. Therefore more and deeper investigation is needed in the further research.

Level Separation

As mentioned before, there is a re-focus procedure applied that focus point of laser beam moves deeper into the material. As the result of cutting experiment done within Taguchi method frame, a separation along the depth direction is occurred, which is introduced by the function in Process Power software in laser system called 'level', meanwhile this separation is alike level or step on cutting surface. An illustration and SEM image of the step separation has been made and obtained below in Fig2.14.

However, this issue only occurs when the laser power is relatively high, which hypothetically can be solved by applied lower power and more repetition.

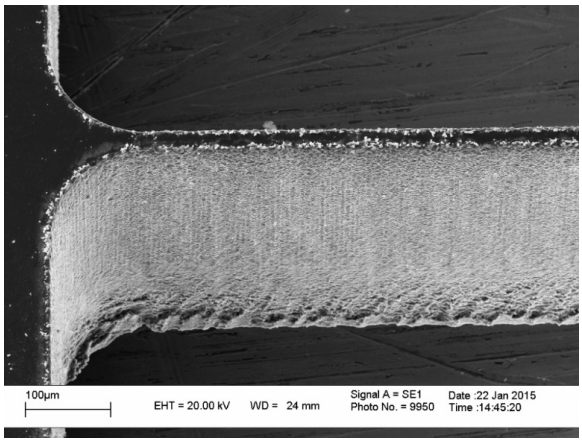

Fig. 2.12: Previous research with bottom adhesion[1]

The white light interferometer in Fig2.13 also proves the same assumption since SEM only gives two dimensional information.

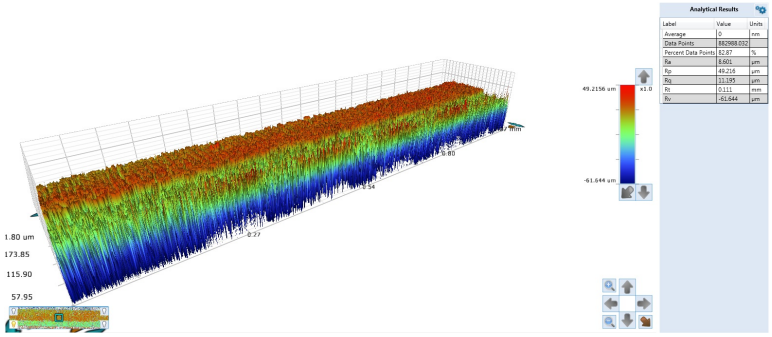

Fig. 2.13: White light interferometer image of level separation

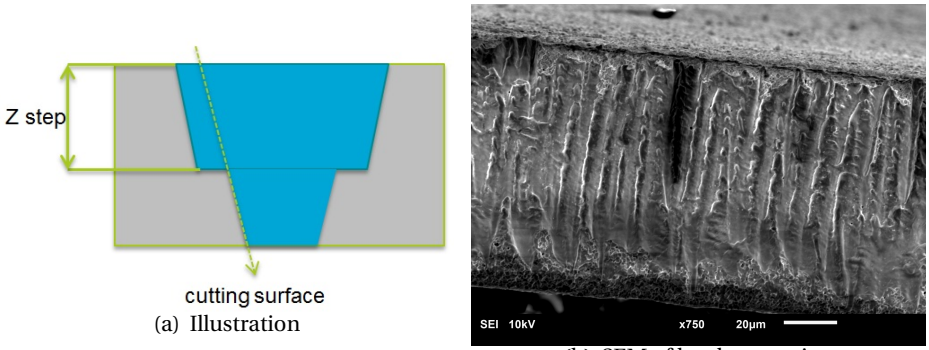

(a) Illustration

(b) SEM of level separation

Fig. 2.14: Illustration and SEM image of level separation

2.4.8 Conclusion

This traineeships has achieved the main aims which are practical experience micro laser operation along with fundamental facilitating equipment training. All those outcomes are essential and important for conducting further graduation project on both producing and testing.

The experience of dealing with multiple types of material gives a in-depth understanding of the behaviour of micro laser system. Several special phenomenon such as the recast, difficulties in releasing, bottom adhesion and level separation have been recorded which were not studied before this traineeships. Furthermore, a systematic approach by utilizing Taguchi process parameters optimization has been conducted. An optimal setting which has the minimum surface roughness value has been obtained, and overall quality has been improved significantly.

However, there are still some obstacles and issues are needed to be investigated further. The trade-off between bottom adhesion and step separation requires more experiment and more systemic investigation. And other factor of describing the cutting quality of micro laser, such as taper angle and production time, have not yet been studied in this traineeships. For quantifying the heat affect zone, an accurate measurement method for piezoelectric coefficient that is sensitive to the thermal damage is desperately needed.

For future research, several improvement can be considered. The minimum feature size of material is a promising direction and essential topic for manufacturing Micro Electro Mechanical System (MEMS). Meanwhile, other static and dynamic mechanical properties can also be considered for quantifying HAZ. Also, beside of the Taguchi optimization method, water-assisted laser system, including both still water immersing and pressured water jet, has also been proved to improve the surface roughness while eliminating thermal damage on variety of materiel in related research.

Bibliography

[1] Pusch T P, D'Auria M, Tolou N, et al. Laser Micromachining of Thin Beams for Silicon MEMS: Optimization of Cutting Parameters Using the Taguchi Method[C]//ASME 2015 International Design Engineering Technical Conferences and Computers and Information in Engineering Conference. American Society of Mechanical Engineers, 2015: V004T09A031-V004T09A031.

[2] Herzog, Dirk, et al. "Investigations on the thermal effect caused by laser cutting with respect to static strength of CFRP." International journal of machine tools and manufacture 48.12 (2008): 1464-1473.

[3] Tangwarodomnukun, Viboon, Jun Wang, and Philip Mathew. "A comparison of dry and underwater laser micromachining of silicon substrates." Key Engineering Materials. Vol. 443. Trans Tech Publications, 2010.

[4] Tangwarodomnukun, V., et al. "An investigation of hybrid laser water jet ablation of silicon substrates." International Journal of Machine Tools and Manufacture 56 (2012): 39-49.

[5] Taguchi G. System of experimental design: engineering methods to optimize quality and minimize costs[M]. UNIPUB/Kraus International Publications, 1987.

[6] Zhang J Z, Chen J C, Kirby E D. Surface roughness optimization in an end-milling operation using the Taguchi design method[J]. Journal of materials processing technology, 2007, 184(1): 233-239.

[7] J. Li and G. Ananthasuresh, "A Quality Study on the Excimer Laser Micromachining of Electro-Thermal-Compliant Micro Devices," J. Micromech. Microeng. 11 (1), 38–47 (2001).

[8] M.D'Auria, N. Tolou "UV-Laser Cutting for Silicon MEMS Prototyping: Improving Etching Rate and Quality". proceedings of the 14th euspen internation conference, 2014.

[9] Nadig S, Ardanuc S, Lal A. Planar laser-micro machined bulk PZT bimorph For in-plane actuation[C]//Applications of Ferroelectric and Workshop on the Piezoresponse Force Microscopy (ISAF/PFM), 2013 IEEE International Symposium on the. IEEE, 2013: 152-155.

3

Appendix C: Literature survey of improving cutting quality

3.1 Introduction

Conventional lithography is not only extremely time-consuming and expensive, specially for thick materials[6] but also complicated with complex skill and sufficient experience needed[7]. Laser micro machining is relatively simple, without contact, no need for mask and effective[8].

Ultra fast laser introduces new problems while bringing the unique advantages. Surface condition of the silicon structure obtained by laser manufacturing is relatively low compared to lithography. Currently the rough and coarse surface is unacceptable for laser machined MEMS devices applied in industry[31] since it would heavily influence the mechanical and optical properties of devices. Therefore improving the surface roughness is urgent for laser micromachining.

In addition, ultra fast laser still introduces small thermal effect, the thermal interaction between the laser and the specimen causes a phenomenon called 'burnt'. During this phenomenon the material properties are negatively affected due to overheating. The burnt area is also referred to as Heat Affected Zone (HAZ) [36]. Normally this can be minimized by carefully tuned laser parameters[9], however, some innovative attempts are also capable to completely avoid HAZ.

To sum up, although ultra fast laser micro machining technique as a new fabrication method has its unique advantages, it also brings drawbacks, such as poor surface condition and HAZ. Several attempts on groove cutting and micro drilling on semiconductor and piezoelectric materials have been carried out[2, 7, 8, 10, 11, 12, 13, 14, 15]. Yet producing practical MEMS devices with minimizing those drawbacks has not been seen in literature, which draws great research potential for future study.

3.2 Background

3.2.1 Laser

The word laser is the abbreviation of Light Amplification by Stimulated Emission of Radiation, the standard laser set needs a cavity to enclose the amplification process happening, an active medium to generate the photon emission reaction, and a 'pump' which is a energy source to pump the energy into the active

medium [19]. A schematic of a typical diode-pumped solid-state laser is shown below in Fig3.1.

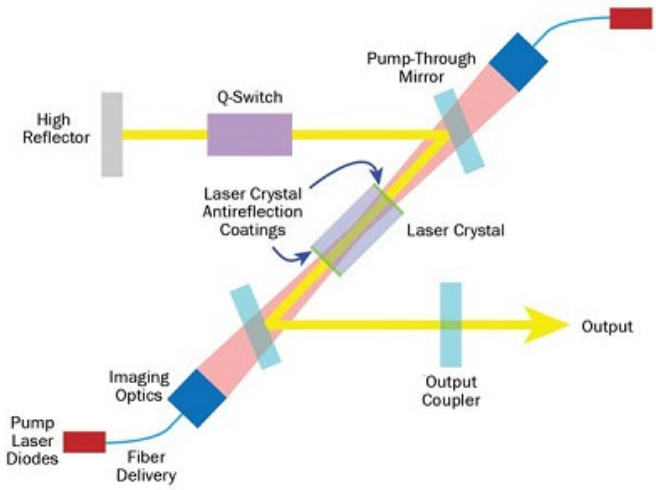

Fig. 3.1: laser configuration[17]

The cavity is shown in pink colour and the active medium is the crystal placed in the middle of cavity, in this case it is so called solid-state rather than gas of liquid, and the 'pump' source is from diode laser of semiconductor laser.

3.2.2 Gaussian Beam

In order to describe the intensity profile of a laser beam while propagation,an ideal Gaussian intensity mode is introduced. However, ideal Gaussian beam does not exist in the real world, therefore, a factor called M-squared is introduced to accommodate this variation between real and ideal Gaussian beams. M-squared factor is equal to 1 for the ideal mode and varies from 1 to 30 for practical beams[18]. A illustration of ideal Gaussian mode can be seen below as Fig3.2.

Two important definitions are widely used to discuss the characteristics of propagation of Gaussian beam, one is the diameter where the intensity of beam is below to $1/e^2$ (13.5 percent) of the peak, and the other is the diameter where the intensity of beam is below 50 percent of the peak. The parameter w in the picture can be calculated as below:

$$w(z) = w_0 \left[1 + \left(\frac{\lambda z}{\pi w_0^2} \right)^2 \right]^{\frac{1}{2}} \tag{3.1}$$

where z is the distance propagated from the plane where the wave front is flat, λ is the wavelength of light, w_0 is the radius of the 13.5 percent contour,

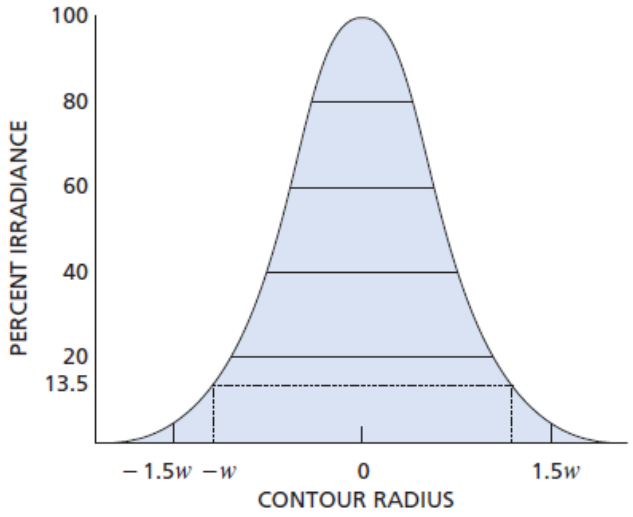

Fig. 3.2: Ideal Gaussian beam[18]

$W(z)$is the radius of the 13.5 percent contour after the wave propagates a distance of z. With the equation3.1 and combination of the Fig3.1, the intensive radius of a ideal Gaussian beam after propagation can be estimated.

3.2.3 Micro Machining

When laser technique applied to the micro scale, the working principle is different from the conventional laser methods. The removal of material is not done by melting, not vaporizing, but as highly ionised plasma[19]. The chemical connection pair in the material is directly broken by the high energy of photons in laser pulse. This process is generally referred as ablation. In order to achieve ablation phenomenon, the important factor is the duration of the laser pulse. When the photons that carry energy applied to the object, the thermal effect will occurs after the relaxation time by the vibration of atoms, therefore, if the laser applied time is short than this relaxation time, the material is ablated in stead of melted[20]. This short time is suggested as 1-10 ps is the favoured duration for high precision laser machining.

Compared to conventional laser technique, the big advantage micro machining brings is the thermal effect is negligible since the material removal is not achieved by melting but ablation. An illustration of comparison between long short and short lasers can be seen below in 3.3.

However, regardless of the advantages shown in the 3.3, when the size scaled down, there is still small heat brought to the material, which is generated by plasma during laser process and would potential have irreversible damage [24].

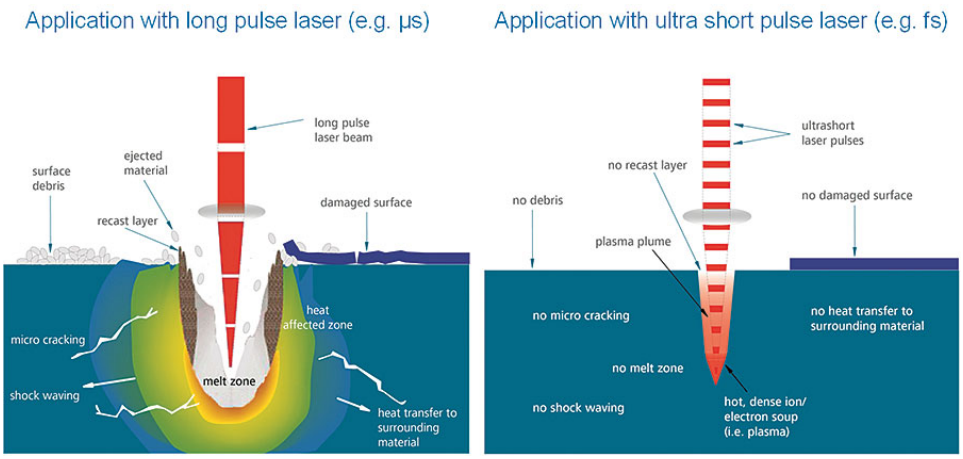

Fig. 3.3: comparison between long and short laser techniques[30]

3.3 Cutting quality

3.3.1 HAZ

As aforementioned, there is a small amount of heat introduced by the plasma generated of ultra fast last micro machining. Therefore, there is thermal interaction between plasma and specimen called 'burnt'. The structural properties of the material such as strength could be negatively influenced by the high temperature reached within the HAZ[26].

An illustration of HAZ on a specimen cut by CO2 laser can be seen below, where the colour is clearly changed between cut edge and base material is HAZ. An example has been shown in 3.4, this picture is the cross-sectional direction of a cutting specimen, the material is fibre reinforced, as some strips shown in the horizontal direction of cutting surface. The right side of the picture is the cutting edge where is the material is removed, and left side with light colour is the location of original material where is not affected by laser cutting. Only the central part of the picture where shows the variation inside of material with colour change is refereed as HAZ. Currently the defining and measuring HAZ is done by observing the the colour change regime around the kerf width.

3.3.2 Surface Roughness

Topography profile of a surface is an important factor for achieving a better performance in terms of lower friction and higher strength. Since the rough surface increase the stress concentration profile where with higher possibility to

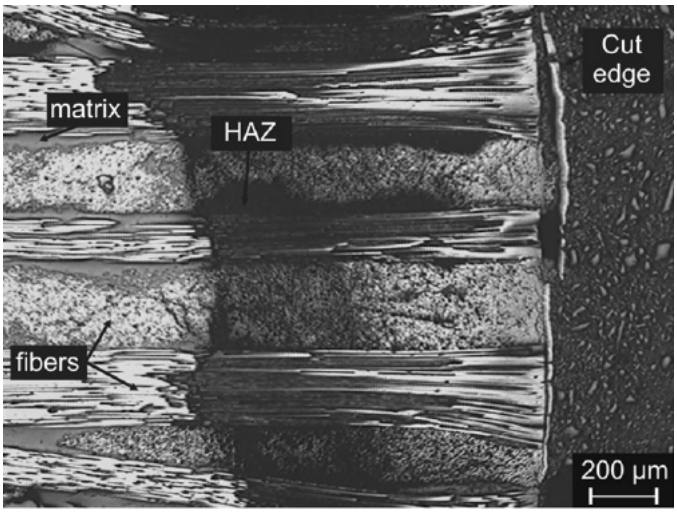

Fig. 3.4: example of Heat Affect Zone by CO2 laser[26]

break. Furthermore, for some application in optics and electronics, rough surface will affect the reflection performance and introduces the surface stroke on the sharp and irregular bumps on the surface. Therefore, the surface roughness as one of the most important factors attracts great interest for fabrication.

The measurement methods can be divided as two categories, contact and non-contact[27]. Stylus Profiler(SP) is a example of contact method of amplifying electronic signal[28], while optical interferometry is a example of non-contact method[29]. Especially, Scanning Tunnelling Microscopy (STM) and Atomic Force Microscopy (AFM) are commonly used as measurements for high precision surface profiling. An amplitude parameter called 'Ra' is normally used to describe the surface roughness. Ra is the arithmetic mean value of the profile measured from the mean line in a sample length, and this parameter is suitable for presenting stochastic surface roughness.

3.3.3 Laser Unit Specification

A Spectra-Physics Talon diode pumped solid-state (DPSS) UV laser system with a wavelength of 355nm and maximum power of 15 watts at 50 KHz along with a pulse width of 30ns is the main equipment in the laboratory. A BOFA extractor and filter is integrated in order to exhaust fumes. The optical steering is achieved by a Galvo head from Rhothor with a scan range of 46x46mm and focal length of 100mm.

Laser

The laser source is from a Q-switched Talon laser 355-15 with a maximum power of 15W at 50 kHz, and with 13W output at 100kHz. The maximum of fre-

quency is 500 kHz and pulse width 35 ns. The M^2 factor is 1.1 which describes the accuracy of the Gaussian TEM00 mode laser, the closer the factor to 1, the closer the actual laser output to the theoretical Gaussian beam. The performance of laser in terms of output power and corresponding pulse width under different frequencies can be found below:

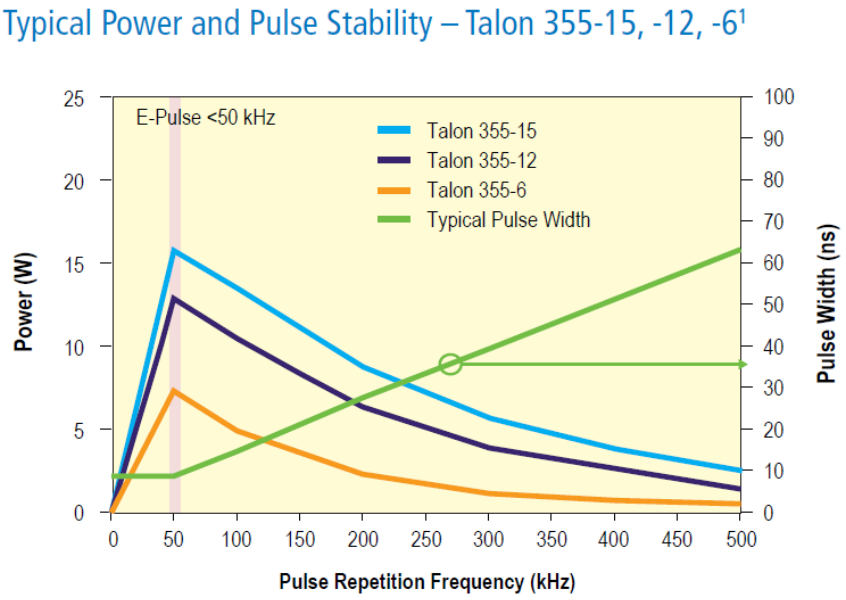

Fig. 3.5: specification of laser

The energy delivered per pulse can be calculated as :

$$E_{pulse} = \frac{W_{output}}{f_{laser}} \tag{3.2}$$

The W is the output power for the laser while irradiating obtained by the internal power monitor, which can be found by clicking 'refresh' button on the laser section Process Power software, and f is the laser frequency which is called as 'firing rate' in the system. For instance with Talon 355-15 laser, the maximum working mode with a 15w output at 50kHz, the energy delivered on every pulse is 300uJ. Fluence is vastly used in literature to describe the energy applied on the surface of object, the fluence can be calculated as:

$$F = \frac{2E_{pulse}}{\pi\omega_0^2} \tag{3.3}$$

As the w is the frequency of the laser.

Beam Delivery

The delivery of laser beam starts from the rear part of the system with a vertical breadboard including attenuator, BET and steering mirrors.The front part contains steering mirror and the optics to focus the beam on the part which is moved with X-Y stages. The vision system consists of a microscope inspection zoom associated to a CCD camera.

The X-Y stage has a range of 80mm square with 1 um effective resolution. The laser beam scanning motion is done by a laser deflection systems based on the Lorentz force motors with internal active optical feedback in order of dramatically reducing sensitivity to external noise. Galvo head had the range of 46x46mm with local length of 100mm, the writing speed is 1300cm per second with position resolution of 8 urad.

Affiliating Equipment

An air purification system BOFA has been integrated in the system to exhaust fumes and nano particles generated due to the laser processing. And a vacuum chuck is underneath the holding plate, in order to avoid the movement of object during the processing due to the motion of stage.

SEM

Scanning Electron Microscopy (SEM) is a type of electron microscope that produces images of a sample by scanning it with a focused beam of electrons. The interaction between atoms in the sample and the electron beams generates various signals that provide information about the topography of the surface of the sample.

For the author's own experience, there are different voltage of electron beams can be selected during the examination, which significantly influence the outcome image. As shown in Fig3.6 and Fig3.7, a lower voltage can provide more structural image that shows peaks and shapes of the surface, which also provides a understanding of the topography information although SEM itself is not capable of obtaining the surface roughness quantitatively.

the other hand, a high voltage provides sharper image that helps for locally inspection, which means more details can be obtained by more electrons interacting. However, stronger electron stream hitting onto the surface may damage the material itself permanently.

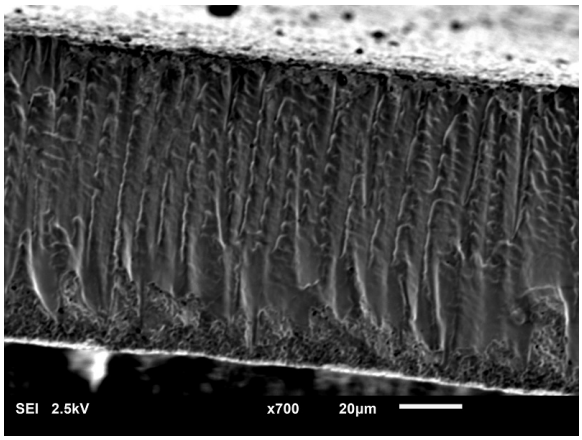

Fig. 3.6: SEM low voltage image

AFM

Atomic Force Microscopy (AFM) can achieve the resolution on the order of fractions of a nanometre, more than 1000 times better than the optical diffraction limit. The surface information is gathered by contacting the surface with a mechanical probe connected with a piezoelectric elements.

There are two working modes of AFM, static swiping modes and taping mode. Static scanning mode provides high resolution result, but damage on probe may happen due to the rough surface. While the tapping mode gives a quicker examination with slightly lower resolution.

For measuring the surface roughness, AFM only subjects to a relatively small area compared to the white light interferometer although AFM is capable to obtain an accurate result.

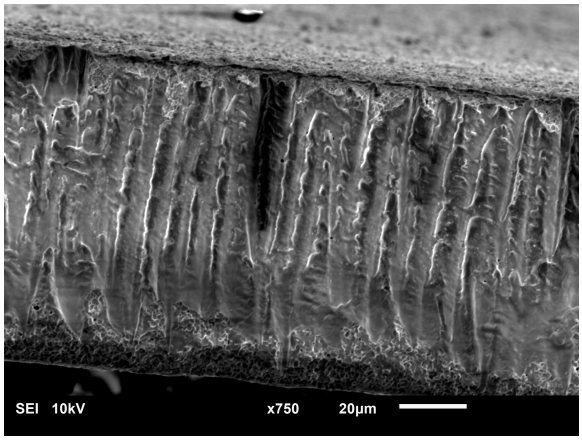

Fig. 3.7: SEM low voltage image

3.4 Quality Improvement

3.4.1 Improve Surface Roughness

Although the laser micromachining has been developed for decades, yet, the surface roughness of the product is still a huge issue due to the periodic structures, which results the surface unacceptable for industry level [31]. At the same time, the conventional UV lithography has reached a smooth surface as 18nm in [32], Yet so far the roughness of temptations of micro machining are mainly in the range of 200nm to 500nm or even rougher[43]. Therefore, improving the surface roughness has became an urgent obstacle of the development of this technique.

Post Treatment

Reheat or reflow is a widely used post treatment method in conventional industry. This process can smooth out the defects and recrystallise the material to obtain an acceptable surface, as well as enhance the mechanical properties like strength. To improve the surface roughness of a resonator micro-machined by laser in a traditional lathe alike setting, a high temperature electric arc was introduced in [33], as shown in 3.8

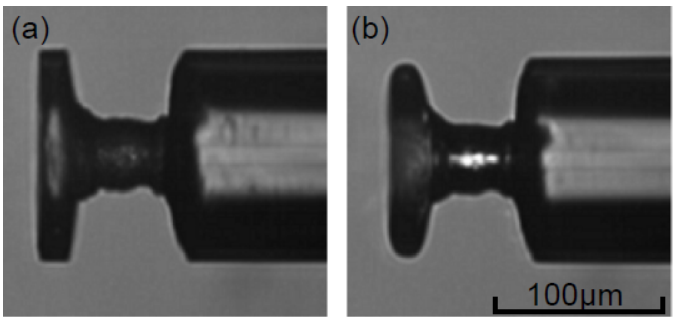

Fig. 3.8: reflow of electric arc of resonator[33]

Another popular post treatment method is chemical etching or wet etching which was suggested to improve the surface condition, but it only subjects to certain types of materials but not all cases. Furthermore, etching method slows the manufacture efficiency[31]. one example is introduced in [35], a micro channel chip is manufactured in the Poly Methyl Methacrylate (PMMA) and Cyclic Olefin Copolymer (COC) material by laser micro machining, and a vapour exposure method is used to improve the surface roughness, the outcome can be seen in 3.9

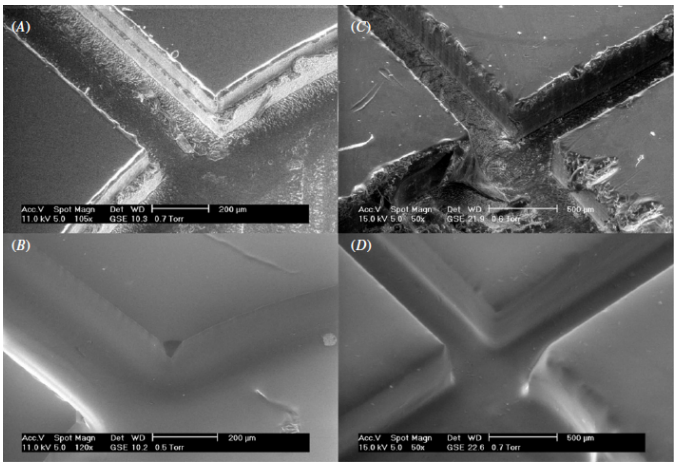

Fig. 3.9: vapour exposure for PMMA(left) and COC(right)[35]

Under Water Cutting

The debris is the main origin of rough surface of laser micro machining, along with the periodic texture introduced at the cut surface. The debris can be controlled by cutting underwater, which means by putting the work piece into the water and creating a very thin water layer between laser source and the work piece. A schematic is shown below in Fig3.10

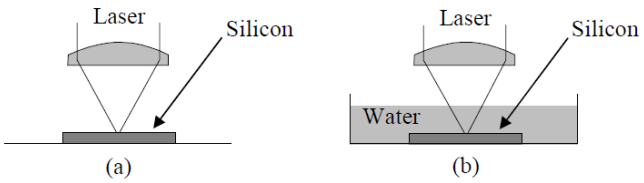

Fig. 3.10: schematicofunderwater [36]

By putting a thin water laying beyond the working surface, the thermal effect can be dramatically decreased since the heat will instantly be dissipated into water . Although original ultra short pulse laser has the advantage of negligible thermal effect, the phenomenon of 'burnt' pieces still existed. There is certain band observed along the kerf band referred as Heat Affected Zones that influences the quality of laser manufacturing. Another obstacle is caused by the high temperature debris recast and gathered around the cur area[37]. The schematic of water cutting is shown below in 3.11, a small eddy flow was generated in water layer which can transport the debris away from cutting area and avoid high temperature. Several successful examples and comparisons are made by [36][38][37], pictures shown following.

The disadvantages of this method are also obvious, part of the laser energy is absorbed by the water layer, which means the higher laser energy is needed

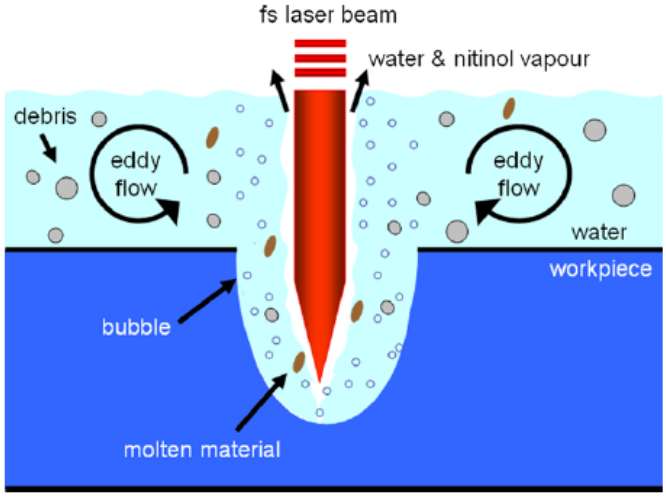

Fig. 3.11: water cutting schmetic[38]

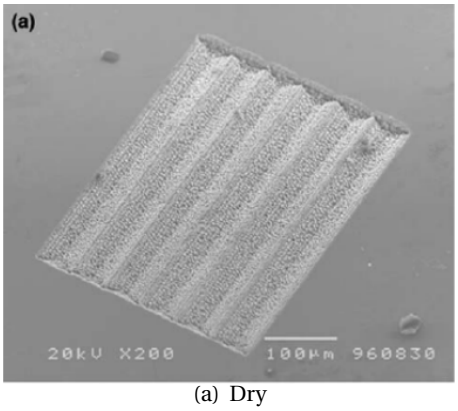

(a) Dry

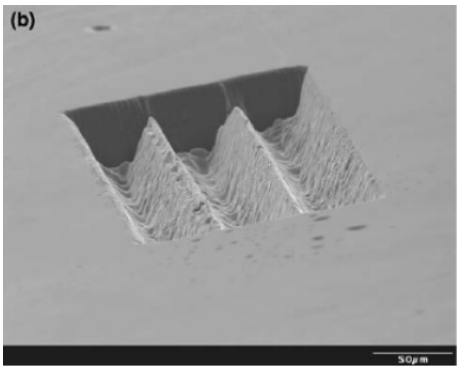

(b) Underwater

Fig. 3.12: One example of underwater cutting

for same workpiece underwater. The energy lost for a single path laser can be calculated by using the Beer-Lambert law:

$$I_w = I_0 \exp\left(-\frac{Z_w}{l_a}\right) \tag{3.4}$$

where I_w is the left laser intensity, Z_w is the distance, and $l_a$andI_0 are the light absorption length and the original laser intensity.

Also, the previous period texture turns into non-period texture, in [37] stated, the possible reason could be the disturbing water wave on the water layer surface, furthermore, due to the high power density hit into the water, some bubbles are generated, and dissociated oxygen has interaction with the laser that can be considered as the moving electromagnetic field. To improve this defeats,

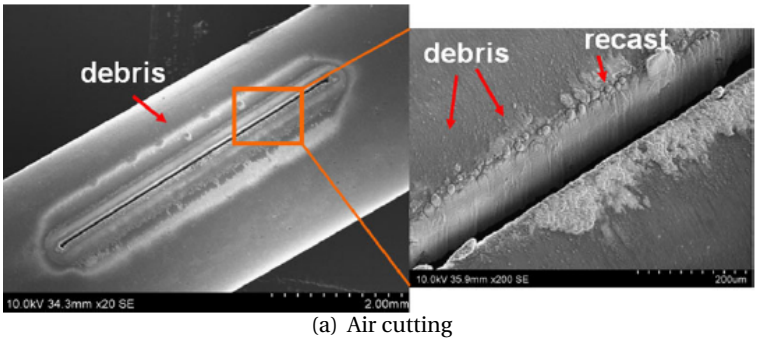

(a) Air cutting

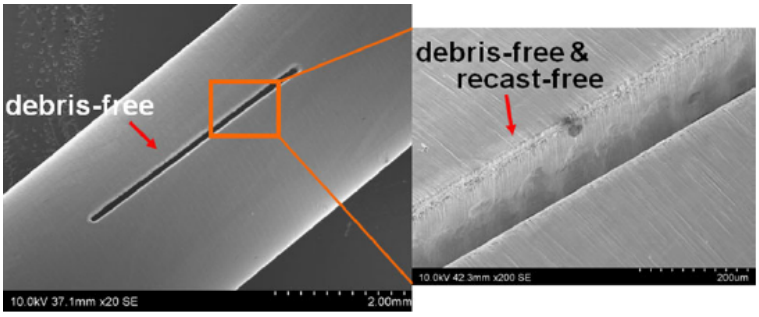

(b) Underwater cutting

Fig. 3.13: Comparison between dry and underwater cuttings[38]

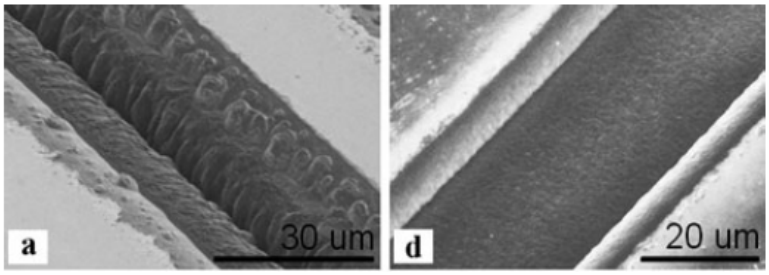

Fig. 3.14: Example of underwater cutting on saphire wafer, (a)dry cutting and (b)underwater cutting[39]

a potential solution was proposed by [36], which is operating this system in a closed water environment that has no disturbing water wave and bubbles.

In addition, the potential safety should be carefully considered since underwater cutting introduces free liquid into experimental environment, the splash of water droplet could possibly damage the laser optical system in some settings.

The underwater laser cutting is also referred as liquid immersion laser micromachining [39].And this method has been investigated with several nice examples shown in the Fig3.12,3.13and3.14. Configurations of this technique can be divided as three settings, as shown in the Fig below, and [40] conducted a research with different cutting parameters on SiC. Silicon based underwater cut-

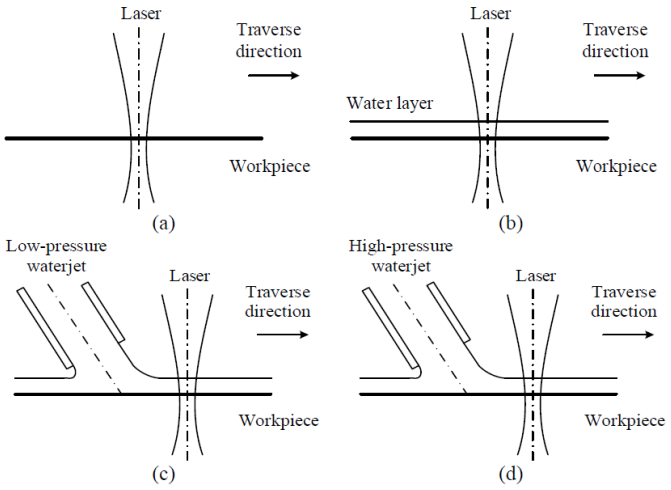

Fig. 3.15: configurations of different underwater cutting[40]

ting researches are shown in [41] and [42], but only single hole or groove were focused. Furthermore, no surface roughness details so far were quantitatively recorded but only observation of 'smoother' result[36].

3.5 Comparisons and Discussion

In order to show the differences among all the current consideration of methods, a table has been made and can be seen below in 3.1. As aforementioned, target effects are improving surface roughness and minimizing heat affected zone. Conventional lithography has tremendous advantages in both aspects, meaning extremely low surface roughness found in[32] and no thermal mechanism at all and relatively mature processing. However, the extremely high cost can only be lowered down by massively bulk parallel producing. Furthermore, enormously time cost and labour requirement terribly limits the prototyping and innovation of MEMS, which were the exact motivation of this research.

Tab. 3.1: Table of comparison among methods

Methods	roughness	heat zone	feasibility	sum
Direct cut	370nm (-)	negligible (-)	developing	–
Underwater cut	not found (0)	none (+)	innovating	+
Reflow and etch	70nm (=)	limited (0)	current	0

Direct cutting by ultra fast laser micromachining has been developed by over decades, and quite a number of research has been carried on, in [43] an advanced optimizing model were used to obtain the best cutting result, and a minimum surface roughness of 370nm was achieved on cutting through silicon, and the HAZ was negligibly small due to the ultra fast lase pause.

Reflow and etching method as post processing are the most commonly used and adapted methods by the current state of art in improving the surface roughness after cutting. However, as considering manufacturing MEMS devices, there are multiple layers of materials cut at the same time. This brings serious problem even for the most commonly used silica and silicon substrate used in this field, since silicon is much more thermal conductive than silica. Different conductivities between layer make the reflow process difficult to achieve.

Although the underwater cutting technique is still being developed, this is the a promising method for improving the surface roughness. Moreover the specific roughness data has not been found in literature yet.

3.6 Conclusion

Laser micromachining as a novel area of laser manufacturing has shown the great potential and unique advantages in MEMS fabrication. This technique can dramatically reduce the cost and time consumed for prototyping compared to lithography. However, the unacceptable surface roughness and heat affected zone around kerf are currently the main drawbacks.

In order to overcome the drawbacks of laser micromachining, reflow or etching have been considered as post treatment process, yet more processing time and cost are added. Therefore, another method called underwater cutting or liquid immersion is investigated. This method can clearly improve the surface condition and almost cause no heat affected zone. Several researches have been conducted on different material such as SiC, glass and silicon, as well as with different configurations. However, current state of art stays only in simple structures like single hole or groove. Furthermore, as examples has shown improved the surfaces, yet no quantified data is found in literature.

More complex cutting profile and quantifying improved the surface could be useful for Further study. And applying micro laser micromachining to fabricate functional MEMS device attracts great interests.

Bibliography

[1] Huang, Yunhan, et al. "MEMS reliability review." IEEE Transactions on Device and Materials Reliability 12.2 (2012): 482-493.

[2] Crawford, T. H. R., A. Borowiec, and H. K. Haugen. "Femtosecond laser micromachining of grooves in silicon with 800 nm pulses." Applied Physics A 80.8 (2005): 1717-1724.

[3] Cheng, Jian, et al. "A review of ultrafast laser materials micromachining." Optics Laser Technology 46 (2013): 88-102.

[4] Bäuerle, Dieter W. Laser processing and chemistry. Springer Science Business Media, 2013.

[5] Mahrle, A., and E. Beyer. "Hybrid laser beam welding—classification, characteristics, and applications." Journal of laser applications 18.3 (2006): 169-180.

[6] X. Jiang, J.R. Yuan, A. Cheng, K. Snook, P.J. Cao, P.W. Rehrig, W.S. Hackenberger, G. Lavalelle, X. Geng, T.R. Shrout, Proc. IEEE Symp. on Ultra (2006) 922.

[7] Peng, Jue, et al. "Micro-patterning of 0.70 Pb (Mg 1/3 Nb 2/3) O 3–0.30 PbTiO 3 single crystals by ultrasonic wet chemical etching." Materials letters 62.17 (2008): 3127-3130.

[8] Lam, K. H., et al. "Kerf profile and piezoresponse study of the laser micromachined PMN-PT single crystal using 355nm Nd: YAG." Materials Research Bulletin 48.9 (2013): 3420-3423.

[9] Karatodorov, S., and M. Grozeva. "The Effect of Process Parameters in Femtosecond Laser Micromachining." Bulg. J. Phys 43 (2016): 110-120.

[10] El Fissi, Lamia, Victor Xhurdebise, and Laurent A. Francis. "Effects of Laser Operating Parameters on Piezoelectric Substrates Micromachining with Picosecond Laser." Micromachines 6.1 (2014): 19-31.

[11] Corbari, Costantino, et al. "Femtosecond versus picosecond laser machining of nano-gratings and micro-channels in silica glass." Optics express 21.4 (2013): 3946-3958.

[12] Li, Xiaomeng, et al. "Lead-Free Piezoelectric Diaphragm Biosensors Based on Micro-Machining Technology and Chemical Solution Deposition." Sensors 16.1 (2016): 69.

[13] Knappe, Ralf, et al. "Scaling ablation rates for picosecond lasers using burst micromachining." SPIE LASE. International Society for Optics and Photonics, 2010.

[14] Chen, Chien-Yu, et al. "Microstructure and lubricating property of ultrafast laser pulse textured silicon carbide seals." Applied Physics A 107.2 (2012): 345-350.

[15] Kam, D. H., L. Shah, and J. Mazumder. "Femtosecond laser machining of multi-depth microchannel networks onto silicon." Journal of Micromechanics and Microengineering 21.4 (2011): 045027.

[16] G.R.Gordon.The laser, light amplification by stimulated emission of radiation. In P.A.Franken and R.H Sands, editors, Processing of the Ann Arbor Conference on Optical Pumping, the University of Michigan, page 128. University og Michigan, 1959.

[17] TREY TURNER AND QUENTIN TURCHETTE, REO INC.Retrieved from http://www.photonics.com/Article.aspx?AID=55003

[18] cvimellesgriot, Gaussian beam optics

[19] Dr.ir. G.R.B.E. Romer. (2012). Laser Material Processing, page 8, page 195. University of Twente

[20] Ruf, Andreas. Modellierung des Perkussionsbohrens von Metallen mit kurz-und ultrakurzgepulsten Lasern. Utz, 2004.

[21] Tao, Sha, et al. "Thermal modeling and experimental study of infrared nanosecond laser ablation of silicon." Journal of Applied Physics 106.12 (2009): 123507.

[22] Cournoyer, Alain, et al. "Maximizing laser ablation efficiency of silicon through optimization of the temporal pulse shape." SPIE LASE. International Society for Optics and Photonics, 2014.

[23] Mannion, P. T., et al. "The effect of damage accumulation behaviour on ablation thresholds and damage morphology in ultrafast laser micromachining of common metals in air." Applied surface science 233.1 (2004): 275-287.

[24] Liu, X., D. Du, and G. Mourou. "Laser ablation and micromachining with ultrashort laser pulses." IEEE journal of quantum electronics 33.10 (1997): 1706-1716.

[25] Cournoyer, Alain, et al. "Maximizing laser ablation efficiency of silicon through optimization of the temporal pulse shape." SPIE LASE. International Society for Optics and Photonics, 2014.

[26] Herzog, Dirk, et al. "Investigations on the thermal effect caused by laser cutting with respect to static strength of CFRP." International journal of machine tools and manufacture 48.12 (2008): 1464-1473.

[27] Poon, Chin Y., and Bharat Bhushan. "Comparison of surface roughness measurements by stylus profiler, AFM and non-contact optical profiler." Wear 190.1 (1995): 76-88.

[28] D.J. Whitehouse, Handbook of Surface Metrology, Institute of Physics,Bristol, 1994.

[29] S.R. Lange and B. Bhushan, Use of two- and three-dimensional noncontact surface profiler for tribology application, Surj: Topography. I (1988) 277-290.

[30] GEOFF SHANNON, "comparison the effects of using a micro second with a femtosecond laser", LASER TECHNOLOGY MANAGER, MIYACHI AMERICA

[31] Han, Yukun, et al. "Femtosecond laser-induced silicon surface morphology in water confinement." Microsystem technologies 15.7 (2009): 1045-1049.

[32] Jung, C., et al. "Silicon micromachining technology for THz applications." 35th International Conference on Infrared, Millimeter, and Terahertz Waves. IEEE, 2010.

[33] Tada, Kazunari, et al. "Fabrication of high-Q microresonators using femtosecond laser micromachining." IEEE Photonics Technology Letters 25.5 (2013): 430-433.

[34] Dong Y, Zorman C, Molian P (2003) Femtosecond laser micromachining of single crystalline 3C-SiC structures based on a laserinduced defect-activation process. J Micromech Microeng 13:680–685. doi:10.1088/0960-1317/13/5/320

[35] Ogilvie, I. R. G., et al. "Reduction of surface roughness for optical quality microfluidic devices in PMMA and COC." Journal of Micromechanics and Microengineering 20.6 (2010): 065016.

[36] Tangwarodomnukun, Viboon, Jun Wang, and Philip Mathew. "A comparison of dry and underwater laser micromachining of silicon substrates." Key Engineering Materials. Vol. 443. Trans Tech Publications, 2010.

[37] Han, Yukun, et al. "Femtosecond laser-induced silicon surface morphology in water confinement." Microsystem technologies 15.7 (2009): 1045-1049.

[38] Muhammad, Noorhafiza, and Lin Li. "Underwater femtosecond laser micromachining of thin nitinol tubes for medical coronary stent manufacture." Applied Physics A 107.4 (2012): 849-861.

[39] Mak, Giuseppe Y., Edmund Y. Lam, and H. W. Choi. "Liquid-immersion laser micromachining of GaN grown on sapphire." Applied Physics A 102.2 (2011): 441-447.

[40] Feng, Shaochuan, et al. "A Comparison among Dry Laser Ablation and Some Different Water-laser Co-machining Processes of Single Crystal Silicon Carbide." Materials Science Forum. Vol. 861. 2016.

[41] Wee, L. M., et al. "Micro-machining of silicon wafer in air and under water." Optics and Laser Technology 43.1 (2011): 62-71.

[42] Das, Alok Kumar, and Partha Saha. "Micromachining of silicon with excimer laser in air and water medium." International Journal of Manufacturing Technology and Management 21.1-2 (2010): 42-53.

[43] Pusch, Tim P., et al. "Laser Micromachining of Thin Beams for Silicon MEMS: Optimization of Cutting Parameters Using the Taguchi Method." ASME 2015 International Design Engineering Technical Conferences and Computers and Information in Engineering Conference. American Society of Mechanical Engineers, 2015.

4

Appendix D: Operation recipes

Material		Laser			Process					Extra	
Type	Thickness (μm)	Firing-rate (KHz)	Speed (mm/s)	Diode current (A)	level	Step[6] (μm)	Lines[4]	Gap[5] (μm)	Repetition	Energy[1] (%)	Note[2]
Spring steel*	50	50	20	6.44[7]	1	60	4	20	65	100	
Spring steel	100	50	20	6.44	2	80	4	20	50	100	
Silicon wafer**	200	20	20	6.44	8	30	4	15	12	100	
Silicon wafer	525	20	20	6.5	20	30	4	15	10	100	
Silicon wafer	300	15	15	6.5	13	30	4	15	18	100	Min.Ra
PZT ceramic***	100	15	60	6.0	4	25	4	20	50	100	Min.HAZ[3]
		15	60	6.0	4	25	4	20	50	100	Min.Ra
PZT ceramic	200	30	80	6.0	2	100	4	20	20	100	Min.HAZ
PZT ceramic	200	20	40	6.5	2	100	4	20	20	100	Min.Ra
PZT polymer****	50	35	110	6.44	3	20	5	10	180	30	

Table 1:Operation Recipe

*: Stainless steel foil with serial number

**:Pure single crystal silicon wafer, doping and polishing does not have obvious influence laser fabrication.

***:PZT-5H ceramic thin foil with two side of thin(<1 μm)electrode (silver and Copper).

****: PVDF(polyvinylidene difluoride) sheet, material property unknown.

1: Controlling overall output by changing percentage of energy may be suitable for junior user.

2: The recipes are based on the Taguchi method optimization and experimental measurement.

3: By mean of minimum loss of piezoelectric coefficient (d_33).

4: More redundant lines provide better releasing for dedicate structures while increasing the machining time.

5: The laser focal spot is roughly 20 μm.

6: The range of working depth is larger than the theoretical thickness of material, in case of low flatness, thermal bending and tolerance in thickness of material.

7: In case of junior users, 6.440 is the default value of system.